学位論文

Mathematical modeling of plasma glucose homeostasis regulated by plasma insulin in humans

（数理モデルを用いたヒト血糖値恒常性制御システムの解析）

平成 29 年　12 月　博士 （理学）申請

東京大学大学院理学系研究科

生物科学専攻

大橋　郁

Abstract

Plasma glucose concentration is regulated to be constant, known as glucose homeostasis, by a complex feedback between circulating glucose and insulin, of which failure leads to type 2 diabetes mellitus (T2DM). The feedback loop is characterized by the abilities of insulin secretion promoted by glucose and glucose uptake promoted by insulin, known as insulin sensitivity. Plasma insulin concentration is affected by insulin clearance ability, which consists of hepatic removal from portal vein and peripheral removal from systemic circulation. However, it is difficult to assess these abilities of body tissues directly from the circulating insulin measurement because of the negative feedback between circulating glucose and insulin. In this study, I developed two kinds of mathematical models based on the consecutive hyperglycemic and hyperinsulinemic-euglycemic clamp analysis performed for 121 subjects including healthy and T2DM. First, I generated the models reproducing the observed time courses of plasma glucose and insulin concentration for specifically quantifying these abilities of insulin secretion, sensitivity, and clearance by accounting for the negative feedback. It was found that peripheral insulin clearance significantly decreased from healthy to T2DM during the progression of glucose intolerance. However, these models did not distinguish the hepatic and peripheral insulin clearance explicitly. Second, I reported another type of models reproducing the time courses of plasma insulin and C-peptide concentrations for separately quantifying hepatic and peripheral insulin clearance as the difference between pre-hepatic and post-hepatic insulin concentrations. An increase in hepatic but a decrease in peripheral insulin clearance from healthy to T2DM were found, respectively.

The model analysis revealed that hepatic and peripheral insulin clearance affected the dynamics of amplitude and temporal patterns, respectively. These results suggest that those two insulin clearance play essential and different roles in regulating plasma insulin concentration and glucose homeostasis.

Table of Contents

Abbreviation List

2-h PG:	2-h after a 75 g oral glucose load plasma glucose
AIC:	Akaike information criterion
AUC:	Area under the curve
DI:	Disposition index
FPG:	Fasting plasma glucose
GIR:	Glucose infusion rate
HEC:	Hyperinsulinemic-euglycemic clamp
HGC:	Hyperglycemic clamp
HOMA:	Homeostatic model assessment
I. I.:	Insulinogenic index
IIR:	Insulin infusion rate
IRI:	Immunoreactive insulin
ISI:	Insulin sensitivity index
IVGTT:	Intravenous glucose tolerance test
MCR:	Metabolic clearance rate
NGT:	Normal glucose tolerance
OGTT:	Oral glucose tolerance test
RSS:	Residual sum of squares
T1DM:	Type 1 Diabetes Mellitus
T2DM:	Type 2 Diabetes Mellitus

1. Introduction

1.1 Plasma glucose homeostasis and Diabetes Mellitus

In human, glucose is the obligate metabolic fuel for most organs, especially the brain, under physiologic conditions, and glucose is supplied through the plasma circulation. In such situation, the regulation of plasma glucose concentration is vital for life and health, and the phenomenon that plasma glucose is maintained in a narrow range in normal individuals [1] is known as glucose homeostasis. This tight regulation is governed by the balance among the biological functions of organs, mainly glucose uptake into peripheral tissues such as adipose tissues and muscles, and glucose production from the liver. These functions are promoted or prevented by insulin, respectively, and the effectiveness of insulin on these target tissues is referred to as insulin sensitivity. Insulin is an essential hormone for glycemia control, secreted from the pancreatic β-cells as plasma glucose concentration rise, and removed from the systemic circulation by insulin-sensitive tissues [2]. Therefore, the concentrations of circulating glucose and insulin are mutually affected, and this negative feedback loop between glucose and insulin plays an essential role in the maintenance of the glucose homeostasis.

Diabetes Mellitus is one of the fastest growing public health problems. Currently, more than 382 million people are afflicted worldwide and the WHO projects that diabetes will be the 7th leading cause of death in 2030 [3]. Diabetes is a metabolic disease that is characterized by chronic hyperglycemia with the failure of such homeostasis [4]. Diabetes can occur because of autoimmune destruction of β-cells (Type 1 Diabetes Mellitus, T1DM) or in a subset of individuals with insulin resistance (Type 2 Diabetes Mellitus, T2DM) or from other reasons.

Diabetes mellitus may present with ketoacidosis or a non-ketotic hyperosmolar state which lead to stupor, coma, and in absence of effective treatment, death. Even if the symptoms are not severe, the long-term effects of diabetes include progressive development of the specific complications of retinopathy with potential blindness, nephropathy that may lead to renal failure, neuropathy with foot ulcers, amputation, Charcot joints, and features of autonomic dysfunction, including sexual dysfunction. People with diabetes are at increased risk of cardiovascular, peripheral vascular, and cerebrovascular diseases [5]. Generally, increased plasma glucose results from low insulin secretion or insufficient secretion for the persons' insulin sensitivity [6].

1.2 Measurements of circulating glucose, insulin dynamics, and indices of glucose tolerance

In clinical diagnosis, the persons' ability of maintenance of plasma glucose concentration against loading glucose, named glucose tolerance, is evaluated. The oral glucose tolerance test (OGTT) is the most commonly used method to classify the level of glucose tolerance: Normal Glucose Tolerance (NGT) is defined as overnight fasting plasma glucose (FPG) of <110 mg/dL (<6.1 mM) and 2-h after a 75 g oral glucose load plasma glucose (2-h PG) of <140 mg/dL (<7.8 mM); T2DM is diagnosed as FPG of ≥126 mg/dL (≥7.0 mM) or 2-h PG of ≥200 mg/dL (≥11.1 mM); Borderline type is defined as falling between the diabetic and normal values of FPG and 2-h PG as FPG of 110–125 mg/dL (6.1–6.9 mM) or 2-h PG of 140–199 mg/dL (7.8–11.0 mM) [7] (Fig. 1).

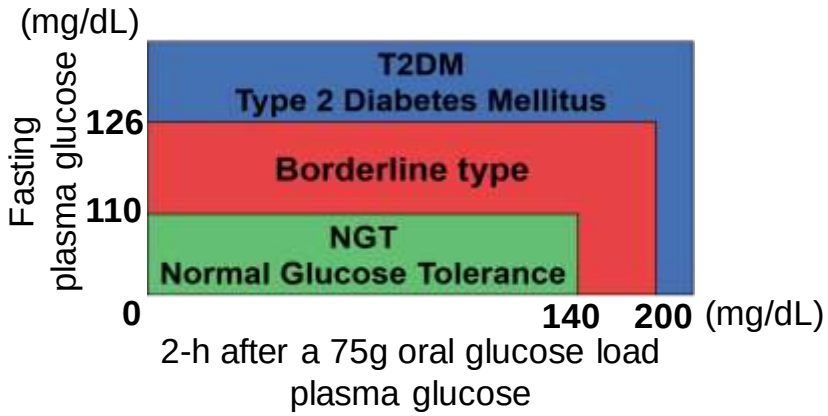

Figure 1. Diagnostic cut-off values of plasma glucose concentration for NGT, borderline type and T2DM.

The measurements of circulating glucose and insulin concentrations dynamics provide information on insulin secretion and sensitivity, therefore, many attempts have been made to assess them. The area under the curves of circulating glucose and insulin has been used as the index of insulin sensitivity [8-11]. The homeostatic model assessment (HOMA) provided the indices of insulin secretion (HOMA-β) and sensitivity (HOMA-R) [12]. Seltzer et al. proposed the insulinogenic index (I. I.) as an index of insulin secretion [13]. Matsuda et al. proposed the index of insulin sensitivity [14].

Since it was suggested that insulin secretion is also affected by intestinal absorption of glucose-independent changes in the circulating glucose concentration, the intravenous glucose tolerance test (IVGTT) is used for quantitating the differential insulinogenic contributions of plasma glucose concentration [15]. However, the methods of OGTT and IVGTT do not directly yield a measure of insulin secretion and sensitivity because of the feedback loop between circulating glucose and insulin. A rise in circulating glucose concentration stimulates insulin secretion from the pancreatic β-cells, and the resultant rise in circulating insulin concentration stimulates glucose uptake, causing circulating glucose concentration to fall. These processes are not sequential but occur simultaneously, and make it difficult to distinguish the effect of insulin secretion and sensitivity directly from the measurements of circulating glucose and insulin concentration in intact human [16].

In order to assess insulin secretion and sensitivity separately, it is necessary to hold the concentration of glucose or insulin constant, like the studies *in vitro*, in which the excised pancreas can be perfused at fixed hyperglycemia. DeFronzo et al. [16] developed the

hyperglycemic clamp technique, in which insulin secretion is measured while circulating glucose concentration is at a fixed hyperglycemic plateau maintained by exogenous continuous glucose infusion. The measurements of circulating insulin concentration during the first 10 min and after 10 min are used to assess the insulin secretion ability and are known as the first and second phase insulin secretions, respectively [16,17].

Conversely, the hyperinsulinemic-euglycemic clamp technique was developed, in which insulin sensitivity is measured while circulating insulin and glucose concentrations are fixed at hyperinsulinemic and euglycemic plateau maintained by exogenous continuous insulin and glucose infusion, respectively [16]. Tissue insulin sensitivity is defined as the ratio of the glucose infusion rate to the circulating insulin and glucose concentrations when they reach plateaus [16,17].

1.3 Relation between dynamics of circulating insulin concentration and the progression of glucose intolerance

According to the mutual relation between circulating glucose and insulin concentration, the dynamics of circulating insulin concentration affects the efficiency of maintaining glucose homeostasis. During the IVGTT, plasma insulin concentration transiently increases during first 10 min, and then continuously increases during 120 min, which are known to be first and second phases of insulin secretion, respectively [18]. In patients with borderline type or in the early stages of T2DM, first-phase insulin release is almost invariably lost despite the enhancement of second-phase secretion [19-21]. A recent longitudinal study has clearly

demonstrated that a defect in acute insulin release occurs early in the natural history of T2DM [22], and it may contribute to the progression from NGT to borderline type, and finally, to overt diabetes. This synopsis illustrates the altered temporal patterns of circulating insulin concentration in T2DM, underscoring the abnormal first and second insulin secretion.

1.4 Mathematical modeling used to assess insulin secretion and sensitivity

Since the clinical indices of insulin secretion and sensitivity introduced above are inferred from circulating glucose and insulin concentrations under the dynamical change and complex interplay in intact humans, it still remains ambiguous that these indices could reflect the real functions of insulin secretion and sensitivity. Mathematical models have been developed for quantifying these biological functions from the observed time courses of circulating glucose and insulin concentrations out of steady state. The minimal model, based on time series data of IVGTT, is a successful example of mathematical models for the assessment of glucose hemostasis [23]. Disposition index (DI), defined as a product of parameters for insulin secretion and insulin sensitivity determined by the minimal model, i.e., DI = insulin secretion × insulin sensitivity, is thought to reflect the ability of insulin secretion adjusted for insulin sensitivity [24,25]. By a number of studies, DI has been proven to tightly constrain the severity of glucose intolerance as well as to predict the development of this condition, showing the validity of the model as well as a concept that glucose tolerance is determined by insulin secretion and sensitivity [26,27]. In addition, mathematical models with the use of the time series data of OGTT have also been developed, and shown to be of clinical utility [28-37]. However, because

circulating glucose and insulin concentrations during IVGTT or OGTT are mutually influenced through the negative feedback loop, it is difficult to accurately determine parameters for insulin sensitivity and insulin secretion.

The model developed for hyperinsulinemic-euglycemic clamp condition made it possible to assess the biological functions in more detail, such as the ability of insulin sensitivity consists of hepatic glucose output and tissue glucose uptake. The parameters revealed that the ability to reduce hepatic glucose output signify decreased from lean to obese subjects, while no difference was found in tissue glucose uptake [38]. However, the time courses of circulating glucose and insulin concentration under both hyperglycemic and hyperinsulinemic-euglycemic clamp conditions were not analyzed by means of mathematical models, and a critical feature(s) of the negative feedback loop may remain to be unclear.

1.5 Mathematical modeling for consecutive hyperglycemic and hyperinsulinemic-euglycemic clamp

In Chapter 2 of this study, I developed the models based on the time courses of circulating glucose and insulin during the consecutive hyperglycemic and hyperinsulinemic-euglycemic clamp [17], in which both insulin secretion and sensitivity can be assessed independently without the effect of the feedback relation. The model of glucose-insulin regulatory system with the glucose and insulin infusion during this clamp analysis was generated, and the parameters of the model were estimated with the observed time courses of plasma glucose and serum insulin concentrations during the clamp analysis for each subject

with variety of glucose tolerance including NGT, borderline type, and T2DM. This model analysis revealed that the rate constant of insulin clearance from the systemic circulation strongly constrain a product of the rate constants of insulin secretion and sensitivity, conceptually corresponding to DI, as well as the progression of glucose intolerance. This study uncovered previously unrecognized relation in biological functions that regulate the capacity of glucose tolerance.

1.6 Dynamics of circulating insulin concentration controlled by insulin secretion and clearance

The remaining problem is how the biological functions control the dynamics of circulating insulin concentration which is also associated with the progression of glucose intolerance. The circulating insulin concentration is controlled by a balance between the insulin secretion and clearance. The major organs responsible for insulin clearance are the liver, which removes portal insulin during first-pass transit [39,40], and insulin-sensitive tissues, such as kidney and muscle, that remove insulin from the systemic circulation [41]. The insulin clearance in the liver and other organs are called hepatic and peripheral insulin clearance, respectively.

Hepatic insulin clearance cannot be assessed directly from circulating insulin concentration because hepatic insulin clearance occurs before delivery of secreted insulin into the systemic circulation. Insulin is secreted at an equimolar ratio with C-peptide, a peptide cleaved from proinsulin to produce insulin in the pancreatic β-cells, which is not extracted in

the liver. Thus, the pre-hepatic insulin concentration can be assessed by simultaneous measurements of circulating insulin and C-peptide concentrations.

1.7 Mathematical modeling with C-peptide used to assess hepatic and peripheral insulin clearance

The clinical indices of insulin clearance were proposed such as the metabolic clearance rate (MCR) [16] calculated by the insulin infusion rate and circulating insulin concentration, and the index calculated as the ratio of plasma insulin against C-peptide concentration [42]. However, the clinical indices of insulin secretion and clearance are indirect indices of insulin secretion and clearance ability, respectively, because the indices are obtained from the time courses of circulating insulin and C-peptide concentrations which are simultaneously affected by their secretion and clearance, and therefore the clinical index of insulin secretion implicitly involves the effect of insulin clearance, and *vice versa*. To directly assess insulin secretion and clearance abilities, the mathematical models have been developed for specifically quantifying these abilities from time courses of plasma measurement by accounting for the mutual dependence [32,38,43]. The models for individual assessment of hepatic and peripheral insulin clearance by using observed circulating C-peptide concentration were also proposed [34,44-51]. However, the relationship between hepatic and peripheral insulin clearance and the progression of glucose tolerance and the roles of both types of clearance in the control of dynamics of circulating of insulin concentration are still unknown.

1.8 Mathematical modeling with C-peptide for consecutive hyperglycemic and

hyperinsulinemic-euglycemic clamp

The models developed in Chapter 2 could not distinguish the hepatic and peripheral insulin clearance, because C-peptide was not incorporated in these models [52]. In Chapter 3, I developed new mathematical models based on the time courses of serum insulin and C-peptide concentrations during the consecutive hyperglycemic and hyperinsulinemic-euglycemic clamp analysis, and estimated hepatic and peripheral insulin clearance for each subject with variety of glucose tolerance including NGT, borderline type, and T2DM. The model analysis revealed the significant decrease in peripheral and increase in hepatic insulin clearance with the progression of glucose intolerance. The distinct roles of hepatic and peripheral insulin clearance in abnormality in the dynamics of circulating insulin concentration during the progression of glucose intolerance were also found; increase of hepatic insulin clearance reduced the amplitude and decrease of peripheral insulin clearance changed temporal patterns from transient to sustained manner of circulating insulin concentration.

2. A homeostatic law between insulin clearance and the progression of glucose intolerance in humans

2.1 Introduction

Glucose concentration in human plasma is tightly maintained within a narrow range [1], known as glucose homeostasis. Type 2 diabetes mellitus, a global health problem with more than 382 million afflicted worldwide, is characterized by the failure of such homeostasis [4]. Although a number of humoral, nutritional and neural factors contribute to the control of circulating glucose concentration, a negative feedback loop linking circulating insulin and glucose is essential to the understanding of this homeostasis control [1].

This negative feedback loop, in which the increase in circulating glucose concentration stimulates insulin secretion and the increase in circulating insulin concentration lowers circulating glucose concentration, has been dissected and analyzed by two major aspects; the ability for insulin secretion and the sensitivity of target tissues to insulin. A number of clinical indices that reflect these two aspects have thus been proposed, and shown to be useful to analyze the physiology of glucose homeostasis and the pathology of glucose intolerance [53]. Given that these clinical indices are usually determined by observed circulating glucose and insulin concentrations at specific conditions, such as glucose and insulin concentrations at fasting or after glucose challenges [54], it is unclear that such indices reflect entire aspects of insulin secretion and insulin sensitivity, however.

Application of a mathematical model is one way to overcome the limitation of the actual measurement of clinical parameters. The early models of the glucose-insulin feedback, which

have been validated by means of the intravenous glucose tolerance test (IVGTT), were reported by Bolie et al. [55] and the Ackerman's research group [56,57]. The most famous model which still widely used in clinical assessments, such as the estimate of the insulin sensitivity index, is known as the minimal model proposed by Bergman et al. [58]. It was conceived from the analysis of the minimal model that glucose tolerance of an individual is related to the product of insulin secretion and sensitivity, referred as the disposition index (DI), i.e., DI = insulin secretion × insulin sensitivity [23]. Many other kinds of models for IVGTT was reported [45,48,59-65] including the models with delay differential equations.

The oral perturbations of circulating glucose and insulin are more physiological than the intravenous ones. The insulin secretion and sensitivity were also assessed by means of models during the oral glucose tolerance test (OGTT) [30,32,66,67]. The parameters showed that insulin sensitivity significantly decreased from NGT to borderline type subjects, while no difference was found insulin secretion [32]. However, the analysis of the OGTT and IVGTT data by a mathematical model is affected by the mutual influence between the time course of circulating glucose and insulin concentrations through the negative feedback loop.

One of the ideal methods for investigating biological phenomena regulated by a feedback loop is to utilize time series data obtained with excluding the feedback relations by clamping one of the components. The patch-clamp method is such a mathematical model analysis of time series data during the voltage-clamp [68]. This analysis in cell biology has uncovered mechanistic insights into excitable system of action potential, which cannot be directly found from experimental data alone. In this study, to further understand the regulatory mechanism of

glucose homeostasis, I took a similar strategy; I mathematically analyzed time series data of the consecutive hyperglycemic and hyperinsulinemic-euglycemic clamp.

In hyperglycemic clamp, circulating glucose concentration is maintained at high concentration by external infusion feedback control in order to circumvent the effect of insulin to change circulating glucose concentration, and the insulin secretion is directly measured as the area under the curve of time course of circulating insulin concentration within 10 min [16,17]. In hyperinsulinemic-euglycemic clamp, insulin infusion is sustainably treated under circulating glucose control at normal concentration, and insulin sensitivity is directly measured as the glucose infusion amount during last 30 min of the clamp test [16,17]. Similar to the DI by IVGTT, Okuno et al. defined the index, a clamp DI, which is a product of insulin sensitivity and secretion measured from the consecutive hyperglycemic and hyperinsulinemic-euglycemic clamps [17]. Using the consecutive clamp analysis, they have shown the inverse correlation between the clamp DI and plasma glucose at 2h during OGTT (2-h PG), which represents the capacity of glucose tolerance, in subjects with normal glucose tolerance (NGT), borderline type, and type 2 diabetes mellitus (T2DM), indicating that the clamp DI is useful measure of the progression of glucose intolerance.

I generated a mathematical model of glucose-insulin regulatory system and determined the parameters of the model using the data of the consecutive clamp analysis for each subject with variety of glucose tolerance including NGT, borderline type, and T2DM. This analysis revealed that the absorption and the degradation of serum insulin, denoted as insulin clearance, strongly constrain a product of insulin secretion and insulin sensitivity as well as

the progression of glucose intolerance. This study uncovered an unrecognized law by a mathematical analysis, and thus shed light on a novel insight into glucose homeostasis and the pathogenesis of diabetes mellitus.

2.2 Materials and Methods

2.2.1 Subjects and measurements

Study subjects were recruited as described previously [17] at Kobe University Hospital from October 2008 to June 2014. This metabolic analysis was approved by the ethics committee of Kobe University Hospital and was registered with the University hospital Medical Information Network (UMIN000002359), and written informed consent was obtained from all subjects. The consecutive hyperglycemic and hyperinsulinemic-euglycemic clamp analyses as well as a standard 75-g OGTT were performed within a period of 10 days for 50 NGT, 18 borderline type, and 53 T2DM subjects (121 in total) as described previously [17]. In brief, before the onset of the consecutive clamp analyses, fasting plasma glucose and serum insulin concentrations were measured as the data for time zero. From 0 to 90 min, a hyperglycemic clamp was applied by intravenous infusion of a bolus of glucose (9622 mg/m^2) within 15 min followed by that of a variable amount of glucose to maintain the plasma glucose level at 200 mg/dL. Ten minutes after the end of the hyperglycemic clamp, a 120-min hyperinsulinemic-euglycemic clamp was initiated by intravenous infusion of human regular insulin (Humulin R, Eli Lilly Japan K.K.) at a rate of 40 mU m^{-2} min^{-1} and with a target plasma glucose level of 90 mg/dL. For the NGT and borderline type subjects whose plasma glucose levels were <90 mg/dL, the plasma glucose concentration was clamped at the fasting level. The plasma glucose level was measured every 1 min during the clamp analyses and the 5-min average values were obtained. The insulin level was also measured in serum samples collected at 5, 10, 15, 60, 75, 90, 100, 190, and 220 min after the onset of the tests.

First-phase insulin secretion during the hyperglycemic clamp was defined as the incremental area under the immunoreactive insulin (IRI) concentration curve (μU mL^{-1} min^{-1}) from 0 to 10 min (AUC_{IRI10}). The insulin sensitivity index (ISI) derived from the hyperinsulinemic-euglycemic clamp was calculated as the mean glucose infusion rate during the final 30 min (i.e. from 190 to 220 min) of the clamp (mg kg^{-1} min^{-1}) divided by both the plasma glucose (mg/dL) and serum insulin (μU/mL) levels at the end of the clamp and then multiplying the result by 100. A clamp-based analogue of the disposition index, the clamp disposition index (clamp DI), was calculated as the product of AUC_{IRI10} and ISI, as described previously [17]. The metabolic clearance rate (MCR) [16], an index of insulin clearance, was calculated as the insulin infusion rate at the steady state (1.46 mU kg^{-1} min^{-1}) divided by the increase in insulin concentration above the basal level in the hyperinsulinemic-euglycemic clamp [17]: 1.46 (mU kg^{-1} min^{-1}) × body weight (kg) × body surface area (m^2)/(end IRI – fasting IRI) (μU/mL), where body surface area is defined as (body weight (kg))$^{1/2}$ × (body height (cm))$^{1/2}$ / 60 (Mosteller formula). Since this study is retrospective analysis of previously collected data, randomization and blinding of the groups with NGT, borderline type, and T2DM were not performed. The actual data for all 121 subjects are shown in Ohashi et al. [52] (Supplementary Table S6)

2.2.2 Mathematical models

I developed mathematical models for the feedback loop between circulating glucose and insulin (Fig. 3 and 4). These models have four variables: *G* and *I* (dimensionless) are plasma

glucose and insulin concentrations, respectively, normalized by dividing them by the respective maximum value among each time course of concentration of each subject (see Section 2.2.3 Parameter estimation below). *Y* (dimensionless) is the effective glucose concentration on insulin secretion, and *X* (dimensionless) is the secreted insulin from pancreatic β-cells.

The actual glucose infusion rate (*GIR* [mg kg^{-1} min^{-1}]) and insulin infusion rate (*IIR* [mU kg^{-1} min^{-1}]) were converted to the corresponding blood concentrations (*cGIR* and *cIIR*, respectively) as follows:

$$cGIR\ (\text{mg dL}^{-1}\ \text{min}^{-1}) = \frac{GIR\ (\text{mg kg}^{-1}\ \text{min}^{-1}) \cdot BW}{BW \cdot BV} \cdot 100 \quad (1)$$

$$cIIR\ (\mu\text{U mL}^{-1}\ \text{min}^{-1}) = \frac{IIR\ (\text{mU kg}^{-1}\ \text{min}^{-1}) \cdot BW}{BW \cdot BV} \cdot 1000 \quad (2)$$

where *BW* and *BV* denote body weight and blood volume (75 and 65 mL/kg for men and women, respectively [69]), respectively.

In these models, glucose and insulin infusions are represented by $influx_G$ and $influx_I$, respectively. These fluxes follow the nonlinear functions f_1 and f_2 that reproduce glucose and insulin infusion concentrations, respectively. Given that the infusion protocol differed between hyperglycemic (from 0 to 90 min) and hyperinsulinemic-euglycemic (from 100 to 220 min) clamps, the functions of the infusion rates f_1 and f_2 and are given by the following equations:

$$f_1(t) = \begin{cases} gc_1 \cdot \exp(gc_2 \cdot t) + gc_3 & (t \le 90) \\ 0 & (90 < t \le 100) \\ gi_1 \cdot \dfrac{\left((t-100)/gi_3\right)^{gi_2}}{1+\left((t-100)/gi_3\right)^{gi_2}} & (100 < t) \end{cases} \quad (3)$$

$$f_2(t) = \begin{cases} 0 & (t \le 100) \\ ii_1 \cdot \exp\left(ii_2 \cdot (t-100)\right) + ii_3 & (100 < t) \end{cases} \quad (4)$$

where the parameters gc_j, gi_j, and ii_j (j = 1, 2, 3) are estimated to reproduce *cGIR* and *cIIR* with functions f_1 and f_2, respectively, for each subject by use of a nonlinear least squares technique [70].

I considered four alternatives of the model structure (*Model A* to *D* in Fig. 4) of infusion of glucose and insulin in order to choose the best model for reproducing the measurements of plasma glucose and serum insulin during the consecutive hyperglycemic and hyperinsulinemic-euglycemic clamp analysis. These models shared the structure of the fluxes between variables, but differed in the structure of infusion of glucose and insulin: $influx_G$ into G or Y, and $influx_I$ into I or X.

2.2.3 Parameter estimation

Nine model parameters for the rate constants (k_1 to k_7) (min^{-1}) and the initial concentrations (Y_b and X_b) (dimensionless) were estimated for each subject to reproduce the normalized time course of plasma glucose G and serum insulin I by a meta-evolutionary programming method to approach the neighborhood of the local minimum, followed by application of the nonlinear least squares technique to reach the local minimum [71]. The four parameters (Y_b, X_b, k_3, and k_7) were calculated as the solution of the four differential equations of the model at a steady state with initial concentrations, and the remaining five parameters are free parameters in the estimation. Each parameter was estimated in the range from 10^{-6} to 10^4. For these methods, the parameters were estimated to minimize the objective function

value, which is defined as residual sum of the square (RSS) between the actual measurements by clamp analyses and the model simulation. RSS is given by:

$$RSS = \frac{n_I}{n_G + n_I} \sum_{n_G} \left[G(t) - G_{sim}(t) \right]^2 + \frac{n_G}{n_G + n_I} \sum_{n_I} \left[I(t) - I_{sim}(t) \right]^2 \quad (5)$$

where n_G and n_I are the total numbers of time points of measuring plasma glucose and serum insulin, respectively, for the hyperglycemic and hyperinsulinemic-euglycemic clamps. $G(t)$ is the normalized and time-averaged plasma glucose concentration within the time range $(t - 5)$ min to t min with every 1-min interval, and $I(t)$ is the normalized serum insulin concentration at t min. $G_{sim}(t)$ and $I_{sim}(t)$ are simulated plasma glucose and serum insulin concentrations, calculated in the same way as $G(t)$ and $I(t)$, respectively. The numbers of parents and generations in the meta-evolutionary programming were 400 and 4000, respectively. Parameter estimation was tried 20 times by changing the initial parameter values for each subject, and the parameter with the smallest *RSS* among 20 trials was taken as the estimated solution of each subject. The estimated parameters for all subjects are shown in Ohashi et al. [52] (Supplementary Table S7).

2.2.4 Determination of parameter outliers

The outliers of model parameters were detected by the adjusted outlyingness (AO) [72]. The cutoff value of AO was $Q_3 + 1.5e^{3MC} \cdot IQR$, where Q_3, *MC*, and *IQR* are the third quartile, medcouple, and interquartile range, respectively. The medcouple is a robust measure of skewness [73]. The number of directions was set at 7000. Subjects found to have outlier

parameters (three NGT, two borderline type and three T2DM subjects) were excluded from further study.

2.2.5 Parameter sensitivity analysis

I defined the individual model parameter sensitivity [74] for each subject as follows:

$$S(f(x),x)=\frac{\partial \log f(x)}{\partial \log x}=\frac{x}{f(x)}\cdot\frac{\partial f(x)}{\partial x} \quad (6)$$

where x is the parameter value and $f(x)$ is ISI or AUC_{IRI10}. The differentiation is numerically approximated by central difference $\frac{\partial f(x)}{\partial x}\approx\frac{f(x+\Delta x)-f(x-\Delta x)}{2\Delta x}$, and $x + \Delta x$ and $x - \Delta x$ were set so as to be increased [x (1.1x)] or decreased [x (0.9x)] by 10%, respectively. Finally, I defined the parameter sensitivity by the median of the individual parameter sensitivity for all subjects.

I examined the parameter sensitivity for 70 parameters consisting of all rate constants, the products of each pair of rate constants, and the quotients of each two rate constants. For the products of each two rate constants, $x = k_i \cdot k_j$, I configured the 10% increased x and 10% decreased x by $1.1x=\sqrt{1.1}k_i\cdot\sqrt{1.1}k_j$ and $0.9x=\sqrt{0.9}k_i\cdot\sqrt{0.9}k_j$, respectively, and I adopted a similar approach for the quotients of each two parameters. The higher the absolute value of parameter sensitivity, the larger the effect of the parameter on ISI or AUC_{IRI10}.

2.2.6 Fitting by power function

I hypothesized that a power function accounted for the relation between two correlated model parameters or clinical indices. I used the function $f(x) = a \cdot x^b$, where x is the model

parameter on the horizontal axis in Fig. 10 and 13A. The parameters *a* and *b* were estimated to minimize the RSS given by:

$$RSS = \sum_{\text{subjects}} \left(y - f(x)\right)^2 \tag{7}$$

where *y* is the model parameter or clinical index on the vertical axis in Fig. 10 and 13A, with the use of a nonlinear least squares technique.

2.2.7 Calculation of clinical indices

HOMA-β [12]:

$$\frac{360 \times \text{F-IRI (uU/mL)}}{\text{FPG (mg/dL)} - 63} \tag{8}$$

where F-IRI and FPG are the fasting serum immunoreactive insulin and plasma glucose, respectively.

HOMA-IR [12]:

$$\frac{\text{F-IRI (uU/mL)} \times \text{FPG (mg/dL)}}{405} \tag{9}$$

Insulinogenic index (I. I.) [13]:

Ratio of the increment of serum IRI to that of plasma glucose at 30 min after the onset of the OGTT:

$$\frac{\text{IRI}(0) - \text{IRI}(30)\,(\text{uU/mL})}{\text{PG}(0) - \text{PG}(30)\,(\text{mg/dL})} \tag{10}$$

where IRI(*t*) and PG(*t*) are the serum immunoreactive insulin and plasma glucose at *t* min, respectively.

$AUC_{IRI10–90}$ [17]:

Incremental area under the serum insulin concentration curve (μU/mL) from 10 to 90 min during the hyperglycemic clamp

$AUC_{IRI120/PG120}$:

Ratio of the area under the insulin concentration curve from 0 to 120 min to that for plasma glucose from 0 to 120 min, without using the data measured at 90 min, in the OGTT:

$$\frac{AUC_{IRI0\text{-}120}\ (uU/mL)}{AUC_{PG0\text{-}120}\ (mg/dL)} \tag{11}$$

Matsuda index [14]:

$$\frac{10000}{\sqrt{FPG\ (mg/dL) \times F\text{-}IRI\ (uU/mL) \times \overline{G} \times \overline{I}}} \tag{12}$$

where $\overline{G}$ and $\overline{I}$ are the mean PG and serum IRI concentrations during the OGTT, respectively.

Oral DI [26,75]:

$$AUC_{IRI120/PG120} \times \text{Matsuda index} \tag{13}$$

2.2.8 Statistical analysis

Unless indicated otherwise, data are expressed as the median with first and third quartiles. Medians of clinical indices and parameter values were compared among NGT, borderline type, and T2DM subjects with the use of the two-sided Wilcoxon rank sum test with Benjamini Hochberg FDR multiple testing correction [76]. An FDR-corrected *P* value <0.05 was considered statistically significant.

2.3 Results

2.3.1 Plasma glucose and serum insulin concentration during consecutive hyperglycemic and hyperinsulinemic-euglycemic clamp

At first, I calculated the mean time courses of measured concentrations of plasma glucose and serum insulin during the consecutive hyperglycemic and hyperinsulinemic-euglycemic clamp analysis of NGT (n = 50), borderline type (n = 18), and T2DM (n = 53) subjects (Fig. 2) [17].

During the hyperglycemic clamp at 0-90 min, plasma glucose concentration of each subject at the hyperglycemic plateau was almost similar among the groups with NGT, borderline type, and T2DM. Serum insulin concentration was higher in the NGT and borderline type subjects than that in the T2DM subjects, meaning that insulin secretion was significantly reduced in the T2DM subjects. The rate of glucose infusion differed significantly among the NGT, borderline type, and T2DM subjects. The mean rate of glucose infusion of the NGT was highest, and that of the T2DM subject was lowest, reflecting the decrease in the ability to remove infused glucose from plasma from NGT to borderline type to T2DM, in other words, the decrease of glucose tolerance.

During the hyperinsulinemic-euglycemic clamp at 100-220 min, serum insulin concentration was at a steady-state plateau of hyperinsulinemia, but serum insulin concentration differed significantly among the three groups. The mean serum insulin concentration of the NGT was lowest, and that of the borderline type subjects was highest, reflecting the difference in the ability to remove infused insulin from serum among the three

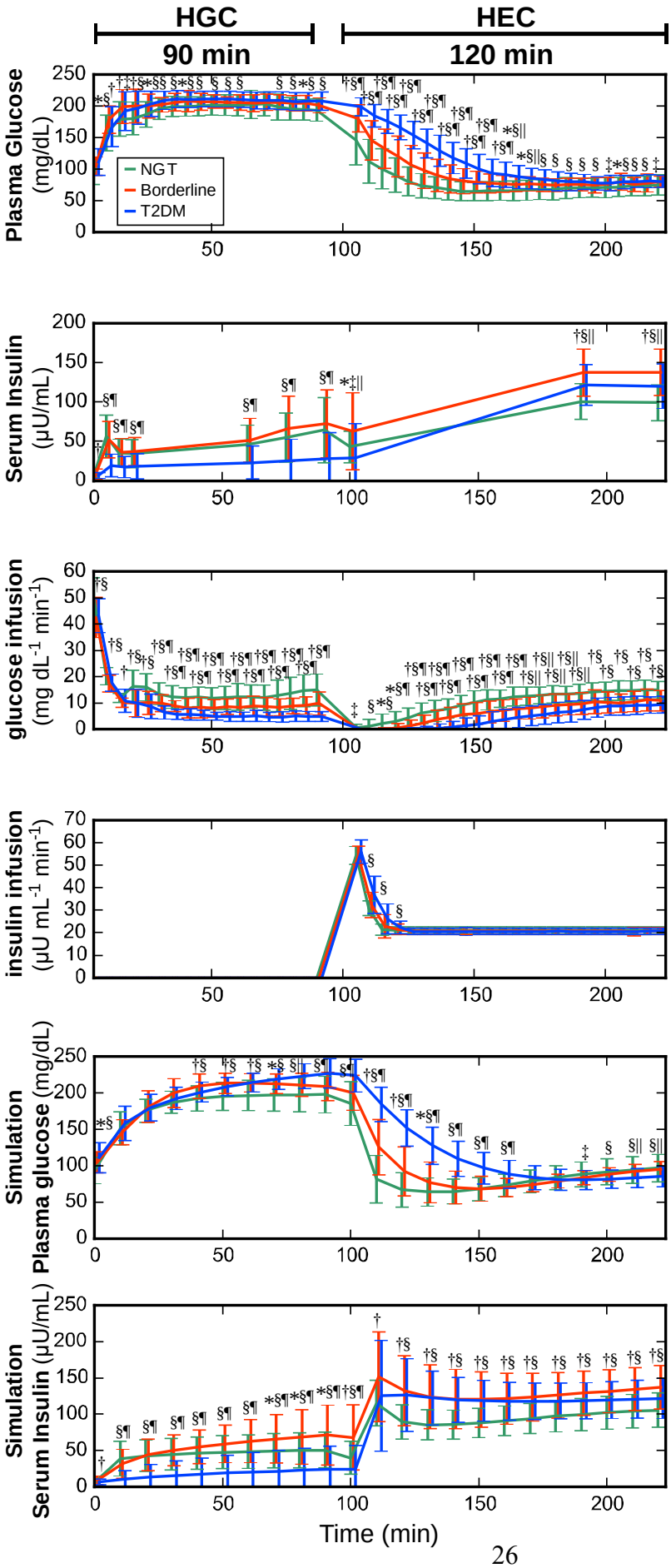
HGC
90 min
HEC
120 min
Plasma Glucose (mg/dL)
NGT
Borderline
T2DM
Serum Insulin (μU/mL)
glucose infusion (mg dL-1 min-1)
insulin infusion (μU mL-1 min-1)
Simulation Plasma glucose (mg/dL)
Simulation Serum Insulin (μU/mL)
Time (min)

Figure 2. Time courses of concentrations of plasma glucose, serum insulin, and glucose and insulin infusion during the consecutive hyperglycemic (HGC) and hyperinsulinemic-euglycemic (HEC) clamp. Experimental (upper 4 panels) and simulation with the model (lower 2 panels) time courses are shown. Simulation time courses are plotted every 10 min. The mean ± SD among the subjects for NGT (green), borderline type (red), and T2DM, and significant differences at each time point are depicted. *$P < 0.05$; †$P < 0.01$, NGT vs. borderline type; ‡$P < 0.05$; §$P < 0.01$, NGT vs. T2DM; ‖$P < 0.05$; ¶$P < 0.01$, borderline type vs. T2DM (two-sample *t*-test with FDR correction).

The actual data for all 121 subjects are provided in Ohashi et al. [52] (Supplementary Table S6).

groups, in other words, the difference of insulin clearance. The plasma glucose concentration returned from hyperglycemia to euglycemic level with different decay rate among the three groups. The mean decay rate was lowest in the T2DM subjects and highest in the NGT subjects, reflecting the decrease in the ability to promote the hypoglycemic effect in response to serum insulin, named insulin sensitivity, from NGT to borderline type to T2DM. The rate of glucose infusion differed significantly among the NGT, borderline type, and T2DM subjects, following the hyperglycemic clamp. The mean rate of glucose infusion of the NGT was highest, and that of the T2DM subject was lowest, reflecting the decrease in the ability to remove infused glucose from plasma in response to serum insulin, corresponding to insulin sensitivity, from NGT to borderline type to T2DM.

2.3.2 Mathematical model for the feedback loop between glucose and insulin

I developed a mathematical model based on the time course of the plasma glucose and serum insulin during the consecutive hyperglycemic and hyperinsulinemic-euglycemic clamps (Fig. 3). In this model, the variables G and I correspond to normalized concentrations of plasma glucose and serum insulin (see Method), respectively. The variable Y is the effective glucose concentration on insulin secretion affected by G. The variable X is the secreted insulin from pancreatic β-cells. The model structure that G regulates I through Y and X, and I directly regulates G, represents the feedback loop. The differential equations of the model are as follows:

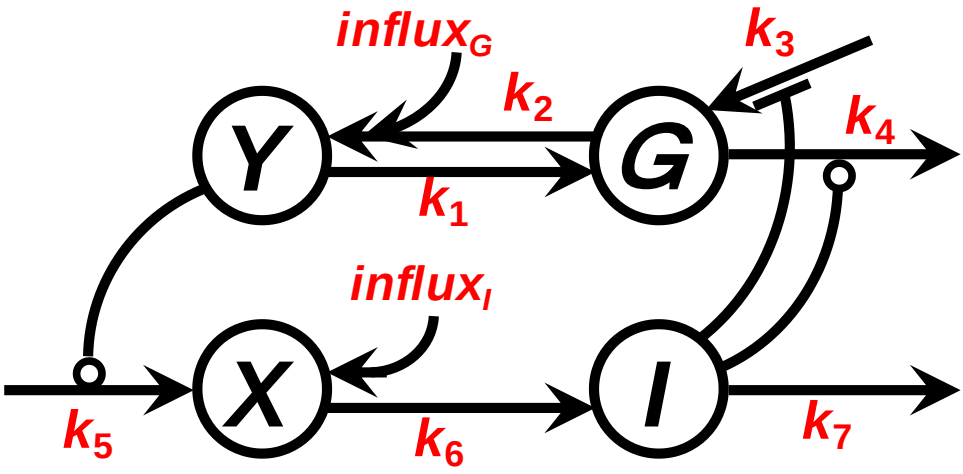

Figure 3. The model structures of the feedback loop between circulating glucose and insulin. G and I are normalized plasma glucose and serum insulin concentration, respectively. Y is the effective glucose concentration on insulin secretion, and X is the secreted insulin from pancreatic β-cells. Arrows indicate fluxes with corresponding parameters (red).

The differential equations of this model are following:

$$\frac{dG}{dt} = v_1 - v_2 + v_3 - v_4 = k_1 \cdot Y - k_2 \cdot G + \frac{k_3}{1+I} - k_4 \cdot G \cdot I, \quad G(0) = G_b \tag{14}$$

$$\frac{dI}{dt} = v_6 - v_7 = k_6 \cdot X - k_7 \cdot I, \quad I(0) = I_b \tag{15}$$

$$\frac{dY}{dt} = -v_1 + v_2 + influx_G = -k_1 \cdot Y + k_2 \cdot G + f_1(t), \quad Y(0) = Y_b \tag{16}$$

$$\frac{dX}{dt} = v_5 - v_6 + influx_I = k_5 \cdot Y - k_6 \cdot X + f_2(t), \quad X(0) = X_b \tag{17}$$

$$\frac{dG}{dt} = v_1 - v_2 + v_3 - v_4 = k_1 \cdot Y - k_2 \cdot G + \frac{k_3}{1+I} - k_4 \cdot G \cdot I, \quad G(0) = G_b \tag{14}$$

$$\frac{dI}{dt} = v_6 - v_7 = k_6 \cdot X - k_7 \cdot I, \quad I(0) = I_b \tag{15}$$

$$\frac{dY}{dt} = -v_1 + v_2 + influx_G = -k_1 \cdot Y + k_2 \cdot G + f_1(t), \quad Y(0) = Y_b \tag{16}$$

$$\frac{dX}{dt} = v_5 - v_6 + influx_I = k_5 \cdot Y - k_6 \cdot X + f_2(t), \quad X(0) = X_b \tag{17}$$

where G_b and I_b correspond to normalized fasting (basal) plasma glucose and insulin concentration, respectively, and Y_b and X_b are initial values of Y and X to be estimated.

Eq. 14 describes how plasma glucose concentration G increases according to the systemic circulation of glucose from the pancreas, v_1, and glucose production by target organs of insulin, v_3, and decreases according to circulation of glucose to the pancreas, v_2, and glucose uptake by target organs of insulin, v_4. v_3 is expanded as $k_3 / (1 + I)$, which corresponds to glucose production inhibited by I, and v_4 is expanded as $k_4 \cdot G \cdot I$, which corresponds to glucose uptake facilitated by both glucose and insulin. The parameters k_3 and k_4 are the rate constants for glucose production and uptake, respectively. The parameters k_1 and k_2 are the rate constants for flux from effective glucose for insulin secretion to plasma glucose, and vice versa, respectively.

Eq. 15 describes how serum insulin concentration I increases according to the systemic circulation of insulin from the pancreas to target organs, v_6, and decreases according to the insulin clearance, v_7. The parameter k_6 is the rate constant for flux from secreted insulin to serum insulin, and k_7 is the degradation rate constant of serum insulin and corresponds to insulin clearance.

Eq. 16 describes how the effective glucose for insulin secretion Y increases according to

the circulation of glucose to the pancreas, v_2, and infused glucose, $influx_G$, and decreases according to the circulation of glucose from the pancreas, v_1. $influx_G$ is the glucose infusion rate during hyperglycemic and hyperinsulinemic-euglycemic clamp. The infusion rate at time t is represented by the function $f_1(t)$ (Methods).

Eq. 17 describes how the secreted insulin from pancreatic β-cells X increases according to the insulin secretion, v_5, and infused insulin, $influx_I$, and decreases according to the systemic circulation of insulin from the pancreas to target organs, v_6, v_5 is expanded as $k_5 \cdot Y$, which corresponds to the insulin secretion in response to the effective glucose concentration, and the parameter k_5 is the rate constant of insulin secretion. $influx_I$ is the insulin infusion rate during hyperinsulinemic-euglycemic clamp. The infusion rate at time t is represented by the function $f_2(t)$ (Methods).

2.3.3 Parameter estimation and model selection for glucose and insulin infusion

Since there was no reported model which had both glucose and insulin infusion in the consecutive hyperglycemic and hyperinsulinemic-euglycemic clamp analysis, I selected the model structure of infusion of glucose and insulin. I considered four alternatives (*Model A* to *D* in Fig. 4) for different kinds of infusion patterns: $influx_G$ into G or Y, and $influx_I$ into I or X. For each of the 121 subjects, parameters of the four models were estimated by using normalized actual measurements of plasma glucose and serum insulin concentration of clamp analysis (Methods). The examples of simulation with the estimated parameters of *Model A* in Fig. 4 in each of NGT, borderline type, and T2DM subjects are shown in Fig. 5, and the

Model structure	Model equation	RSS mean ± SD
Model A 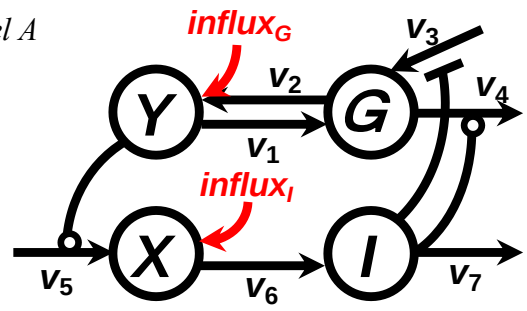	$\begin{cases} \frac{dG}{dt} = v_1 - v_2 + v_3 - v_4 \\ \frac{dI}{dt} = v_6 - v_7 \\ \frac{dY}{dt} = -v_1 + v_2 + influx_G \\ \frac{dX}{dt} = v_5 - v_6 + influx_I \end{cases}$	0.1395 ± 0.1037
Model B 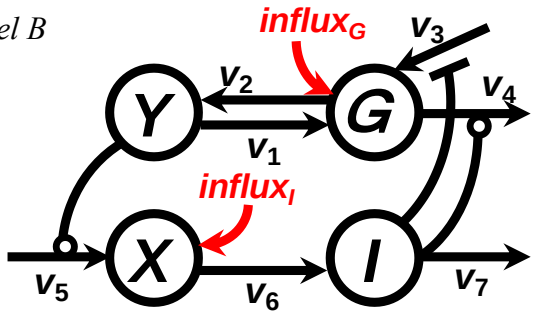	$\begin{cases} \frac{dG}{dt} = v_1 - v_2 + v_3 - v_4 + influx_G \\ \frac{dI}{dt} = v_6 - v_7 \\ \frac{dY}{dt} = -v_1 + v_2 \\ \frac{dX}{dt} = v_5 - v_6 + influx_I \end{cases}$	0.5132± 0.5784
Model C 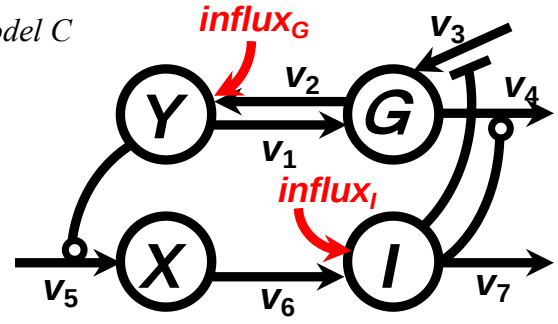	$\begin{cases} \frac{dG}{dt} = v_1 - v_2 + v_3 - v_4 \\ \frac{dI}{dt} = v_6 - v_7 + influx_I \\ \frac{dY}{dt} = -v_1 + v_2 + influx_G \\ \frac{dX}{dt} = v_5 - v_6 \end{cases}$	0.1457 ± 0.1003
Model D 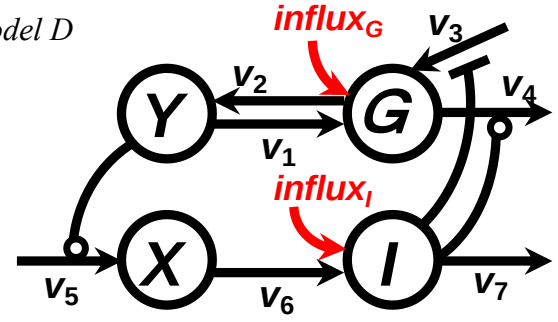	$\begin{cases} \frac{dG}{dt} = v_1 - v_2 + v_3 - v_4 + influx_G \\ \frac{dI}{dt} = v_6 - v_7 + influx_I \\ \frac{dY}{dt} = -v_1 + v_2 \\ \frac{dX}{dt} = v_5 - v_6 \end{cases}$	0.5159 ± 0.5764

Figure 4. Four model alternatives for glucose and insulin infusion.

Model structures differ according to which variables were increased by $influx_G$ and $influx_I$.

Each model was fitted for the actual measurements of clamp analyses of each subject, and

individual RSS between the actual time course and the model trajectories were calculated.

Left panel: The structure of models. G is normalized plasma glucose concentration, I is normalized serum insulin concentration, Y is the effective glucose concentration on insulin secretion, and X is the concentration of secreted insulin.

Middle panel: The differential equations of each model. The fluxes v_1 to v_7 are shown in Results.

Right panel: Means ± SD of RSS among all 121 subjects for each model. The significant differences of RSS between the four models are shown in Table 1.

Table 1. Significant differences of RSS between models

Model pair	*P*
Model A vs. *B*	5.46×10^{-13}
Model A vs. *C*	2.15×10^{-8}
Model A vs. *D*	3.43×10^{-13}
Model B vs. *C*	1.54×10^{-12}
Model B vs. *D*	6.28×10^{-5}
Model C vs. *D*	9.69×10^{-13}

P values were determined by paired *t*-test, and the value of $<8.33\times10^{-3}$ (=0.05/6, corrected by the number of tests, divided by 6) is considered statistically significant.

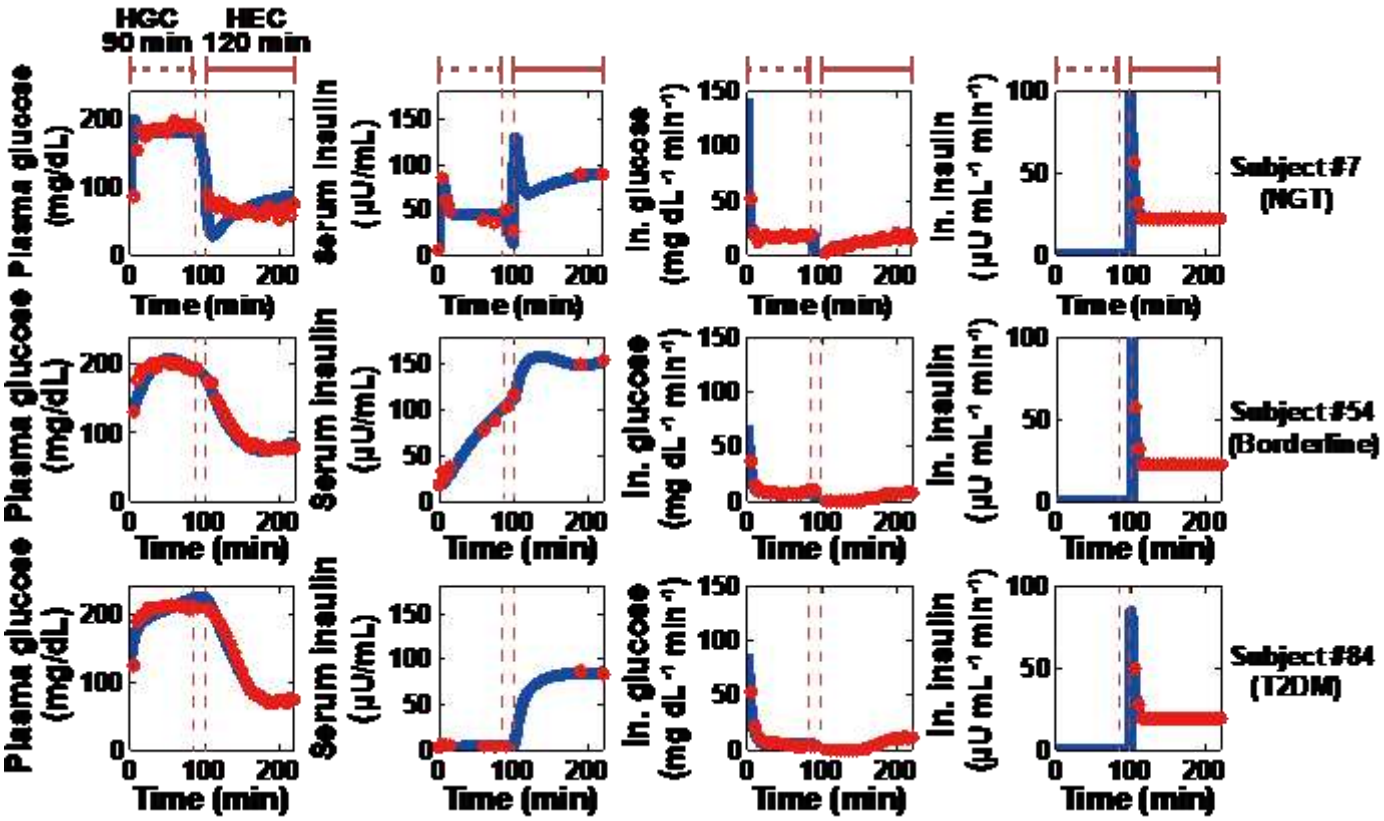

Figure 5. Time courses of plasma glucose, serum insulin, infused (In.) glucose, and infused insulin for typical NGT, borderline type, and T2DM subjects. Red circles and blue curves are actual measurement during the clamp analysis and simulation with the *Model A*, respectively. The simulated values of plasma glucose and serum insulin were rescaled to absolute concentrations from the normalized values.

simulations for all subjects are provided in Ohashi et al. [52] (Supplementary Fig. S1).

Since mean of RSS calculated for all subjects was the lowest in *Model A* and RSS differed significantly between the four models (Table 1), I performed analyses using *Model A* for further study (Fig. 3). The simulation with the model (Fig. 2) reproduced measured concentrations of glucose and insulin, and reflected significant differences among the NGT, borderline type, and T2DM subjects.

Eight subjects (three NGT, two borderline type, and three T2DM subjects) were excluded because their estimated model parameters were detected as outliers based on the adjusted outlyingness (Methods), and I analyzed the model for the remaining 113 subjects (47 NGT, 16 borderline type, and 50 T2DM) (Table 2).

To confirm that the simulation appropriately reflects characteristics of the subjects, I evaluated the consistency between the clinical indices calculated from the actual measurements and those calculated from the simulation with the model (Fig. 6). ISI calculated from the simulated concentrations of plasma glucose and serum insulin and infused glucose was greater for the NGT subjects than for the borderline type or T2DM subjects, whereas it did not differ significantly between the latter two groups of subjects. AUC_{IRI10} calculated in the simulation decreased significantly from NGT to borderline type to T2DM. These characteristics of ISI and AUC_{IRI10} in the simulation almost mimicked those calculated from the actual measurements (Fig. 6), but AUC_{IRI10} in the actual measurements did not differ significantly between the NGT and borderline type subjects. The disposition index (DI), originally defined as the product of indices for insulin secretion and insulin sensitivity

Table 2. Characteristics of the three groups of study subjects.

	NGT	Borderline	T2DM	Total
Number	47	16	50	113
Sex (male/female)	20/27	9/7	32/18	61/52
Age (years)	30.9 ± 8.74	42.9 ± 11.9	55.2 ± 14.1	43.2 ± 16.3
BMI (kg/m^2)	21.1 ± 3.43	26.7 ± 6.89	26.0 ± 4.93	24.1 ± 5.31
FPG (mg/dL)	85.6 ± 6.70	93.0 ± 14.6	110 ± 22.4	97.5 ± 20.0
2-h PG (mg/dL)	112 ± 17.3	167 ± 16.2	266 ± 74.2	187 ± 87.8
F-IRI (μU/mL)	5.65 ± 2.24	8.50 ± 5.56	6.80 ± 4.14	6.56 ± 3.82

Data are means ± SD. BMI, body mass index; FPG, fasting plasma glucose concentration; 2-h PG, 2-h plasma glucose level during the oral glucose tolerance test; F-IRI, fasting serum immunoreactive insulin concentration.

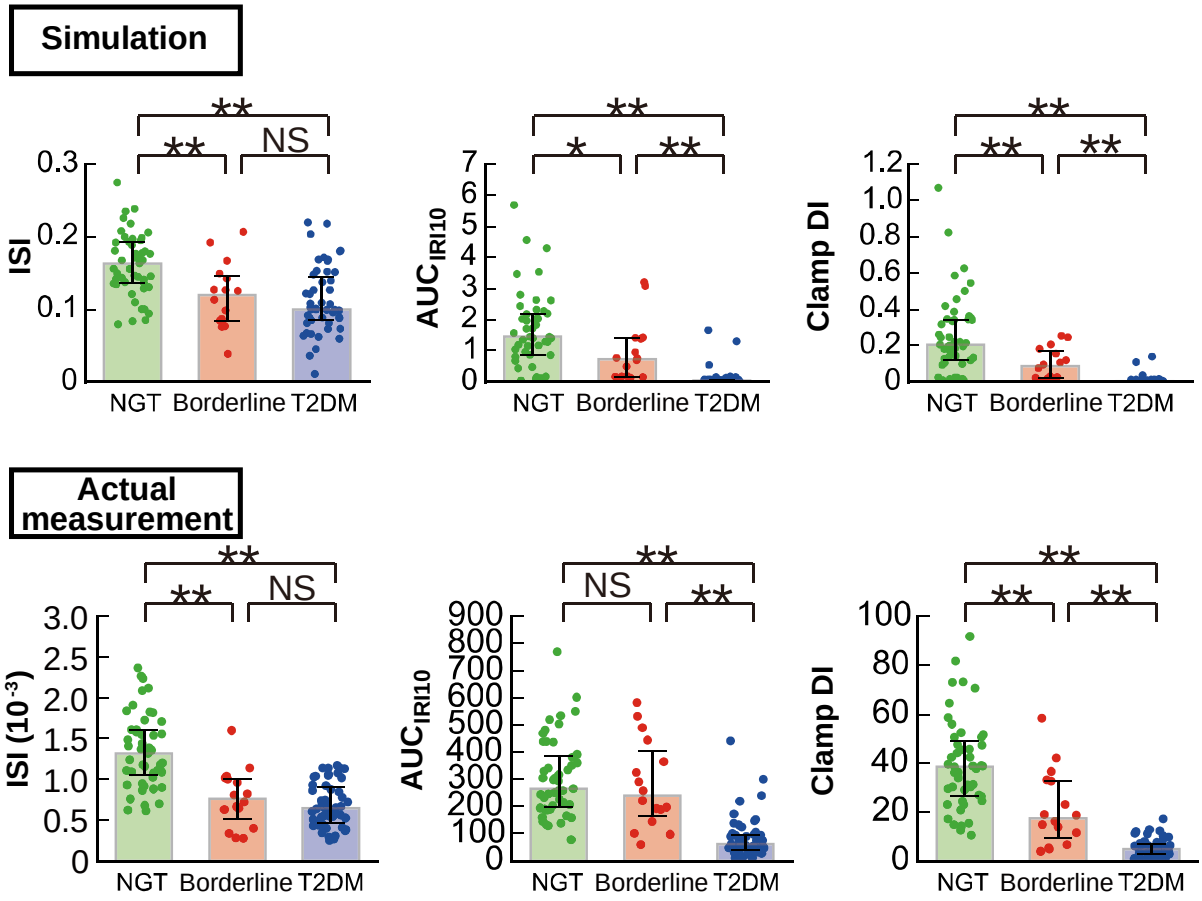

Figure 6. The insulin sensitivity index (ISI), insulin secretion as the incremental area under the curve of immunoreactive insulin concentration during the first 10 min (AUC_{IRI10}) of the hyperglycemic clamp, and the clamp disposition index (DI), which is given by the product of ISI and AUC_{IRI10}, both in the simulation and actual measurements. Note that the indices in the simulation are calculated by normalized time course, and are dimensionless value. *$P < 0.05$, **$P < 0.01$, NS: not significant by two-sided Wilcoxon rank sum test with FDR-correction.

determined by the minimal model [23], is thought to reflect the capacity for insulin secretion adjusted for insulin sensitivity and therefore to represent the integrated capacity for glucose tolerance. An analog of DI determined for clamp analysis (clamp DI) has been shown to possess clinical characteristics similar to those of the original DI [17]. The value of clamp DI in the simulation, the product of ISI and AUC_{IRI10} in the simulation, decreased significantly from NGT to borderline type to T2DM (Fig. 6). This characteristic was also similarly observed with clamp DI calculated from the actual measurements (Fig. 6). These results thus suggested that the simulation with the model retains well the essential characteristics of the capacity for glucose tolerance among the study subjects.

2.3.4 Relation between model parameters and the progression of glucose intolerance

I statistically compared the model parameters among the NGT, borderline type, and T2DM subjects (Fig. 7 and 8; Methods), the parameters Y_b and k_5 differed significantly between T2DM and each of the other two groups; k_3 and k_4 differed significantly between NGT and each of the other two groups; k_1, k_2 and k_7 differed significantly between each pair of all three groups.

The parameter Y_b is the initial value of effective glucose concentration for insulin secretion (Fig. 3). This parameter in the T2DM subjects was significantly higher than that in the NGT and borderline type subjects, consistent with observations that the fasting plasma glucose (FPG) concentration increases in T2DM patients [7].

The parameters k_3 and k_4 are the rate constants for glucose production and uptake,

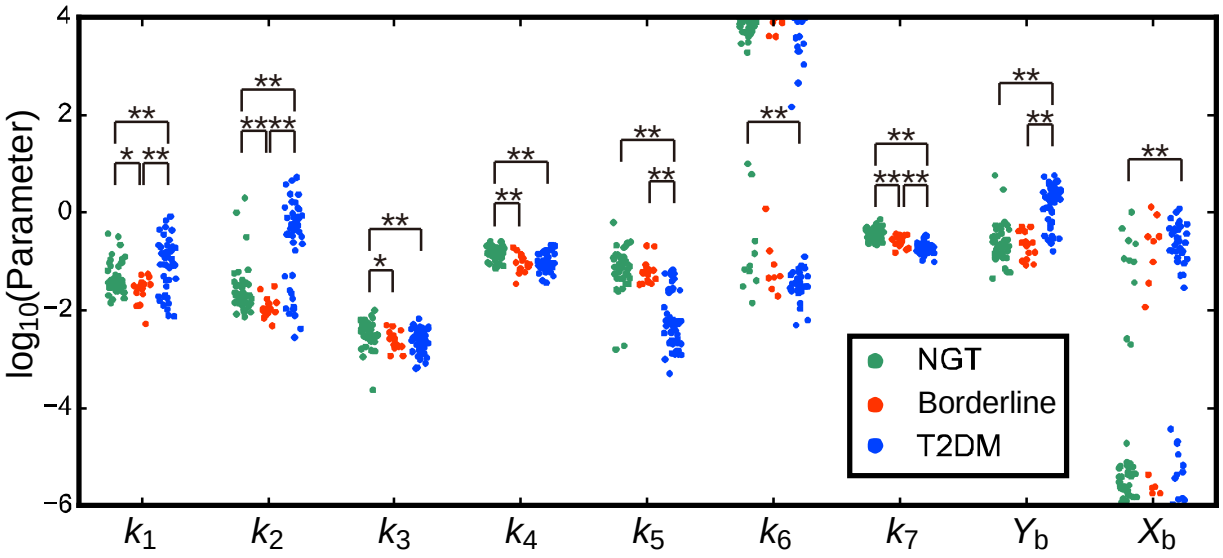

Figure 7. The estimated parameters for the NGT (green), borderline type (red), and T2DM (blue) subjects. Each dot corresponds to the indicated parameter for an individual subject. *P < 0.05, **P < 0.01, NS: not significant (two-sided Wilcoxon rank sum test with FDR-correction).

Model parameters for all subjects are provided in Ohashi et al. [52] (Supplementary Table S7).

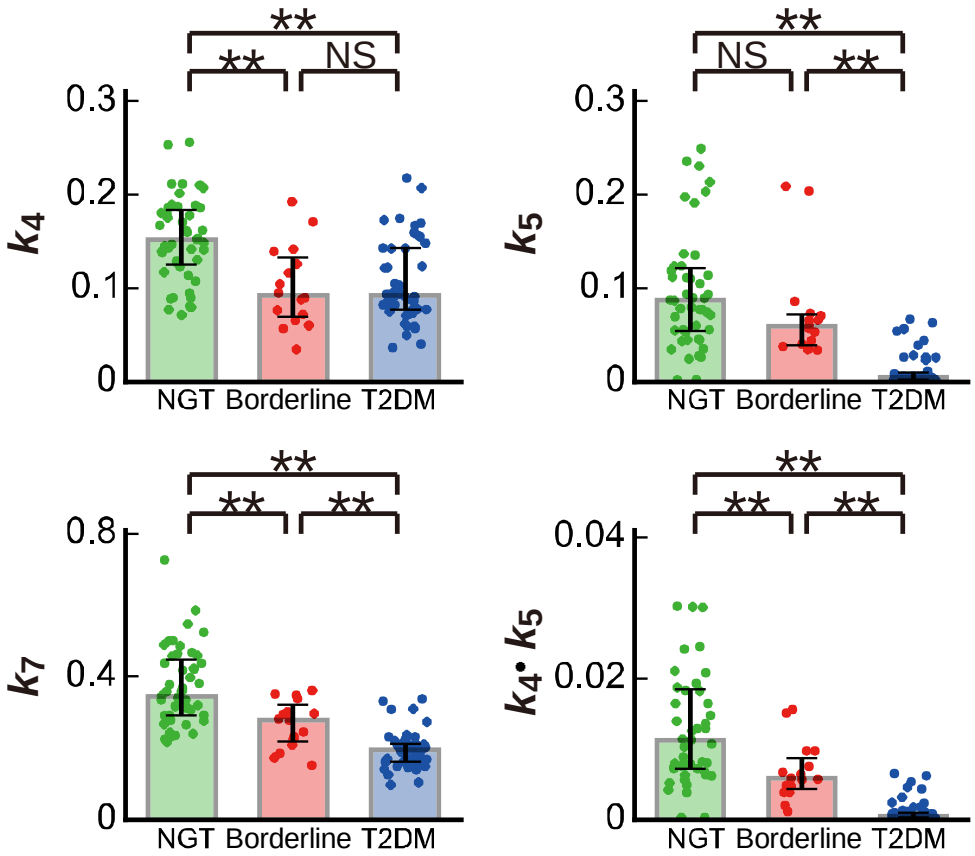

Figure 8. The parameters of k_4, k_5, k_7, and $k_4 \cdot k_5$, corresponding to insulin sensitivity, insulin secretion, insulin clearance, and DI, respectively. *$P < 0.05$, **$P < 0.01$, NS: not significant (two-sided Wilcoxon rank sum test with FDR-correction). The bar and error bar show the median and lower and upper quantiles, respectively. Each dot corresponds to the indicated parameter for an individual subject.

respectively (Fig. 3), and both correspond to insulin sensitivity. The values of k_3 and k_4 in the NGT subjects were significantly higher than that for borderline type or T2DM subjects. This is consistent with the finding that ISI calculated from both simulation and actual measurements for the borderline type or T2DM subjects was lower than those for the NGT subjects (Fig. 6).

The parameter k_5 is the rate constant for insulin secretion and corresponds to the capacity for insulin secretion. The value of k_5 in the T2DM subjects was significantly lower than that for the NGT or borderline type subjects. This indicated that insulin secretion is reduced in T2DM subjects compared with NGT and borderline type subjects, consistent with the result that AUC_{IRI10} calculated from both simulation and actual for T2DM subjects were lower than those for the other two groups (Fig. 6).

The parameter k_7 is the degradation rate of serum insulin and corresponds to insulin clearance (Fig. 3). The value of k_7 decreased significantly from NGT to borderline type to T2DM. The same characteristics were shown in clamp DI calculated from both simulation and actual measurements, indicating the relationship between insulin clearance and the capacity for glucose tolerance.

The parameters k_1 and k_2 are the rate constants for flux from effective glucose for insulin secretion to plasma glucose, and vice versa, respectively, differed significantly among the three groups. These parameters decreased in the rank order T2DM > NGT > borderline type, indicating that k_1 and k_2 do not represent progression of glucose intolerance. The physiological relevance of this difference remains to be elucidated.

I next performed parameter sensitivity analysis on ISI and AUC_{IRI10} in the simulation (Table 3) in order to evaluate the responsibility of each parameter for the simulated time courses of plasma glucose and serum insulin concentrations. I examined all 70 parameters including the seven rate constants (k_1 to k_7), the 21 products of each pair of rate constants, and the 42 quotients for each two rate constants. This analysis revealed that the most sensitive parameter for ISI was k_4, and that for AUC_{IRI10} was k_7, although k_5 was also one of the most sensitive parameters for AUC_{IRI10} (Table 3). These results are consistent with the functional roles of k_4 (insulin sensitivity) and k_5 (insulin secretion) in the feedback model. For further study, the parameter k_4, not the parameter k_3, is considered as a representative of parameters corresponding to insulin sensitivity.

The product of k_4 and k_5 ($k_4 \cdot k_5$), which conceptually corresponds to DI, decreased significantly from NGT to borderline type to T2DM (Fig. 8), as did the DIs in the simulation and actual measurements (Fig. 6). Of note, the parameter k_7, the rate constant of insulin clearance, also significantly declined from NGT to borderline type to T2DM (Fig. 8). These results thus suggested that k_7 is correlated with $k_4 \cdot k_5$, with DI, and, consequently, with the capacity for glucose tolerance.

Table 3. Parameter sensitivity analysis for ISI and AUC_{IRI10}.

Rank	ISI			AUC_{IRI10}		
		Median	*P*		Median	*P*
1	k_4	9.77×10^{-1}		k_7	–2.28	
2	k_1/k_4	-5.29×10^{-1}	1.40×10^{-38}	k_7/k_5	–1.90	1.87×10^{-1}
3	k_4/k_1	5.26×10^{-1}	1.40×10^{-38}	k_5/k_7	1.90	2.03×10^{-1}
4	k_3/k_4	-5.08×10^{-1}	1.40×10^{-38}	$k_5\bullet k_6$	1.60	2.26×10^{-3}
5	k_4/k_3	5.06×10^{-1}	1.40×10^{-38}	k_5	1.50	4.60×10^{-1}
6	$k_4\bullet k_7$	4.96×10^{-1}	1.40×10^{-38}	k_6/k_7	1.36	2.02×10^{-3}
7	$k_2\bullet k_4$	4.95×10^{-1}	1.40×10^{-38}	k_7/k_6	–1.35	2.09×10^{-3}
8	$k_4\bullet k_6$	4.93×10^{-1}	1.40×10^{-38}	$k_1\bullet k_7$	–1.27	5.51×10^{-5}
9	k_5/k_4	-4.91×10^{-1}	1.40×10^{-38}	k_7/k_2	–1.24	3.40×10^{-5}
10	$k_4\bullet k_5$	4.90×10^{-1}	1.40×10^{-38}	k_2/k_7	1.24	3.43×10^{-5}
11	k_2/k_4	-4.89×10^{-1}	1.40×10^{-38}	k_7/k_3	–1.14	2.15×10^{-5}
12	k_4/k_5	4.88×10^{-1}	1.40×10^{-38}	$k_4\bullet k_7$	–1.14	2.17×10^{-5}
13	k_4/k_2	4.86×10^{-1}	1.40×10^{-38}	$k_3\bullet k_7$	–1.14	2.11×10^{-5}
14	k_7/k_4	-4.84×10^{-1}	1.40×10^{-38}	k_7/k_4	–1.14	2.11×10^{-5}
15	k_6/k_4	-4.83×10^{-1}	1.40×10^{-38}	k_3/k_7	1.14	2.15×10^{-5}
16	k_4/k_7	4.81×10^{-1}	1.40×10^{-38}	k_4/k_7	1.14	2.11×10^{-5}
17	k_4/k_6	4.81×10^{-1}	1.40×10^{-38}	$k_2\bullet k_7$	-9.47×10^{-1}	9.99×10^{-6}

Rank	ISI			AUC_{IRI10}		
		Median	*P*		Median	*P*
18	k_3•k_4	4.73×10^{-1}	1.40×10^{-38}	k_1/k_7	9.06×10^{-1}	7.74×10^{-6}
19	k_1•k_4	4.42×10^{-1}	1.40×10^{-38}	k_7/k_1	-9.03×10^{-1}	7.45×10^{-6}
20	k_1	-8.79×10^{-2}	1.40×10^{-38}	k_1/k_5	-8.13×10^{-1}	1.51×10^{-8}
21	k_1•k_3	-6.16×10^{-2}	1.40×10^{-38}	k_5/k_1	8.09×10^{-1}	1.04×10^{-8}
22	k_6/k_1	5.97×10^{-2}	1.40×10^{-38}	k_2•k_5	7.69×10^{-1}	1.20×10^{-10}
23	k_1/k_6	-5.97×10^{-2}	1.40×10^{-38}	k_4/k_5	-7.53×10^{-1}	9.89×10^{-12}
24	k_1/k_7	-5.51×10^{-2}	1.40×10^{-38}	k_3/k_5	-7.52×10^{-1}	8.58×10^{-12}
25	k_7/k_1	5.33×10^{-2}	1.40×10^{-38}	k_5/k_4	7.49×10^{-1}	6.84×10^{-12}
26	k_1/k_2	-4.91×10^{-2}	1.40×10^{-38}	k_3•k_5	7.49×10^{-1}	6.74×10^{-12}
27	k_2/k_1	4.88×10^{-2}	1.40×10^{-38}	k_5/k_3	7.49×10^{-1}	6.46×10^{-12}
28	k_1/k_5	-4.74×10^{-2}	1.40×10^{-38}	k_4•k_5	7.48×10^{-1}	6.10×10^{-12}
29	k_5/k_1	4.71×10^{-2}	1.40×10^{-38}	k_2/k_5	-7.15×10^{-1}	6.26×10^{-13}
30	k_1•k_5	-3.54×10^{-2}	1.40×10^{-38}	k_5/k_2	7.11×10^{-1}	4.44×10^{-13}
31	k_1•k_2	-3.43×10^{-2}	1.40×10^{-38}	k_1•k_5	6.79×10^{-1}	7.81×10^{-14}
32	k_3	-3.32×10^{-2}	1.40×10^{-38}	k_6/k_5	-5.69×10^{-1}	2.82×10^{-6}
33	k_1•k_6	-3.25×10^{-2}	1.40×10^{-38}	k_5/k_6	5.66×10^{-1}	2.60×10^{-6}
34	k_1•k_7	-3.04×10^{-2}	1.40×10^{-38}	k_6•k_7	-4.50×10^{-1}	1.66×10^{-17}
35	k_3/k_7	-2.51×10^{-2}	1.40×10^{-38}	k_6/k_1	3.05×10^{-1}	5.30×10^{-10}

Rank	ISI			AUC_{IRI10}		
		Median	*P*		Median	*P*
36	k_7/k_3	2.48×10^{-2}	1.40×10^{-38}	k_1/k_6	-3.05×10^{-1}	5.37×10^{-10}
37	k_1/k_3	-2.44×10^{-2}	1.40×10^{-38}	$k_2 \bullet k_6$	2.78×10^{-1}	4.36×10^{-10}
38	k_3/k_1	2.29×10^{-2}	1.40×10^{-38}	k_1	-1.71×10^{-1}	5.77×10^{-35}
39	k_3/k_2	-1.90×10^{-2}	1.40×10^{-38}	$k_5 \bullet k_7$	1.69×10^{-1}	1.92×10^{-12}
40	k_2/k_3	1.90×10^{-2}	1.40×10^{-38}	k_2/k_1	1.11×10^{-1}	2.99×10^{-35}
41	k_5/k_3	1.85×10^{-2}	1.40×10^{-38}	k_1/k_2	-1.11×10^{-1}	2.44×10^{-35}
42	k_3/k_5	-1.84×10^{-2}	1.40×10^{-38}	$k_1 \bullet k_4$	-8.63×10^{-2}	1.40×10^{-38}
43	k_6/k_3	1.84×10^{-2}	1.40×10^{-38}	k_3/k_1	8.63×10^{-2}	1.40×10^{-38}
44	k_3/k_6	-1.84×10^{-2}	1.40×10^{-38}	k_1/k_3	-8.60×10^{-2}	1.40×10^{-38}
45	$k_6 \bullet k_7$	1.57×10^{-2}	1.40×10^{-38}	k_4/k_1	8.58×10^{-2}	1.40×10^{-38}
46	$k_3 \bullet k_5$	-1.54×10^{-2}	1.40×10^{-38}	$k_1 \bullet k_3$	-8.56×10^{-2}	1.40×10^{-38}
47	k_7	1.49×10^{-2}	1.40×10^{-38}	k_1/k_4	-8.53×10^{-2}	1.40×10^{-38}
48	$k_2 \bullet k_3$	-1.22×10^{-2}	1.40×10^{-38}	k_2	5.47×10^{-2}	1.54×10^{-35}
49	$k_3 \bullet k_6$	-1.20×10^{-2}	1.40×10^{-38}	$k_1 \bullet k_6$	-4.80×10^{-2}	2.55×10^{-10}
50	$k_2 \bullet k_7$	9.26×10^{-3}	1.40×10^{-38}	$k_1 \bullet k_2$	-3.13×10^{-2}	1.40×10^{-38}
51	$k_5 \bullet k_7$	7.79×10^{-3}	1.40×10^{-38}	k_4/k_2	-2.84×10^{-2}	1.40×10^{-38}
52	$k_3 \bullet k_7$	-7.18×10^{-3}	1.40×10^{-38}	k_2/k_4	2.82×10^{-2}	1.40×10^{-38}
53	k_5/k_6	-6.73×10^{-3}	1.40×10^{-38}	$k_2 \bullet k_3$	2.79×10^{-2}	1.40×10^{-38}

Rank	ISI			AUC_{IRI10}		
		Median	*P*		Median	*P*
54	k_6/k_5	6.68×10^{-3}	1.40×10^{-38}	k_3/k_2	-2.70×10^{-2}	1.40×10^{-38}
55	k_2	6.33×10^{-3}	1.40×10^{-38}	k_2/k_3	2.69×10^{-2}	1.40×10^{-38}
56	k_2/k_7	-5.83×10^{-3}	1.40×10^{-38}	$k_2\bullet k_4$	2.65×10^{-2}	1.40×10^{-38}
57	k_7/k_2	5.82×10^{-3}	1.40×10^{-38}	k_6/k_2	-1.09×10^{-2}	3.03×10^{-10}
58	$k_2\bullet k_6$	5.25×10^{-3}	1.40×10^{-38}	k_2/k_6	1.09×10^{-2}	3.19×10^{-10}
59	k_5/k_7	-5.09×10^{-3}	1.40×10^{-38}	k_6/k_4	5.88×10^{-3}	3.78×10^{-10}
60	k_7/k_5	4.98×10^{-3}	1.40×10^{-38}	k_4/k_6	-5.88×10^{-3}	3.83×10^{-10}
61	k_2/k_5	3.46×10^{-3}	1.40×10^{-38}	$k_3\bullet k_6$	4.28×10^{-3}	3.78×10^{-10}
62	k_5/k_2	-3.11×10^{-3}	1.40×10^{-38}	k_4	-2.21×10^{-3}	1.40×10^{-38}
63	k_6/k_7	-2.22×10^{-3}	1.40×10^{-38}	k_3/k_4	1.73×10^{-3}	1.40×10^{-38}
64	k_7/k_6	1.94×10^{-3}	1.40×10^{-38}	k_4/k_3	-1.59×10^{-3}	1.40×10^{-38}
65	$k_2\bullet k_5$	1.94×10^{-3}	1.40×10^{-38}	k_3	1.04×10^{-3}	1.40×10^{-38}
66	$k_5\bullet k_6$	1.71×10^{-3}	1.40×10^{-38}	$k_3\bullet k_4$	-3.63×10^{-4}	1.17×10^{-38}
67	k_6/k_2	-1.10×10^{-3}	1.40×10^{-38}	k_6	3.56×10^{-4}	4.12×10^{-7}
68	k_2/k_6	1.05×10^{-3}	1.40×10^{-38}	$k_4\bullet k_6$	-2.57×10^{-4}	3.78×10^{-10}
69	k_5	6.87×10^{-4}	1.40×10^{-38}	k_3/k_6	0.00	3.82×10^{-10}
70	k_6	0.00	4.34×10^{-39}	k_6/k_3	0.00	3.77×10^{-10}

Medians of the indicated parameters for all 113 subjects were used for parameter sensitivity analysis for clinical indices of insulin sensitivity, ISI, and insulin secretion AUC_{IRI10} (see

Methods). The higher the absolute value of the parameter, as listed, the higher the sensitivity. *P* values relative to the median for the top-ranked parameter were determined by two-sided Wilcoxon rank sum test, and the value of $<3.57\times10^{-4}$ (=0.05/140, corrected by the number of tests, divided by 140) is considered statistically significant. Parameter sensitivity of k_7 (-2.28) and that of k_5 (1.50) for AUC_{IRI10} did not differ significantly ($P = 0.460$).

2.3.5 Parameters reflecting the abilities to control glucose and insulin concentration

I examined the correlation of the estimated model parameters with clinical indices of insulin sensitivity, secretion, and clearance (Fig. 9). The model parameter showing the highest correlation with insulin sensitivity index (ISI) was k_7 ($r = 0.804$, $P < 0.001$), and the parameter showing second highest correlation was k_4 ($r = 0.625$, $P < 0.001$). k_4 is the rate constant for glucose uptake facilitated by both glucose and insulin, and corresponding to insulin sensitivity. k_7 is the degradation rate of serum insulin, which depends on the number of insulin receptors on target tissues [77], indicating that serum insulin degradation and insulin sensitivity are mutually correlated. Therefore, it is reasonable that both k_7 and k_4 are correlated with ISI.

The model parameter showing the highest correlation with insulin secretion during the first 10 min (AUC_{IRI10}) was k_5 ($r = 0.703$, $P < 0.001$). Because the parameter k_5 is the rate constant for insulin secretion, its correlation with the clinical index of insulin secretion is reasonable.

The model parameter showing the highest correlation with metabolic clearance rate (MCR), which is the index of insulin clearance calculated from the insulin infusion rate and circulating insulin levels during hyperinsulinemic-euglycemic clamp analysis [16] (see Methods for details), was k_7 ($r = 0.551$, $P < 0.001$). Because the parameter k_7 is the rate constant for insulin clearance, its correlation with the clinical index of insulin clearance is reasonable.

Given that the results suggested that the rate constant for insulin clearance, k_7, might be related to the capacity for glucose tolerance, I next examined the correlation between model

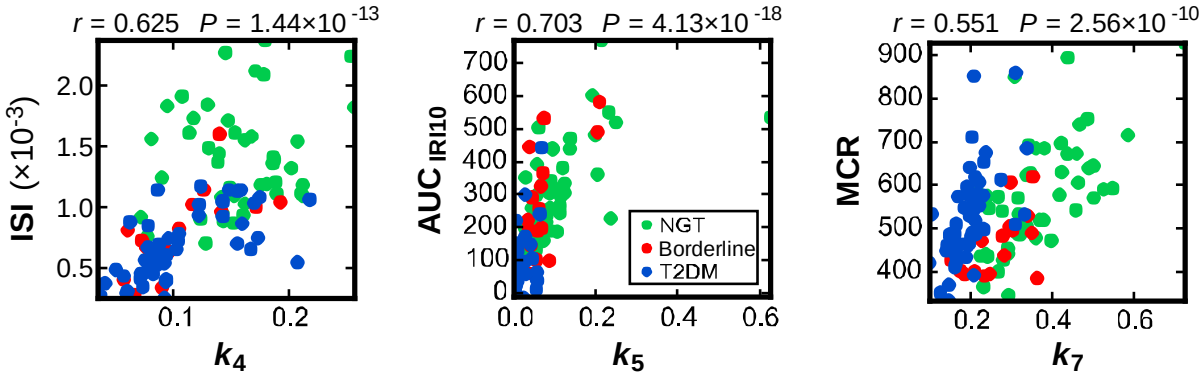

Figure 9. The correlations between parameters and clinical indices related to control of insulin concentration. Scatter plots for the indicated measured clinical indices versus the parameters correspond to insulin sensitivity (k_4), secretion (k_5), DI ($k_4 \cdot k_5$), and clearance (k_7). Each dot indicates the value of an individual subject. Green, red, and blue dots indicate NGT, borderline type, and T2DM subjects, respectively.

Correlation coefficients of all clinical indices with model parameters are provided in Ohashi et al. [52] (Supplementary Table S4).

parameters and various clinical indices determined by the OGTT performed in each subject (Fig. 10; Methods). Among the 70 parameters consisting of each rate constant as well as the products and quotients for each pair of rate constants, k_7 showed the highest correlation with 90-min plasma glucose (PG) and AUC_{PG} values, the latter being the integrated glucose concentration during the OGTT, as well as the second highest correlation with FPG, 60-min PG, and 120-min PG during the OGTT, indicating that k_7 is highly correlated with the capacity for glucose tolerance. An analog of DI calculated from indices measured during an OGTT (oral DI) has been proposed and shown to possess characteristics similar to those of the original DI (Methods). The parameter k_7 also showed the highest correlation with oral DI (Fig. 10), whereas the correlation of k_7 with each index of insulin sensitivity or insulin secretion, including the components of oral DI (Matsuda index and $AUC_{IRI120/PG120}$), was not especially high (data shown in Supplementary Table S4 in Ohashi et al. [52]). The tight relation between the capacity for glucose tolerance and k_7 was thus confirmed by the results of the OGTT as following:

$$k_7 \approx PG_{OGTT}^{-1} \tag{18}$$

In addition, k_7 showed the highest correlation with the insulinogenic index (Fig. 10), which is thought to be an important determinant of the capacity for glucose tolerance.

MCR is a clinical index of insulin clearance rate, and corresponds to k_7 in the mathematical model. However, MCR was not highly correlated with either 30-min PG (r = –0.22), 60-min PG (r = –0.22), 90-min PG (r = –0.16), 120-min PG (r = –0.17), AUC_{PG} (r = –0.20), oral DI (r = 0.23), or clamp DI (r = 0.32) (Fig. 11; data shown in Supplementary

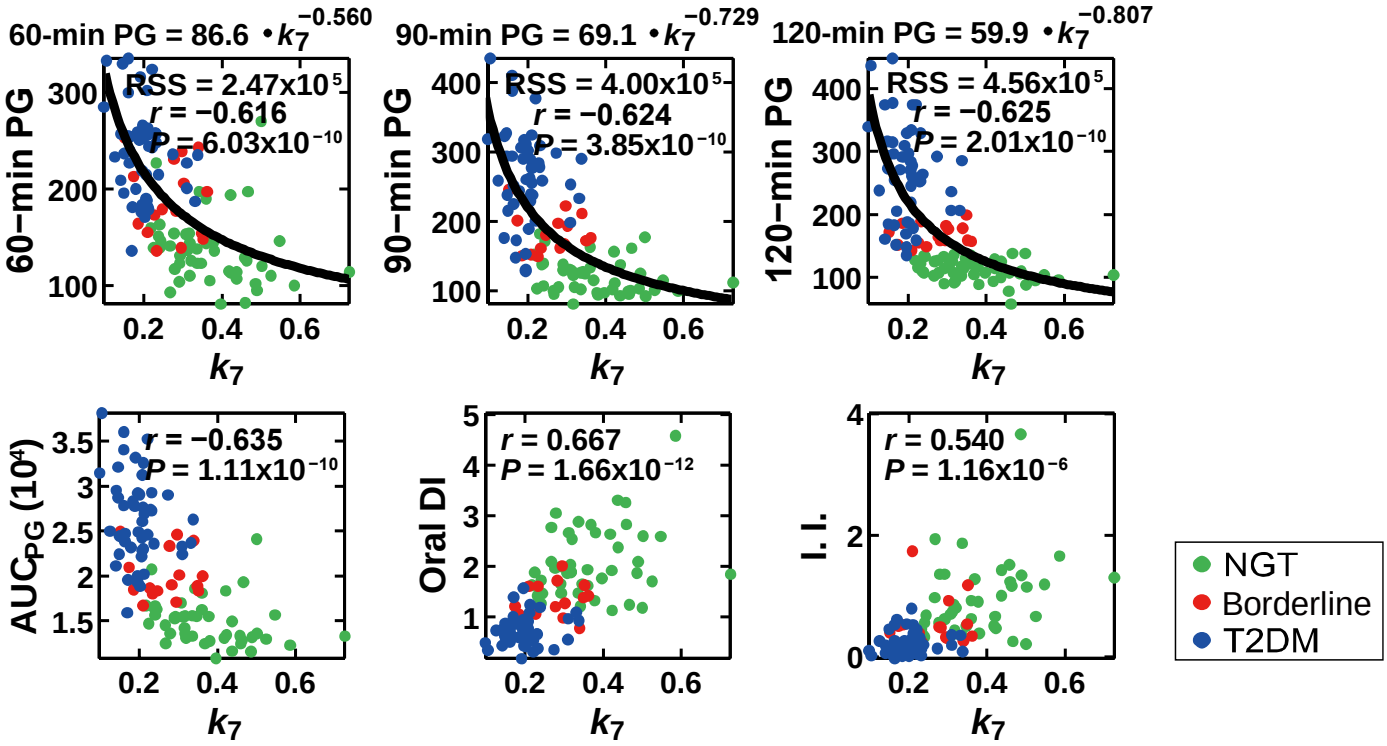

Figure 10. The correlations between the parameter corresponds to insulin clearance (k_7) and clinical indices related to control of glucose and insulin concentration. Scatter plots for the indicated measured clinical indices versus the parameter k_7. Each dot indicated the value of an individual subject. *t*-min PG, plasma glucose concentration at *t* min during oral glucose tolerance test (OGTT); AUC_{PG}, the area under the plasma glucose concentration curve from 0 to 120 min; Oral DI, the disposition index calculated from indices measured during OGTT; I.I., insulinogenic index. The correlation coefficient, *r*, and the *P* value for testing the hypothesis of no correlation are shown. Each distribution in the axis of k_7 and *t*-min PG was fitted by a power function (see Methods), plotted as black curves. RSS, residual sum of the square between the *t*-min PG and the estimated function is also shown at the top of the corresponding plots.

Correlation coefficients of all clinical indices with model parameters are provided in Ohashi et al. [52] (Supplementary Table S4).

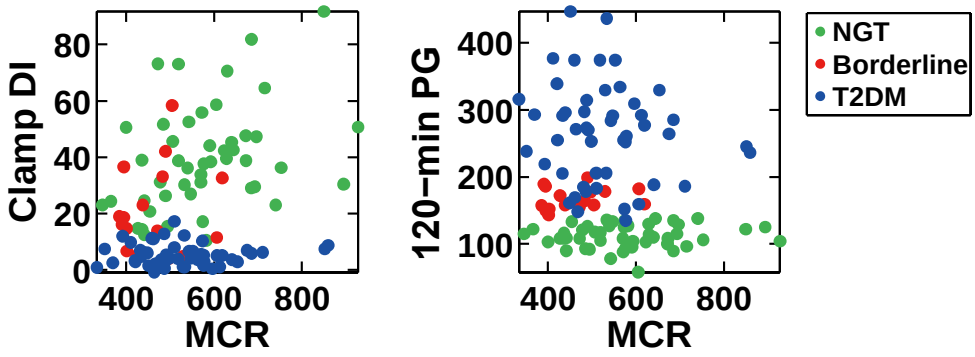

Figure 11. The correlations between the clinical indices of metabolic clearance rate (MCR) and clamp DI and 120-min PG related to the capacity for glucose tolerance. Each dot in Scatter plots indicated the value of an individual subject. The correlation coefficient, *r*, and the *P* value for testing the hypothesis of no correlation are shown.

Table S5 in Ohashi et al. [52]). It should be noted that MCR is not exactly the same as insulin clearance; MCR indicates the ratio between insulin infusion rate and serum insulin level at steady state whereas k_7 indicates the rate of insulin degradation, which is denoted as insulin clearance in this study.

2.3.6 Conserved relationship between insulin clearance and the capacity of glucose tolerance

The clinical indices that differed significantly among each of the NGT, borderline type, and T2DM groups were clamp DI calculated from simulation and actual measurements (Fig. 6), and the parameters in the model that differed significantly among each of the three groups were k_7 and $k_4 \cdot k_5$ (Fig. 8). These indices and parameters therefore reflect the capacity of glucose tolerance of the subject, then I examined the correlation between them (Fig. 12). The clamp DI calculated from simulation and actual measurements showed a high correlation with both k_7 and $k_4 \cdot k_5$.

The similarity of this characteristics between k_7 and $k_4 \cdot k_5$ suggests the existence of an unrecognized relation between insulin clearance and both insulin sensitivity and insulin secretion. I further investigated the relation between $k_4 \cdot k_5$ and k_7 by fitting their distribution with a power function, resulting in the power index appearing to be 1.98 (Fig. 13A), indicative of a square-law relation between k_7 and $k_4 \cdot k_5$ as following:

$$k_7 \approx \sqrt{k_4 \cdot k_5} \tag{19}$$

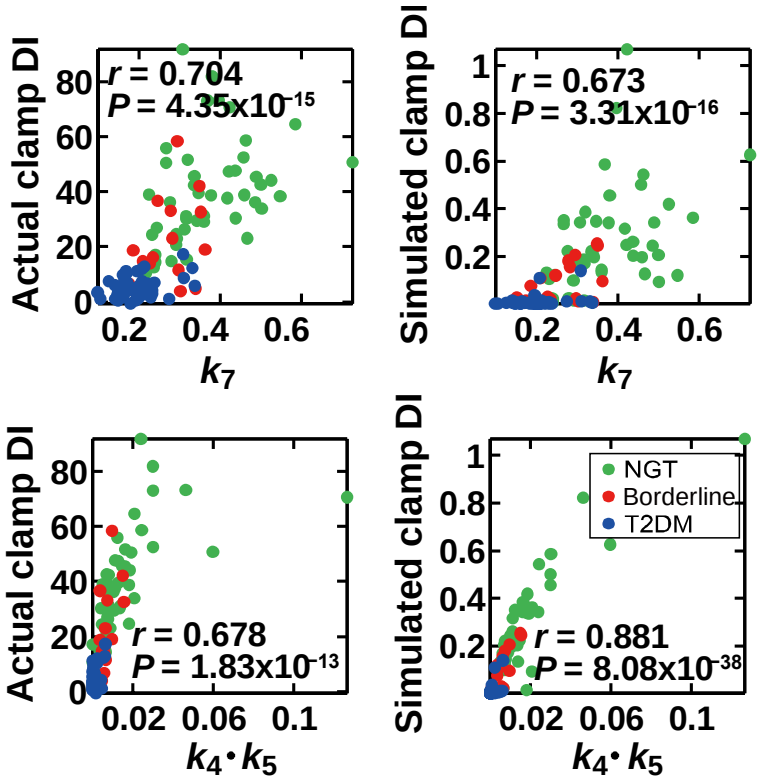

Figure 12. The correlations between the parameter corresponds to insulin clearance (k_7) and clinical indices of clamp DI calculated from simulation and actual measurements. Each dot indicates the value of an individual subject. Green, red, and blue dots indicate NGT, borderline type, and T2DM subjects, respectively.

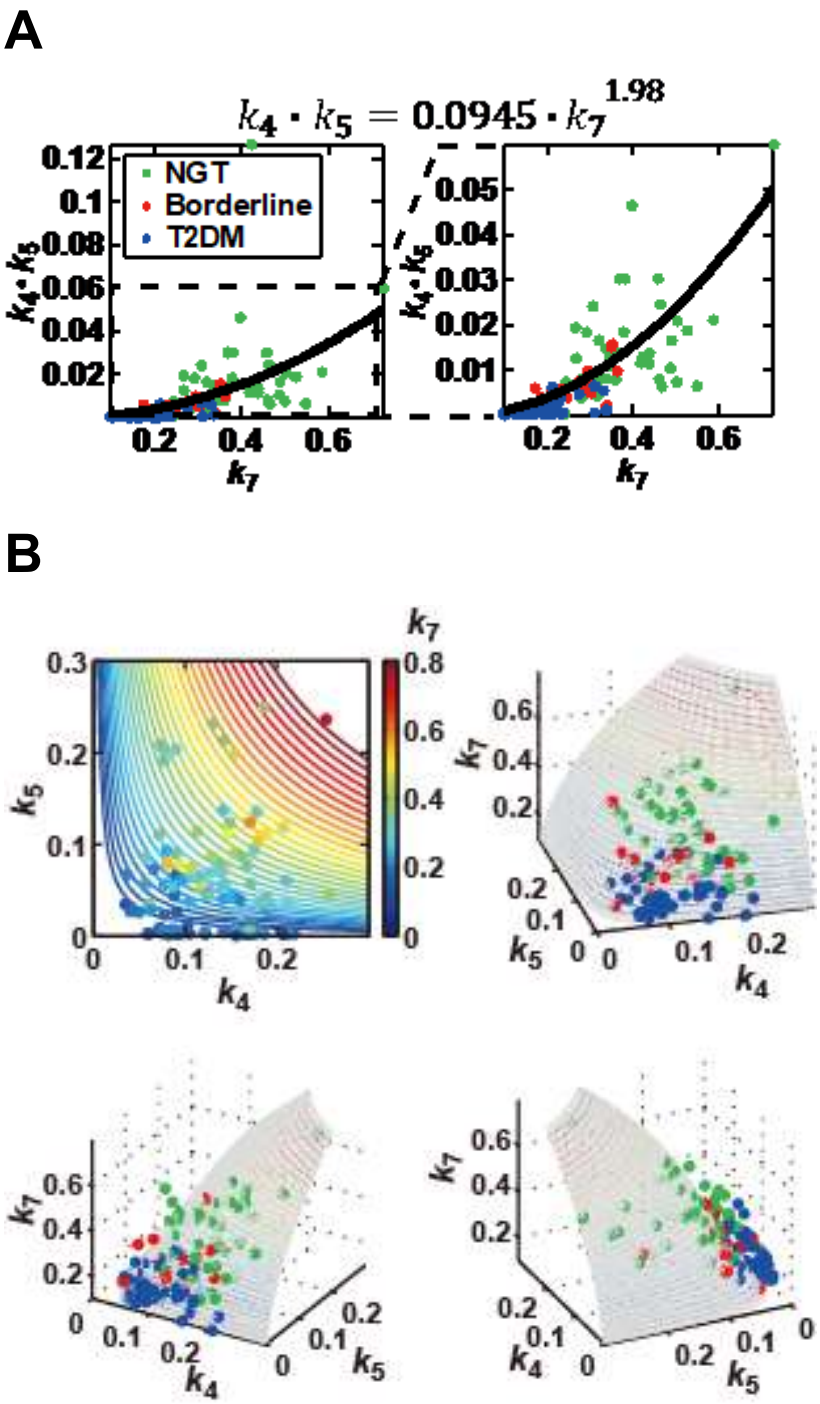

Figure 13. Square-law relation between parameters corresponding to insulin clearance (k_7) and DI ($k_4 \cdot k_5$).

(**A**) Scatter plot of the parameter k_7 versus the parameter k_7, with dots indicating the parameters of each subject. The distribution in the axis of k_7 and $k_4 \cdot k_5$ was fitted by a power function (see Methods), plotted as black curves. The estimated function is shown at the top.

(**B**) The contour plot of k_4, k_5, and k_7 (upper left), with the value of k_7 being indicated by colors, as well as three-dimensional plots of k_4, k_5, and k_7, where circle colors of green, red and blue indicate NGT, borderline type, and T2DM subjects, respectively. RSS was 0.0168. Parameters with $k_4 \leq 0.3$ and $k_5 \leq 0.3$ are plotted.

I plotted the distribution of k_4, k_5, and k_7 in a contour plot (Fig. 13B), with each parameter appearing along the curve surface of the square-law equation. Analysis of the mathematical model thus made it possible to infer the hidden square-law relation between two functionally different parameters, $k_4 \cdot k_5$ and k_7.

2.4 Discussion

I developed a mathematical model for the feedback loop between circulating glucose and insulin, and estimated parameters from the time courses of plasma glucose and serum insulin during the consecutive hyperglycemic and hyperinsulinemic-euglycemic clamp. The parameters estimated for each subject with NGT, borderline type, and T2DM revealed that the rate constants correspond to insulin sensitivity (k_5) and secretion (k_5) as well as clearance (k_7) decreased with the progression of glucose intolerance (Fig. 14). The analyses between model parameters inferred a square-law relation between the rate constant of insulin clearance (k_7) and the product of the rate constants of insulin sensitivity (k_4) and insulin secretion (k_5) (Eq. 19; Fig. 14). Of note, the right and left sides of the fitted equation in Fig. 13A have almost the same dimension (min^{-2}), and the ratio between k_7 and $\sqrt{k_4 \cdot k_5}$ always remains constant among NGT, borderline type, and T2DM subjects. The ratio between k_7 and $\sqrt{k_4 \cdot k_5}$ may therefore indicate a homeostasis constant of glucose tolerance that constrains the rate constant of insulin clearance as well as those of insulin sensitivity and insulin secretion. As far as I am aware, such a relation between insulin secretion, sensitivity, and clearance has not previously been proposed on the basis of actual measurement of clinical indices. The reason why this relation could be discovered may be because of using both the consecutive hyperglycemic and hyperinsulinemic-euglycemic clamp and mathematical modeling. Hyperglycemic clamp data involves quantitative relation between insulin clearance and secretion, and hyperinsulinemic-euglycemic clamp data involves quantitative relation between insulin clearance and sensitivity. In addition, because model structure constrained the relation between insulin

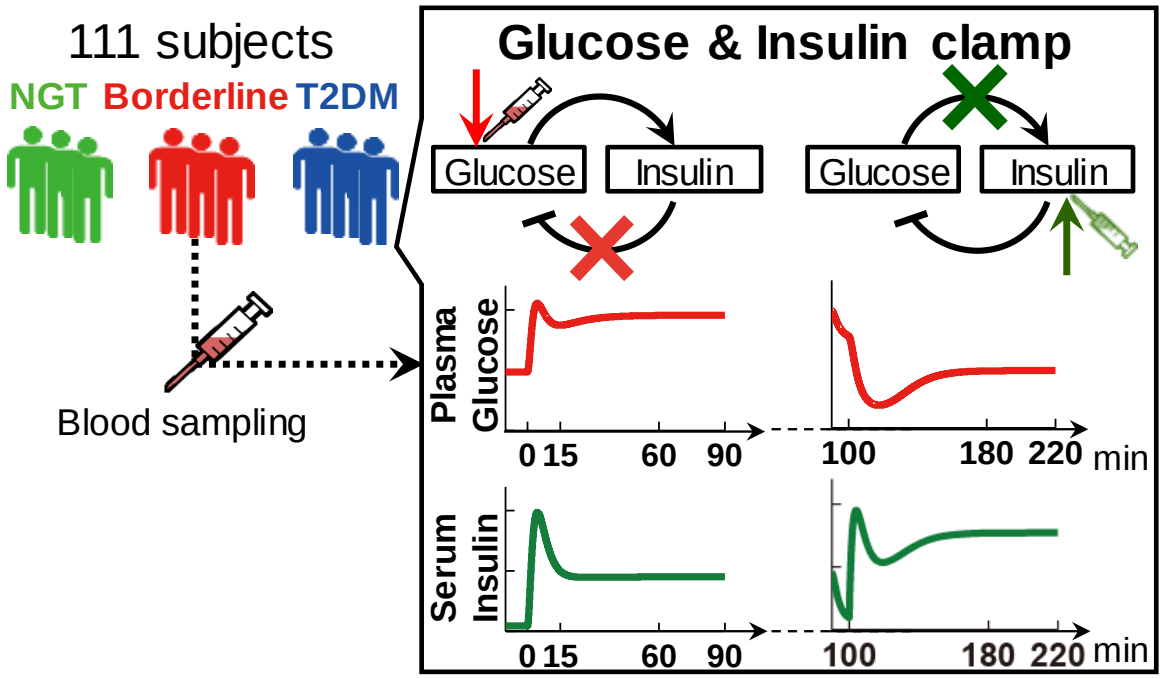

Mathematical model

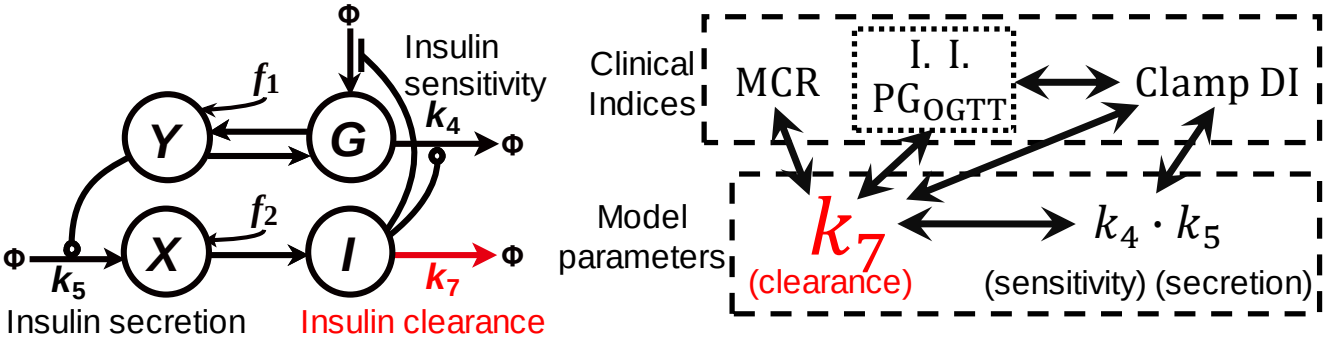

Simple glucose homeostatic law

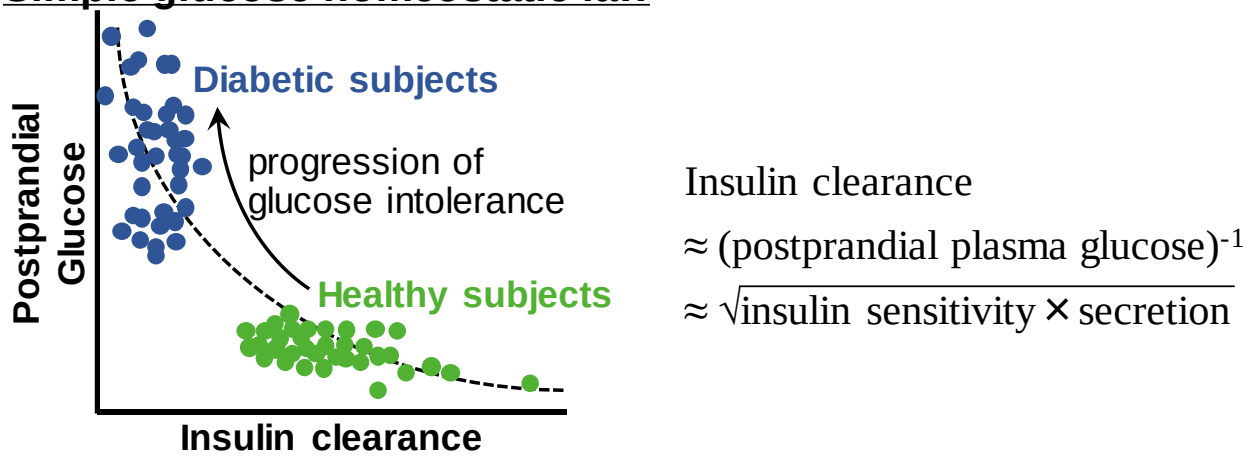

Figure 14. The mathematical model analysis with the consecutive clamp and the relation between clinical indices and parameters in the model.

Solid arrows between clinical indices and model parameters indicate the correlations for which $|r| \geq 0.5$. The parameter corresponding to insulin clearance (k_7) was found to be tightly related to the progression of glucose intolerance.

clearance, secretion and sensitivity, parameter estimation based on the consecutive hyperglycemic and hyperinsulinemic-euglycemic clamps uncovered quantitative relation between k_7 and $\sqrt{k_4 \cdot k_5}$ conserved among NGT, borderline type, and T2DM subjects. This study has thus elucidated an unrecognized relation between factors that play important roles in the regulation glucose homeostasis.

The role of insulin clearance in glucose intolerance has thus far been studied, however, the role of insulin clearance remains controversial. Insulin clearance has been reported to be negatively correlated with the progression of glucose intolerance[78-84]. On the other hand, it has been reported that insulin clearance is increased in subjects carrying diabetes-susceptible gene[85], and that insulin clearance is not affected by decreasing insulin secretion by free fatty acid administration[86]. The controversial role of insulin clearance may be because the data obtained by OGTT or single clamp alone contain less information regarding insulin clearance than that obtained by the consecutive clamps in this study, or because the insulin clearance directly calculated from the measured data, such as MCR, is less quantitative than that obtained by the mathematical modeling. This study strongly supports the conclusion in the former studies[78-84].

Insulin secretion and insulin sensitivity are thought to determine the capacity for glucose tolerance, and DI, defined as the product of indices for these two parameters, has indeed been shown to reflect the integrated capacity for glucose tolerance. Given that $k_4 \cdot k_5$ conceptually corresponds to DI, it is not surprising that it correlates with actual measurements for glucose tolerance to a certain extent. An unexpected finding in the current study, however, is that k_7,

the rate constant of insulin clearance, showed the highest or one of the highest correlations with PG level as well as with AUC_{PG} during an OGTT (Eq. 18). This finding, together with the high correlations of k_7 with oral and clamp DIs, is indicative of the strong relation between insulin clearance and the capacity for glucose tolerance.

Although this analysis suggests the existence of a previously unrecognized relation among the three important components of insulin-regulated glucose homeostasis—insulin secretion, insulin sensitivity, and insulin clearance—the mechanism for the overall control of these components remains unknown. Insulin is degraded in cells after its receptor-mediated internalization, with this internalization being tightly linked to the intrinsic tyrosine kinase activity of the insulin receptor, a key signaling function of this protein [2]. Both insulin clearance and insulin sensitivity may thus be strongly influenced by the integral of the abundance and activity of the insulin receptor. Indeed, insulin clearance in the liver has been shown to be an important determinant of insulin sensitivity in dogs [87]. However, insulin clearance and insulin sensitivity may be distinguished because insulin clearance is related to receptor down-regulation, while insulin sensitivity is also related to the subsequent signaling cascade, such as the negative feedback through mTOR/S6K1.

Insulin secretion in the living body manifests a pulsatile pattern, and the maintenance of this pattern is thought to be important for both insulin sensitivity and glucose tolerance. Although the mechanistic link between pulsatile insulin secretion and insulin sensitivity is not fully understood, I have recently shown that certain elements of insulin signaling respond not to the absolute value but to the temporal profile of insulin concentration [88,89]. Loss of the

pulsatile pattern of insulin secretion induced by partial pancreatectomy was also found to result in a decrease not only in insulin sensitivity but also in insulin clearance [90]. Theoretically, if insulin clearance is impaired, the retention period of circulating insulin would be expected to be prolonged and rapid temporal changes in insulin secretion would not be well reflected by circulating insulin levels [91], suggesting that the pulsatile pattern is observed only when insulin clearance is fully operative. I found that k_7 also showed the highest correlation with the insulinogenic index, an index of early insulin secretion. It is possible that the higher k_7 is, the more the rapid temporal changes in insulin secretion are reflected in circulating insulin levels. A high level of insulin clearance is thus likely important for full transmission of information from pancreatic β-cells to the whole body. This notion may be related, at least in part, to the underlying relation between the secretion, sensitivity, and clearance of insulin.

Many mathematical models of systemic insulin-glucose dynamics have been reported [23,30,32,45,48,55,58-67]. One of the differences between these previous models and the present model is incorporation of the infusion of glucose and insulin in the model. Another key difference is the experimental method of both hyperglycemic and hyperinsulinemic-euglycemic clamps, which made it possible to evaluate indices for insulin secretion and insulin sensitivity without an effect of the feedback relation. To examine whether both hyperglycemic and hyperinsulinemic-euglycemic clamps are necessary to uncover the relation between insulin clearance and glucose intolerance, I estimated parameters using hyperglycemic or hyperinsulinemic-euglycemic clamp data alone, and found that insulin clearance did not

significantly differ between three groups (Fig. 15). In the model with hyperinsulinemic-euglycemic clamp, insulin clearance declined from the NGT to borderline type subjects (Fig. 15), suggesting that addition of hyperglycemic clamp data is necessary to find the difference of insulin clearance from the borderline type to T2DM subjects.

I am aware that some of the results of this analysis only hold if the parameters are identifiable based on plasma glucose and serum insulin data. I performed 20 trials of parameter estimation for each subject (Methods), but for most subjects (90 subjects), estimated parameters varied among trials that returned the same RSS, especially the parameters k_6 and X_b differed to a large extent, while the parameters k_4, k_5, and k_7 did not largely differ (Fig. 16). The remaining 23 subjects had only one trial which minimized RSS. The values of estimated parameters and RSS varied among the 20 trials of each subject. If the number of estimated trials, parents, and generations of evolutionary programming increases, a trial that gives a different parameter solution with smaller RSS than that reported in this study might be obtained. Structural or a priori identifiability of parameters based on the system equations [92], which tests if model parameters can be determined from the available data, was not performed in this study. Large variability in the fitted parameters, like for instance in k_6 and X_b, could be due to the identifiability of the parameters and not due to biological variance, and interpretation of the results has to take this into account.

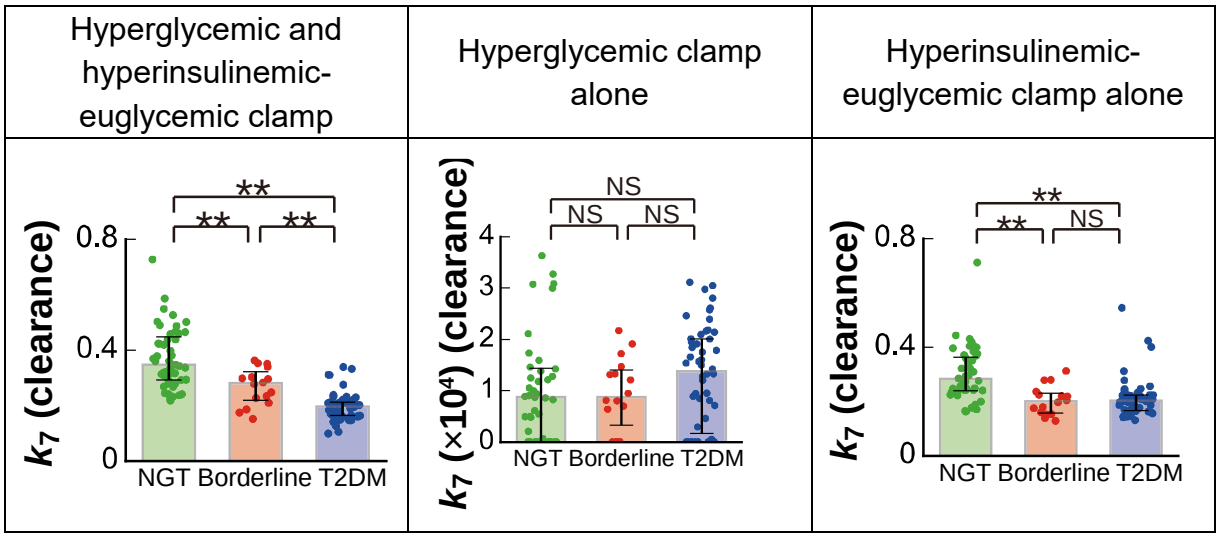

Figure 15. The parameter corresponding to insulin clearance (k_7) estimated by use of both hyperglycemic and hyperinsulinemic-euglycemic clamps or either one of them. *P <0.05, **P <0.01, NS: not significant by two-sided Wilcoxon rank sum test with FDR-correction.

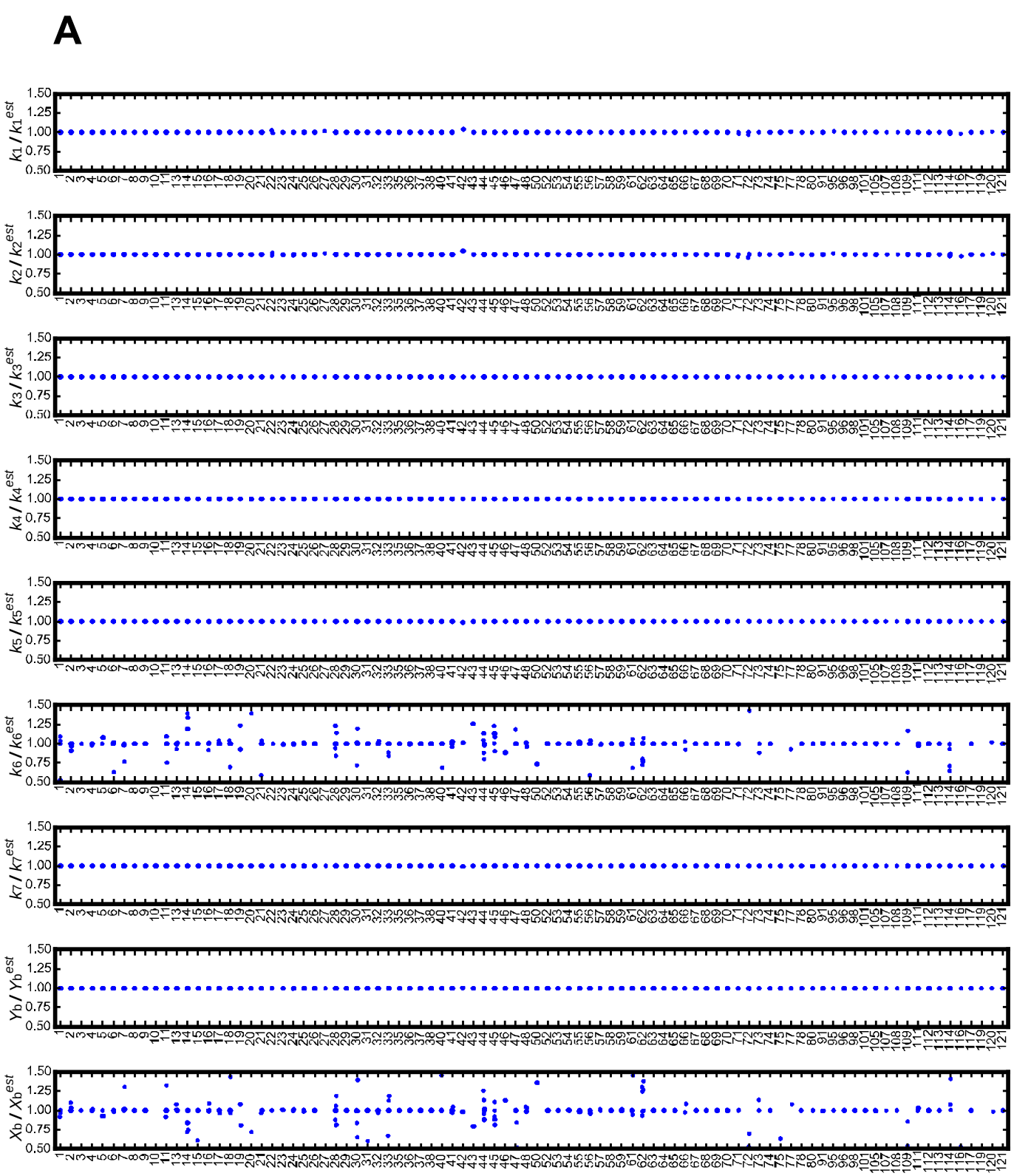
A
k1 / k1est
k2 / k2est
k3 / k3est
k4 / k4est
k5 / k5est
k6 / k6est
k7 / k7est
Yb / Yb est
Xb / Xb est
1.50
1.25
1.00
0.75
0.50

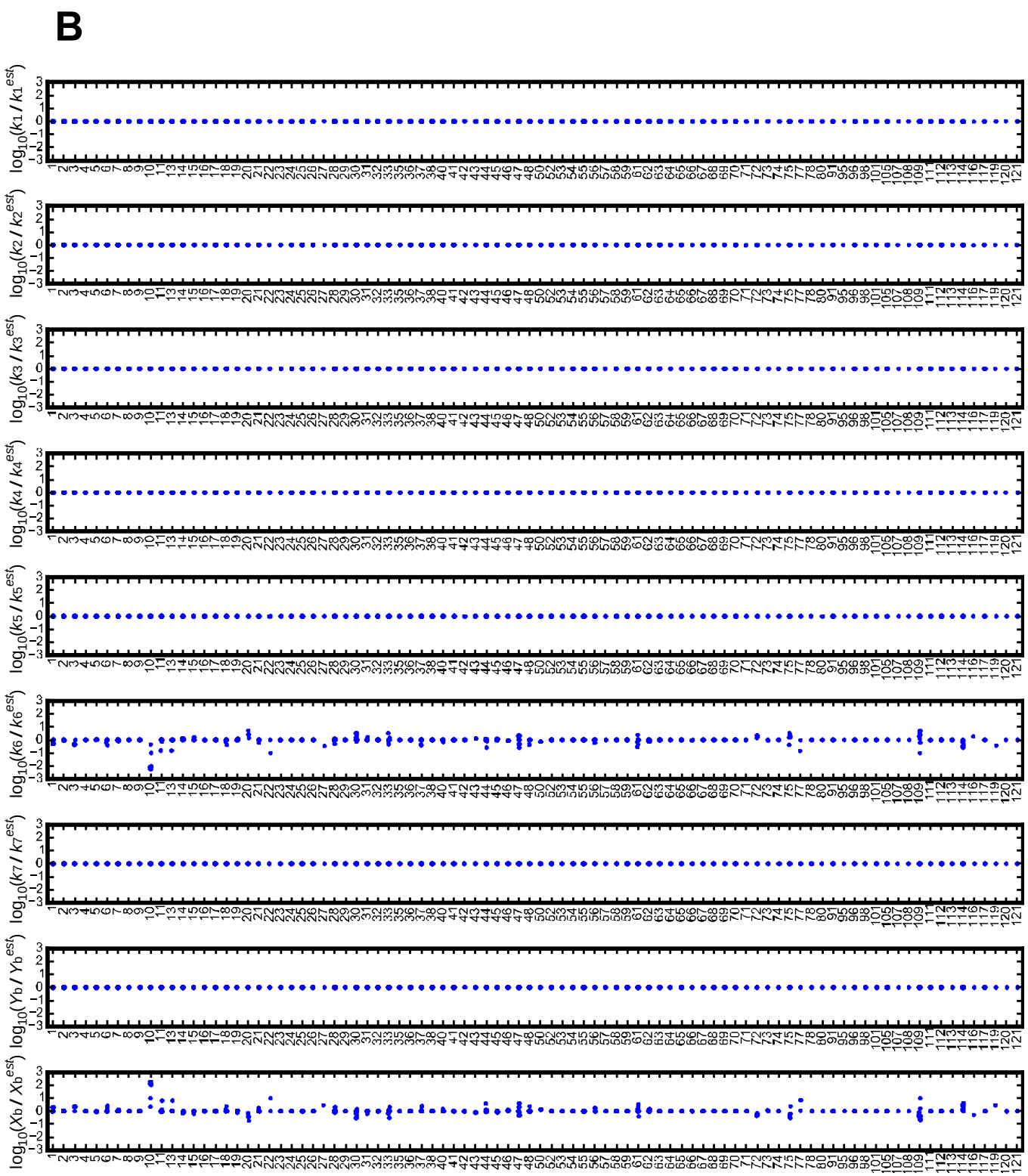

Figure 16. The ratio of parameters estimated in trials other than the trial used in this study to parameters estimated in the trial used in this study (*parameter*^{est}) for 90 subjects (46 NGT: #1 to #50, 16 borderline type: #52 to #68, and 28 T2DM: #69 to #121) who had two or more

trials which minimized RSS. Each dot corresponds to the indicated parameter ratio of an individual trial of an individual subject in linear (**A**) and log-10 (**B**) scale.

3. Increase in hepatic and decrease in peripheral insulin clearance characterize progression of glucose intolerance and temporal patterns of serum insulin in humans

3.1 Introduction

Insulin is the major anabolic hormone regulating the glucose homeostasis. The impaired action of insulin is a characteristics of type 2 diabetes mellitus (T2DM) [93], accompanied by abnormality in the temporal patterns of circulating insulin concentration [19-21]. In physiological condition, the circulating insulin concentration changes over the course of 24 h, including a persistently low level during fasting and a surge in response to food ingestion, which are known to be basal and additional secretions from the pancreas, respectively [94,95].

Ability of additional insulin secretion is assessed by the oral glucose tolerance test (OGTT) [96], in which a subject's ability to tolerate the glucose load (glucose tolerance) is evaluated by measuring the circulating glucose concentration after an overnight fast (fasting plasma glucose concentration; FPG) and again 2 h after a 75-g oral glucose load (2-h post-load glucose concentration; 2-h PG) [7]. During this test, the circulating insulin concentration transiently increases and then continuously increases or decreases, known as the early and late phases of insulin secretion, respectively [97,98]. The direct contribution of circulating glucose concentration to circulating insulin concentration is assessed by use of an intravenous glucose tolerance test (IVGTT) [15]. This test excludes the effects of intestinal absorption of glucose and incretins secretion that trigger insulin secretion, thus permitting quantitative estimates of the ability of circulating glucose to initiate insulin secretion. During this test, the circulating

insulin concentration transiently increases during the first 10 min and then continuously increases during the following 120 min, which are known as the first and second phase of insulin secretion, respectively [18].

These temporal patterns of circulating insulin concentration differ across the stages of progression from normal glucose tolerance (NGT) over borderline type to T2DM. In general, plasma insulin concentration during the late-phase secretion of an OGTT in borderline type subjects is higher than in NGT subjects, whereas the concentration during the early-phase secretion is similar in NGT and borderline type subjects [97,98]. Plasma insulin concentration during the first-phase secretion of an IVGTT decreases as glucose intolerance progresses, whereas that during the second-phase secretion is relatively maintained [19-21]. Such changes of the temporal patterns of circulating insulin concentration during the progression of glucose intolerance from NGT to T2DM suggest these temporal patterns are involved in the maintenance and impairment of glucose homeostasis. Together with the measurement of circulating glucose concentration, the time course of circulating insulin concentration is used to assess insulin secretion from the pancreas and insulin sensitivity.

However, it is difficult to assess the insulin secretion and sensitivity of body tissues directly from the circulating insulin concentration because of the negative feedback between circulating insulin and glucose. A rise in circulating glucose concentration stimulates insulin secretion, and the resultant rise in circulating insulin concentration stimulates glucose uptake, causing circulating glucose concentration to fall. This feedback means there is mutual dependence between glucose and insulin, making it difficult to distinguish the effect of

insulin secretion and sensitivity directly from the circulating insulin concentration [16].To directly assess insulin secretion without the effect of the feedback from insulin to glucose, DeFronzo et al. [16] developed the hyperglycemic and hyperinsulinemic-euglycemic clamp techniques, in which indices for insulin secretion and insulin sensitivity are independently obtained without an effect of the feedback relation, respectively.

The body controls the circulating insulin concentration by balancing insulin secretion and insulin clearance. The major organs responsible for insulin clearance are the liver, which removes portal insulin during first-pass transit [39,40], and insulin-sensitive tissues such as muscle, which remove insulin from the systemic circulation [41]. The insulin clearance from portal vein in the liver and from peripheral plasma in other organs is called hepatic and peripheral insulin clearance, respectively. Although the relationship between changes of insulin clearance and the progression of glucose intolerance have been reported, the effects of insulin clearance are controversial. Some studies found that during the progression of glucose intolerance, insulin clearance decreased [78-81], whereas hepatic insulin clearance increased [85] or decreased [78,84]. Thus, the hepatic and peripheral insulin clearances were not explicitly distinguished, making it difficult to interpret the effect of both types.

Hepatic insulin clearance cannot be assessed directly from circulating insulin concentration because insulin is extracted from the liver before secreted insulin is delivered into the systemic circulation. However, insulin is secreted at an equimolar ratio with C-peptide, a peptide cleaved from proinsulin to produce insulin, which is not extracted in the liver. Thus, by measuring circulating C-peptide concentration simultaneously with circulating

insulin concentration, the pre-hepatic insulin concentration can be accurately assessed. The C-peptide index, which is the ratio of circulating glucose to C-peptide concentration, is an index of insulin secretion with clinical utility [99]. Hepatic insulin clearance is clinically quantified as the ratio of circulating insulin to C-peptide concentration during the first 10 min under the hyperglycemic clamp condition [42].

The clinical indices of insulin secretion and clearance are indirect measures because they are obtained from temporal patterns of circulating concentrations, which are simultaneously affected by insulin secretion and clearance. Therefore, the clinical index of insulin secretion implicitly involves the effect of insulin clearance and vice versa. Mathematical models have been developed for specifically quantifying insulin secretion, sensitivity, and clearance abilities from temporal patterns of circulating concentration by accounting for this mutual dependence [32,38,43]. The model known as the minimal model is used to estimate insulin sensitivity and insulin secretion abilities for each individual based on the time courses of circulating glucose and insulin concentrations during IVGTT [23]. Furthermore, from the parameters of the model, Bergman et al. [23] identified a relationship between the subject's glucose intolerance and the product of insulin secretion and sensitivity.

In Chapter 2, I developed a mathematical model based on time courses of plasma glucose and serum insulin during the consecutive hyperglycemic and hyperinsulinemic-euglycemic clamp conditions, and estimated the parameters of insulin secretion, sensitivity, and peripheral insulin clearance for each subject. I found that peripheral insulin clearance significantly decreased from NGT to borderline type to T2DM [52]. However, the hepatic and

peripheral insulin clearance could not be distinguished because C-peptide was not incorporated in the model [52].

Hepatic insulin clearance is calculated as the difference between pre-hepatic and post-hepatic insulin concentrations assessed by comparing circulating C-peptide and insulin concentrations, because C-peptide, unlike insulin, is not removed by the liver. Since the circulating C-peptide concentration is also controlled by its secretion and clearance, a mathematical model for C-peptide kinetics was developed [62]. The models for circulating insulin and C-peptide have been used to estimate the secretion and kinetics of insulin and C-peptide, as well as hepatic insulin clearance [34,44-50]. However, peripheral insulin clearance was not assessed in the models, because exogenous insulin infusion, which is required for accurate estimation of peripheral insulin clearance, was not performed.

Recently, Polidori et al. [51] reported that both hepatic and extrahepatic insulin clearance, corresponding to peripheral insulin clearance, can be estimated by modeling analysis using plasma insulin and C-peptide concentrations obtained from the insulin-modified frequently sampled IVGTT. The parameters of hepatic and peripheral insulin clearance in the model were not highly correlated, suggesting that the two types of insulin clearance are regulated differently. In addition, hepatic insulin clearance was negatively correlated with insulin secretion, and peripheral insulin clearance was positively correlated with insulin sensitivity. However, hepatic and peripheral insulin clearance in T2DM subjects and the roles of both types of clearance in the changes in temporal pattern of circulating insulin concentration during the progression of glucose intolerance have yet to be examined.

In Chapter 3, I developed a mathematical model based on the time course of the serum insulin and C-peptide concentrations during the consecutive hyperglycemic and hyperinsulinemic-euglycemic clamp conditions, and estimated hepatic and peripheral insulin clearance for each subject. The parameters from 111 subjects (47 NGT, 17 borderline type, and 47 T2DM) showed a significant increase in hepatic insulin clearance and significant decrease in peripheral insulin clearance from NGT to borderline type and T2DM, respectively. It was also found that hepatic and peripheral insulin clearance play distinct roles in the abnormal temporal patterns of serum insulin concentration from NGT to borderline type and T2DM, namely an increase in hepatic insulin clearance reduces the amplitude of serum insulin concentration, whereas a decrease in peripheral insulin clearance changes the temporal patterns of serum insulin concentration from transient to sustained.

3.2 Materials and Methods

3.2.1 Subjects and measurements

The data of actual measurement of 121 subjects (50 NGT, 18 borderline type, and 53 T2DM) during the consecutive hyperglycemic and hyperinsulinemic-euglycemic clamp analysis [17,52] were shared with the previous study in Chapter 2.

The clamp data contained measured concentration of plasma glucose and serum insulin as well as serum C-peptide in serum samples collected at 5, 10, 15, 60, 75, 90, 100, 190, and 220 min after the onset of the clamp analysis. First-phase insulin secretion during the hyperglycemic clamp was defined as the incremental area under the immunoreactive insulin (IRI) concentration curve (μU mL^{-1} min^{-1}) from 0 to 10 min (AUC_{IRI10}). The insulin sensitivity index (ISI) derived from the hyperinsulinemic-euglycemic clamp was calculated by dividing the mean glucose infusion rate during the final 30 min of the clamp (mg kg^{-1} min^{-1}) by both the plasma glucose (mg/dL) and serum insulin (μU/mL) levels at the end of the clamp and then multiplying the result by 100. A clamp-based analogue of the disposition index, the clamp disposition index (clamp DI), was calculated as the product of AUC_{IRI10} and ISI, as described previously [17]. The metabolic clearance rate (MCR) [16], an index of insulin clearance, was calculated by dividing the insulin infusion rate at the steady state (1.46 mU kg^{-1} min^{-1}) by the increase in insulin concentration above the basal level in the hyperinsulinemic-euglycemic clamp [17]: 1.46 (mU kg^{-1} min^{-1}) × body weight (kg) × body surface area (m^2)/(end IRI – fasting IRI) (μU/mL), where body surface area is defined as (body weight (kg))$^{1/2}$ × (body height (cm))$^{1/2}$ / 60 (Mosteller formula). The actual data for all 121 subjects are shown

in Ohashi *et at*. (in preparation) (Supplementary Fig. S10 and Supplementary Table S8).

3.2.2 Mathematical models

I developed six mathematical models for serum insulin and C-peptide kinetics based on the proposed models in order to choose the best model for reproducing the measurement of serum insulin and C-peptide during the consecutive hyperglycemic and hyperinsulinemic-euglycemic clamp (Fig. 18). In these models, *I* represents serum insulin concentration (pM), and *CP* and CP_1 represent serum C-peptide concentration (pM) including insulin and C-peptide secretion and hepatic and peripheral clearance. I used a conversion factor of insulin (6.00 nmol/U) [100] and the molecular weights of glucose (180.16 g/mol) and C-peptide (3020.3 g/mol) to convert the unit of serum insulin, plasma glucose, and serum C-peptide, respectively. Plasma glucose concentration *G* (mM) was used as input in the models, which was determined by stepwise interpolation of the measured plasma glucose data. Note that plasma glucose data were obtained as the 5-min average values, and each sampling time was reduced by 2 min in the calculation of stepwise interpolation.

The actual insulin infusion rate (*IIR*, mU kg^{-1} min^{-1}) was converted to the corresponding serum concentrations (*cIIR*) as follows:

$$cIIR(\mathrm{pM\,min^{-1}}) = \frac{IIR(\mathrm{mU\,kg^{-1}\,min^{-1}}) \cdot 6.00 \cdot 10^{-3}\,(\mathrm{pmol\,mU^{-1}}) \cdot BW}{BW \cdot BV} \cdot 10^{3} \qquad (20)$$

where *BW* and *BV* denote body weight and blood volume (75 and 65 mL/kg for men and women, respectively [69]).

In the models, insulin infusions are represented by *influx*. This flux follows the nonlinear

function *f* that predicts insulin infusion concentrations. Given that insulin infusion was performed only during the hyperinsulinemic-euglycemic (from 100 to 220 min) clamp, the function *f* was given by the following equations:

$$f(t) = \begin{cases} 0 & (t \le 100) \\ ii_1 \cdot \exp(ii_2 \cdot (t - 100)) + ii_3 & (t > 100) \end{cases} \quad (4)$$

where the parameters ii_j (j = 1, 2, 3) are estimated to reproduce *cIIR* with the function *f* for each subject by use of a nonlinear least squares technique [70]. Parameters for all subjects are shown in Ohashi et al. (in preparation) (Supplementary Table S9).

3.2.3 Parameter estimation

The model parameters for each subject were estimated to reproduce the actual measurement of time course of serum insulin *I* and C-peptide *CP* and CP_1 by a meta-evolutionary programming method to approach the neighbourhood of the local minimum, followed by application of the nonlinear least squares technique to reach the local minimum [71]. Each parameter was estimated in the range from 10^{-6} to 10^4. For these methods, the model parameters were estimated to minimize the objective function value, which is defined as the residual sum of squares (RSS) between the actual measurements by clamp analyses and the model simulation. *RSS* is given by:

$$RSS = \sum_{\text{points}} \left\{ \frac{I(t) - I_{\text{sim}}(t)}{I_{\text{mean}}} \right\}^2 + \sum_{\text{points}} \left\{ \frac{CP(t) - CP_{\text{sim}}(t)}{CP_{\text{mean}}} \right\}^2 \quad (21)$$

where

$$I_{\text{mean}} = \frac{\sum_{\text{subjects}} \sum_{\text{points}} I(t)}{\sum_{\text{subjects}} \text{points}} \tag{22}$$

$$CP_{\text{mean}} = \frac{\sum_{\text{subjects}} \sum_{\text{points}} CP(t)}{\sum_{\text{subjects}} \text{points}} \tag{23}$$

$I(t)$ and $CP(t)$ are the serum insulin and C-peptide concentration, and $I_{\text{sim}}(t)$ and $CP_{\text{sim}}(t)$ are simulated serum insulin and C-peptide concentrations at t min, respectively. Serum insulin and C-peptide concentrations were normalized by dividing them by the averages of serum concentrations over all time points of all subjects of insulin (I_{mean}, 302.7 pM) and C-peptide (CP_{mean}, 1475 pM), respectively. The numbers of parents and generations in the meta-evolutionary programming were 400 and 4000, respectively. Parameter estimation was tried 20 times by changing the initial parameter values for each subject, and the parameter with the smallest *RSS* among 20 trials was taken as the estimated solution of each subject. The estimated parameters for all subjects are shown in Ohashi et al. (in preparation) (Supplementary Table S9).

3.2.4 Model selection

The model was chosen among the six models according to Akaike information criterion (AIC). For a given model and an individual subject, AIC was calculated as follows:

$$AIC = n \ln\left(\frac{2\pi \cdot RSS}{n}\right) + n + 2K \tag{24}$$

where n is the total number of sampling time points of serum insulin and C-peptide concentration, and K is the number of estimated parameters of the model.

3.2.5 Determination of outliers of RSS and parameters

The outliers of RSS and model parameters were detected by the adjusted outlyingness (AO) [72]. The cutoff value of AO was $Q_3 + 1.5e^{3MC} \cdot IQR$, where Q_3, MC, and IQR are the third quartile, medcouple, and interquartile range, respectively. The medcouple is a robust measure of skewness [73]. The number of directions was set at 8000. Subjects found to have outlier RSS (2 NGT and 1 T2DM subjects) and outlier parameters (1 NGT, 1 borderline type, and 5 T2DM subjects) were excluded from further study.

3.2.6 Parameter sensitivity analysis

I defined the individual model parameter sensitivity [74] for each subject as follows:

$$S(f(x), x) = \frac{\partial \log f(x)}{\partial \log x} = \frac{x}{f(x)} \cdot \frac{\partial f(x)}{\partial x} \tag{6}$$

where x is the parameter value and $f(x)$ is *ipeak* or *iTPI*. The differentiation is numerically approximated by central difference $\frac{\partial f(x)}{\partial x} \approx \frac{f(x+\Delta x) - f(x-\Delta x)}{2\Delta x}$, and $x + \Delta x$ and $x - \Delta x$ were set so as to be increased [x (1.1x)] or decreased [x (0.9x)] by 10%, respectively. Finally, I defined the parameter sensitivity by the median of the individual parameter sensitivity for all subjects. I examined the parameter sensitivity in *Model VI* for six parameters of the rate constant related to serum insulin concentration, except X_b and k_{CPout}, which are nothing to do with changing the serum insulin concentration. The higher the absolute value of parameter sensitivity, the larger the effect of the parameter on *ipeak* or *iTPI*.

3.2.7 Statistical analysis

Unless indicated otherwise, data are expressed as the median with first and third quartiles. Medians of parameter values were compared among the NGT, borderline type, and T2DM subjects with the use of the two-sided Wilcoxon rank sum test with Benjamini Hochberg FDR multiple testing correction [76]. An FDR-corrected *P* value <0.05 was considered statistically significant.

3.3 Results

3.3.1 Plasma glucose, serum insulin, and C-peptide concentration during consecutive hyperglycemic and hyperinsulinemic-euglycemic clamp

At first, I calculated the mean time courses of measured concentrations of plasma glucose, serum insulin, and C-peptide during the consecutive hyperglycemic and hyperinsulinemic-euglycemic clamp analysis of NGT (n = 50), borderline type (n = 18), and T2DM (n = 53) subjects (Fig. 17) [17]. The time courses of plasma glucose and serum insulin were the same as those reported in Chapter 2.

During the hyperglycemic clamp at 0-90 min, plasma glucose concentration of each subject at the hyperglycemic plateau was similar among the groups with NGT, borderline type, and T2DM. Insulin secretion during both the first (0-15 min) and second phases (15-90 min) was clearly observed in the NGT and borderline type subjects, whereas insulin secretion during both phases was significantly reduced in the T2DM subjects. Serum C-peptide concentration showed a similar increase with insulin secretion during the first and second phase in the NGT and borderline type subjects, whereas serum C-peptide concentration was significantly lower in the T2DM subjects during both two phases. Although insulin and C-peptide should be secreted in an equimolar manner, the serum C-peptide concentration was higher than the serum insulin concentration. That is because insulin—but not C-peptide—was removed by the liver, and C-peptide clearance was slower than insulin clearance in the periphery.

During the hyperinsulinemic-euglycemic clamp at 100-220 min, serum insulin

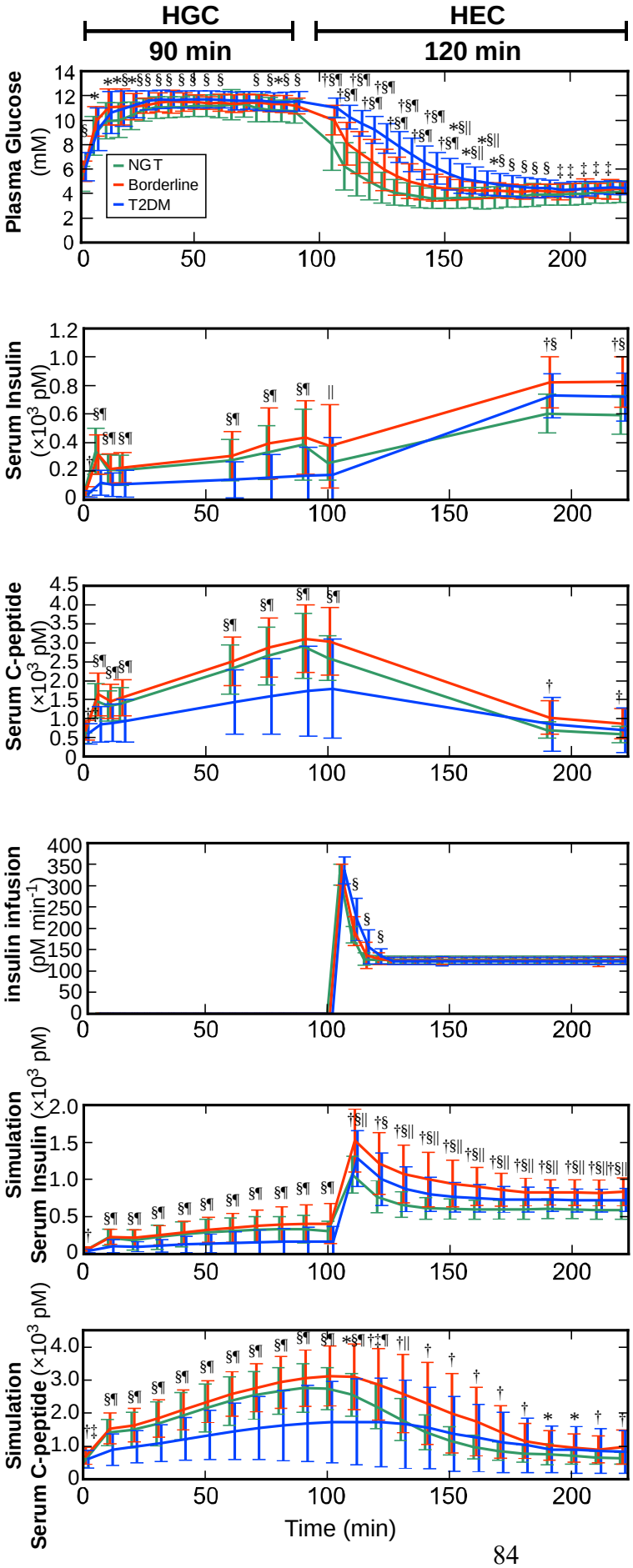
HGC
90 min
HEC
120 min
Plasma Glucose (mM)
NGT
Borderline
T2DM
Serum Insulin (×10³ pM)
Serum C-peptide (×10³ pM)
insulin infusion (pM min⁻¹)
Simulation Serum Insulin (×10³ pM)
Simulation Serum C-peptide (×10³ pM)
Time (min)

Figure 17. Time courses of concentrations of plasma glucose, serum insulin and C-peptide, and insulin infusion during the consecutive hyperglycemic (HGC) and hyperinsulinemic-euglycemic (HEC) clamp. Experimental (upper 4 panels) and simulation with *Model VI* (lower 2 panels) time courses are shown. Simulation time courses are plotted every 10 min. The mean ± SD among the subjects for NGT (green), borderline type (red), and T2DM, and significant differences at each time point are depicted. **P* < 0.05; †*P* < 0.01, NGT vs. borderline type; ‡*P* < 0.05; §*P* < 0.01, NGT vs. T2DM; ||*P* < 0.05; ¶*P* < 0.01, borderline type vs. T2DM (two-sample *t*-test with FDR correction).

The FDR-corrected *P* values are provided in Ohashi et al. (in preparation) (Supplementary Table S1).

concentration was at a steady-state plateau of hyperinsulinemia, but serum insulin concentration differed significantly from the NGT to borderline type and T2DM subjects. The mean serum insulin concentration of the NGT subjects was lowest, and that of the borderline type subjects was highest. These differences reflect the difference in the ability to remove infused insulin from serum among the three groups, in other words, the difference of the peripheral insulin clearance. The plasma glucose concentration returned to the basal level from hyperglycemia with different decay rate among the three groups. The mean decay rate was lowest in the T2DM subjects and highest in the NGT subjects. These differences reflect the decrease in the ability to promote the hypoglycemic effect in response to serum insulin, named insulin sensitivity, from NGT to borderline type to T2DM. The serum C-peptide concentration return to the fasting level in all groups, because only insulin was infused during the hyperinsulinemic-euglycemic clamp and C-peptide was derived only from endogenous secretion. The small but significant differences in serum C-peptide concentration between the NGT and borderline type subjects were shown.

3.3.2 Mathematical model alternatives for serum insulin and C-peptide kinetics

Many mathematical models that reproduce circulating insulin and C-peptide concentrations have been developed [23,34,44-48]. I developed six mathematical models based on these reported models, and selected one model which is appropriate for reproducing measured serum insulin and C-peptide concentrations during the consecutive hyperglycemic and hyperinsulinemic-euglycemic clamp [17,52] (Fig. 18). These models consist of the compartments

Model structure	Model equation	No. parameters
Model I 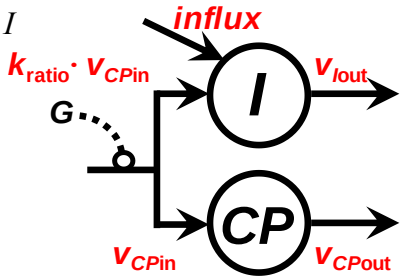	$v_{CPin} = CPS^{I} + CPS^{II}$ $CPS^{I} = k_{CP0}\delta(t)$ $CPS^{II} = \begin{cases} \gamma(G-h)t & (G > h) \\ 0 & (G \le h) \end{cases}$ $v_{Iout} = k_{Iout}(I - I_b)$ $v_{CPout} = k_{CPout}(CP - CP_b)$	6 k_{ratio}, k_{Iout}, k_{CPout}, k_{CP0}, γ, h
Model II 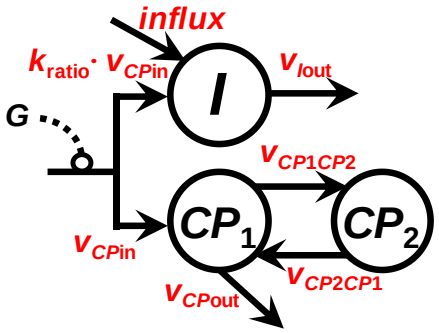	$v_{CPin} = CPS^{I} + CPS^{II}$ $CPS^{I} = k_{CP0}\delta(t)$ $CPS^{II} = \begin{cases} \gamma(G-h)t & (G > h) \\ 0 & (G \le h) \end{cases}$ $v_{Iout} = k_{Iout}(I - I_b)$ $v_{CP1CP2} = k_{12}(CP_1 - CP_b)$ $v_{CP2CP1} = k_{21}CP_2, \quad CP_2(0) = 0$ $v_{CPout} = k_{CPout}(CP_1 - CP_b)$	8 k_{ratio}, k_{Iout}, k_{CPout}, k_{12}, k_{21}, k_{CP0}, γ, h
Model III 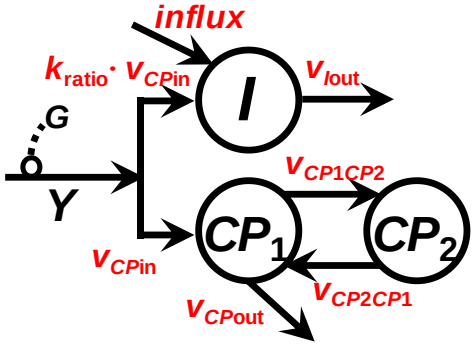	$\frac{dY}{dt} = \begin{cases} \alpha\{\beta(G-h) - Y\} & (G > h) \\ -\alpha Y & (G \le h) \end{cases}, Y(0) = 0$ $v_{CPin} = CPS^{III} + Y$ $CPS^{III} = \begin{cases} k_{CPd} \cdot \frac{dG}{dt} & \left(\frac{dG}{dt} > 0\right) \\ 0 & \left(\frac{dG}{dt} \le 0\right) \end{cases}$ $v_{Iout} = k_{Iout}(I - I_b)$ $v_{CP1CP2} = k_{12}(CP_1 - CP_b)$ $v_{CP2CP1} = k_{21}CP_2, \quad CP_2(0) = 0$ $v_{CPout} = k_{CPout}(CP_1 - CP_b)$	9 k_{ratio}, k_{Iout}, k_{CPout}, k_{12}, k_{21}, k_{CPd}, α, β, h

Model IV 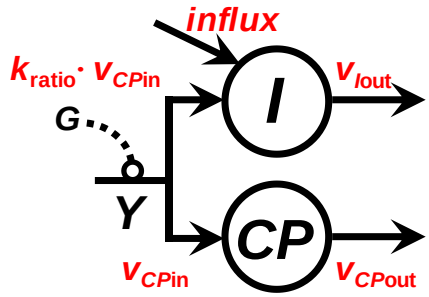	$\frac{dY}{dt} = \begin{cases} \alpha\{\beta(G-h)-Y\} & (G>h) \\ -\alpha Y & (G \le h) \end{cases}, Y(0)=0$ $v_{CPin} = CPS^{III} + Y$ $CPS^{III} = \begin{cases} k_{CPd} \cdot \frac{dG}{dt} & \left(\frac{dG}{dt} > 0\right) \\ 0 & \left(\frac{dG}{dt} \le 0\right) \end{cases}$ $v_{Iout} = k_{Iout}(I - I_b)$ $v_{CPout} = k_{CPout}(CP - CP_b)$	7 k_{ratio}, k_{Iout}, k_{CPout}, k_{CPd}, α, β, h
Model V 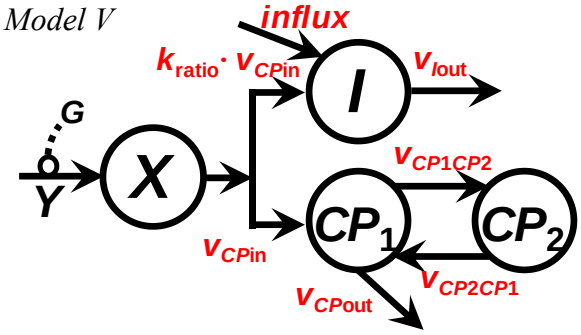	$\frac{dY}{dt} = \begin{cases} \alpha\{\beta(G-h)-Y\} & (G>h) \\ -\alpha Y & (G \le h) \end{cases}, Y(0)=0$ $v_{CPin} = \begin{cases} m \cdot X & (G>h) \\ 0 & (G \le h) \end{cases}, X(0) = X_b$ $v_{Iout} = k_{Iout}(I - I_b)$ $v_{CP1CP2} = k_{12}(CP_1 - CP_b)$ $v_{CP2CP1} = k_{21}CP_2, \quad CP_2(0) = 0$ $v_{CPout} = k_{CPout}(CP_1 - CP_b)$	10 k_{ratio}, k_{Iout}, k_{CPout}, k_{12}, k_{21}, m, X_b, α, β, h
Model VI 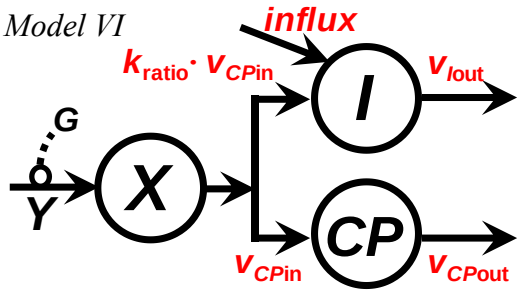	$\frac{dY}{dt} = \begin{cases} \alpha\{\beta(G-h)-Y\} & (G>h) \\ -\alpha Y & (G \le h) \end{cases}, Y(0)=0$ $v_{CPin} = \begin{cases} m \cdot X & (G>h) \\ 0 & (G \le h) \end{cases}, X(0) = X_b$ $v_{Iout} = k_{Iout}(I - I_b)$ $v_{CPout} = k_{CPout}(CP - CP_b)$	8 k_{ratio}, k_{Iout}, k_{CPout}, m, X_b, α, β, h

Figure 18. Six model alternatives for serum insulin and C-peptide kinetics.

Left panel: The structure of models. I (pM) is serum insulin concentration, CP and CP_1 (pM) are serum C-peptide concentration, CP_2 (pM) is C-peptide concentration in the extravascular compartment, and X (pM) is the amount of stored insulin and C-peptide. Insulin secretion and provision rate Y (pM min^{-1}) are controlled by plasma glucose concentration G (mM).

Middle panel: Mathematical representation of fluxes. Equations related to insulin infusion rate *influx* are shown in Methods.

Right panel: The number of parameters for estimation, referred to as *K* in the calculation of AIC (Methods).

corresponding to serum insulin and C-peptide concentration, including the structures of insulin and C-peptide secretion and their hepatic and peripheral clearance. Plasma glucose concentration and insulin infusion were used as inputs (Fig. 17).

Model I. The model for serum insulin and C-peptide kinetics derived from the combined model [44]. The model for insulin and C-peptide secretions (CPS^{I} and CPS^{II}) are from the insulin minimal model [23], instead of a cubic spline function in the combined model [44]. This model has two variables, three fluxes, and six parameters, which is the simplest structure among the six models. The differential equations of this model are as follows:

$$\begin{aligned}\frac{dI}{dt} &= k_{\text{ratio}} \cdot v_{CP\text{in}} - v_{I\text{out}} + influx \\ &= \begin{cases} k_{\text{ratio}} \cdot \left(k_{CP0}\delta(t) + \gamma(G-h)t\right) - k_{I\text{out}} \cdot \left(I - I_{\text{b}}\right) + f(t) & \left(G > h\right) \\ k_{\text{ratio}} \cdot k_{CP0}\delta(t) - k_{I\text{out}} \cdot \left(I - I_{\text{b}}\right) + f(t) & \left(G \le h\right) \end{cases}\end{aligned} \tag{25}$$

$$\begin{aligned}\frac{dCP}{dt} &= v_{CP\text{in}} - v_{CP\text{out}} \\ &= \begin{cases} k_{CP0}\delta(t) + \gamma(G-h)t - k_{CP\text{out}} \cdot \left(CP - CP_{\text{b}}\right) & \left(G > h\right) \\ k_{CP0}\delta(t) - k_{CP\text{out}} \cdot \left(CP - CP_{\text{b}}\right) & \left(G \le h\right) \end{cases}\end{aligned} \tag{26}$$

Eq. 25 describes how serum insulin concentration I increases according to the post-hepatic insulin delivery $k_{\text{ratio}} \cdot v_{CP\text{in}}$ and infused insulin *influx*, and decreases according to peripheral insulin clearance $v_{I\text{out}}$. $v_{CP\text{in}}$ is expanded as $k_{CP0}\delta(t) + \gamma(G - h)t$ when $G > h$, otherwise $k_{CP0}\delta(t)$, which corresponds to the sum of first-phase (CPS^{I}) and second-phase (CPS^{II}) secretion of insulin and C-peptide. The parameter k_{CP0} (pM) is the zero-intercept immediately after the start of hyperglycemic clamp, and $\delta(t)$ is the Dirac delta function approximated as follows:

$$\delta(t) = \begin{cases} 10^{6} & \left(t \le 10^{-6}\right) \\ 0 & \left(t > 10^{6}\right) \end{cases} \tag{27}$$

$k_{\text{ratio}} \cdot v_{CP\text{in}}$ indicates that only a fraction k_{ratio} of secreted insulin is delivered into

peripheral circulation after passage through the liver, when $G > h$, otherwise zero. The parameter k_{ratio} is the molar ratio of post-hepatic insulin to C-peptide, which represents the fraction of insulin delivered to the peripheral circulation without being extracted by the liver. Given that C-peptide is not extracted by the liver, k_{ratio} can represent the remaining fraction of insulin after the extraction by the liver over the total amount of secreted insulin, and changes from 0 to 1. Therefore, $(1 - k_{ratio})$ represents the fraction of insulin extracted by the liver and not delivered to the peripheral circulation, and corresponds to hepatic insulin clearance. *influx* is the insulin infusion rate during hyperinsulinemic-euglycemic clamp. The serum rate at time t is represented by $f(t)$ (Methods). $v_{I\text{out}}$ represents serum insulin degradation with the rate parameter $k_{I\text{out}}$ (min^{-1}). Therefore, $k_{I\text{out}}$ represents insulin degradation in the periphery and corresponds to peripheral insulin clearance.

Eq. 26 describes how serum C-peptide concentration CP increases according to the C-peptide secretion $v_{CP\text{in}}$, and decreases according to peripheral C-peptide clearance $v_{CP\text{out}}$. $v_{CP\text{in}}$ is C-peptide secretion and is delivered to peripheral circulation without hepatic clearance. $v_{CP\text{out}}$ represents serum C-peptide degradation with the rate parameter $k_{CP\text{out}}$ (min^{-1}).

Model II. This model is identical to *Model I*, except the two-compartmental structure for the serum C-peptide kinetics [45,62], and has three variables, five fluxes, and eight parameters. The differential equations of CP_1 and CP_2 are as follows:

$$\frac{dCP_1}{dt} = v_{CP\text{in}} - v_{CP1CP2} + v_{CP2CP1} - v_{CP\text{out}}$$
$$= \begin{cases} k_{CP0}\delta(t) + \gamma(G-h)t - k_{12}\left(CP_1 - CP_\text{b}\right) + k_{21}CP_2 - k_{CP\text{out}} \cdot \left(CP_1 - CP_\text{b}\right) & (G > h) \\ k_{CP0}\delta(t) - k_{12}\left(CP_1 - CP_\text{b}\right) + k_{21}CP_2 - k_{CP\text{out}} \cdot \left(CP_1 - CP_\text{b}\right) & (G \le h) \end{cases} \quad (28)$$

$$\frac{dCP_2}{dt} = v_{CP1CP2} - v_{CP2CP1}$$
$$= k_{12}\left(CP_1 - CP_\text{b}\right) - k_{21}CP_2 \quad (29)$$

Eq. 28 describes how serum C-peptide concentration CP_1 increases according to the C-peptide secretion $v_{CP\text{in}}$ and transfer from extravascular compartment v_{CP2CP1}, and decreases according to peripheral C-peptide clearance $v_{CP\text{out t}}$ and transfer to extravascular compartment v_{CP1CP2}. v_{CP2CP1} and v_{CP1CP2} represents C-peptide distribution from extravascular compartment to serum and vice versa, with the rate parameter k_{21} and k_{12} (min^{-1}), respectively.

Eq. 29 describes how C-peptide in the extravascular compartment CP_2 increases according to transfer from serum v_{CP1CP2}, and decreases according to transfer to serum v_{CP2CP1}.

Model III. The model for serum insulin and C-peptide kinetics is same as *Model II*, and the model for insulin and C-peptide secretions (CPS^{III} and Y) are from another model [34,46,47]. This model has four variables, seven fluxes, and nine parameters. The differential equations of I, CP_1, and Y are as follows:

$$\frac{dI}{dt} = k_\text{ratio} \cdot v_{CP\text{in}} - v_{I\text{out}} + influx$$
$$= \begin{cases} k_\text{ratio} \cdot \left(k_{CP\text{d}} \cdot \frac{dG}{dt} + Y\right) - k_{I\text{out}} \cdot \left(I - I_\text{b}\right) + f(t) & \left(\frac{dG}{dt} > 0\right) \\ k_\text{ratio} \cdot Y - k_{I\text{out}} \cdot \left(I - I_\text{b}\right) + f(t) & \left(\frac{dG}{dt} \le 0\right) \end{cases} \quad (30)$$

$$\frac{dCP_1}{dt} = v_{CP\text{in}} - v_{CP1CP2} + v_{CP2CP1} - v_{CP\text{out}}$$

$$= \begin{cases} k_{CP\text{d}} \cdot \dfrac{dG}{dt} + Y - k_{12}\left(CP_1 - CP_\text{b}\right) + k_{21}CP_2 - k_{CP\text{out}} \cdot \left(CP_1 - CP_\text{b}\right) & \left(\dfrac{dG}{dt} > 0\right) \\ Y - k_{12}\left(CP_1 - CP_\text{b}\right) + k_{21}CP_2 - k_{CP\text{out}} \cdot \left(CP_1 - CP_\text{b}\right) & \left(\dfrac{dG}{dt} \le 0\right) \end{cases} \quad (31)$$

$$\frac{dY}{dt} = \begin{cases} a\{b(G - h) - Y\} & (G > h) \\ -aY & (G \le h) \end{cases}, \; Y(0) = 0 \quad (32)$$

Eq. 30 and 31 describe the changes of serum insulin and C-peptide concentration similar to Eq. 25 and 28, respectively, except that $v_{CP\text{in}}$ is expanded as $k_{CPd} \cdot dG/dt + Y$ when $dG/dt > 0$, otherwise Y, which corresponds to the sum of insulin and C-peptide secretion controlled by the rate of change of plasma glucose concentration (CPS^{III}) and by glucose concentration (Y). The parameter k_{CPd} describes the effect of the rate of change of glucose on insulin secretion when glucose concentration is increasing.

Eq. 32 describes how insulin provision rate Y increases according to $\alpha\beta(G - h)$ when $G > h$, otherwise zero, and decreases with αY. This means that provision of insulin and C-peptide tends with a time constant $1/\alpha$ (min) toward a steady-state value linearly related via parameter β (min^{-1}) to plasma glucose concentration G (mM) above its basal level h.

Model IV. This model is identical to *Model III*, except the one-compartmental structure for the serum C-peptide kinetics is similar to *Model I*, and has three variables, five fluxes, and seven parameters. The differential equations of *CP* are as follows:

$$\frac{dCP}{dt} = v_{CP\text{in}} - v_{CP\text{out}}$$
$$= \begin{cases} k_{CPd} \cdot \dfrac{dG}{dt} + Y - k_{CP\text{out}} \cdot \left(CP - CP_b\right) & \left(\dfrac{dG}{dt} > 0\right) \\ Y - k_{CP\text{out}} \cdot \left(CP - CP_b\right) & \left(\dfrac{dG}{dt} \le 0\right) \end{cases} \quad (33)$$

Eq. 33 describes the change of serum C-peptide concentration similar to Eq. 26, except that $v_{CP\text{in}}$ is expanded as $k_{CPd} \cdot dG/dt + Y$ when $dG/dt > 0$, otherwise Y, similarly described in Eq. 31.

Model V. The model for serum insulin and C-peptide kinetics is same as *Model II*, and the model for insulin and C-peptide secretions (X and Y) are from the C-peptide minimal model [46,48]. This model has five variables, eight fluxes, and 10 parameters. The differential equations of I, CP_1, and X are as follows:

$$\frac{dI}{dt} = k_{\text{ratio}} \cdot v_{CP\text{in}} - v_{I\text{out}} + influx$$
$$= \begin{cases} k_{\text{ratio}} \cdot m \cdot X - k_{I\text{out}} \cdot \left(I - I_b\right) + f(t) & \left(G > h\right) \\ -k_{I\text{out}} \cdot \left(I - I_b\right) + f(t) & \left(G \le h\right) \end{cases} \quad (34)$$

$$\frac{dCP_1}{dt} = v_{CP\text{in}} - v_{CP1CP2} + v_{CP2CP1} - v_{CP\text{out}}$$
$$= \begin{cases} m \cdot X - k_{12}\left(CP_1 - CP_b\right) + k_{21}CP_2 - k_{CP\text{out}} \cdot \left(CP_1 - CP_b\right) & \left(G > h\right) \\ -k_{12}\left(CP_1 - CP_b\right) + k_{21}CP_2 - k_{CP\text{out}} \cdot \left(CP_1 - CP_b\right) & \left(G \le h\right) \end{cases} \quad (35)$$

$$\frac{dX}{dt} = Y - v_{CP\text{in}} = \begin{cases} Y - m \cdot X & \left(G > h\right) \\ Y & \left(G \le h\right) \end{cases} \quad (36)$$

Eq. 34 and 35 describe the change of serum insulin and C-peptide concentration similar to Eq. 25 and 28, except that $v_{CP\text{in}}$ is expanded as $m \cdot X$, which corresponds to insulin and C-peptide secretion when $G > h$, otherwise zero.

Eq. 36 describes that X (pM) increases according to the provision rate Y (pM min^{-1}) and decreases according to the insulin and C-peptide secretion $v_{CP\mathrm{in}}$. $v_{CP\mathrm{in}}$ is X secreted at the rate m (min^{-1}) when $G > h$, otherwise zero. The initial value of X, X_b (pM), is the parameter and is responsible for the first-phase secretion, whereas the slower second-phase secretion derives from provision Y.

Model VI. This model is identical to *Model V*, except the one-compartmental structure for the serum C-peptide kinetics is similar to *Model I*, and has four variables, six fluxes, and eight parameters. The differential equations of CP are as follows:

$$\begin{aligned}\frac{dCP}{dt} &= v_{CP\mathrm{in}} - v_{CP\mathrm{out}} \\ &= \begin{cases} m \cdot X - k_{CP\mathrm{out}} \cdot \left(CP - CP_\mathrm{b}\right) & \left(G > h\right) \\ -k_{CP\mathrm{out}} \cdot \left(CP - CP_\mathrm{b}\right) & \left(G \le h\right) \end{cases}\end{aligned} \tag{37}$$

Eq. 37 describes the change of serum C-peptide concentration similar to Eq. 26, except that $v_{CP\mathrm{in}}$ is expanded as $m \cdot X$, which corresponds to insulin and C-peptide secretion when $G > h$, otherwise zero, similarly described in Eq. 35.

3.3.3 Selected model for serum insulin and C-peptide kinetics

For each of the 121 subjects, parameters of the six models were estimated by using actual measurements of plasma glucose, serum insulin, and C-peptide concentration of clamp analysis (Methods). The examples of simulation with the estimated parameters of *Model VI* in Fig. 18 in each of NGT, borderline type, and T2DM subjects are shown in Fig. 19, and the simulations for all subjects are provided in Ohashi et al. (in preparation) (Supplementary Fig.

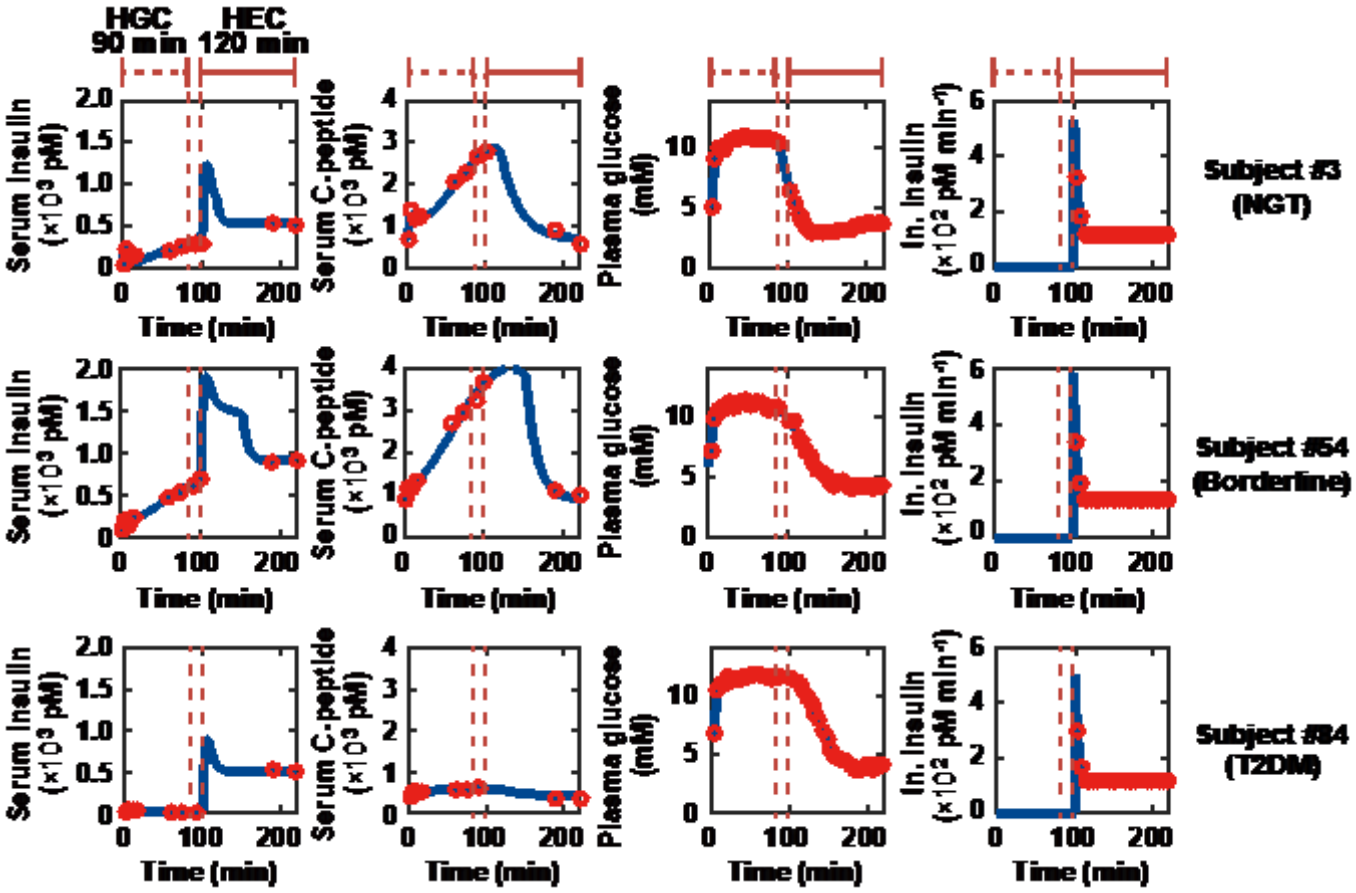

Figure 19. Time courses of serum insulin and C-peptide, plasma glucose, and infused (In.) insulin for typical NGT, borderline type, and T2DM subjects. Red circles and blue curves are actual measurement during the clamp analysis and simulation with *Model VI*, respectively. Note that plasma glucose concentration was not reproduced by the model, just determined by linear interpolation and used as input in the model.

S10).

Since I hypothesized that the structure of the control of circulating insulin concentration may differ among the pathogenesis of T2DM, I employed the model to reproduce time courses of serum insulin and C-peptide concentration for each subject with a simpler model structure, which took the minimum value of Akaike information criterion (AIC) [101] in the six mathematical models. The AIC is the statistical criterion for comparing the goodness of fit of a model with each other.

The model consisting of four variables (*Model VI* in Fig. 18) was selected as the best model with the minimum AIC for 76 of 121 subjects (Fig. 20; Table 4). In this model, the variables *I* and *CP* correspond to serum concentration of insulin and C-peptide, respectively. The variable *X* corresponds to stored insulin and C-peptide in β-cells or β-cell masses. Because insulin and C-peptide are stored in equimolar through the synthesis, a single variable, *X*, is used to represent both. The variable *Y* is the insulin provision rate depending on plasma glucose concentration, *G*. The differential equations of the model are as follows:

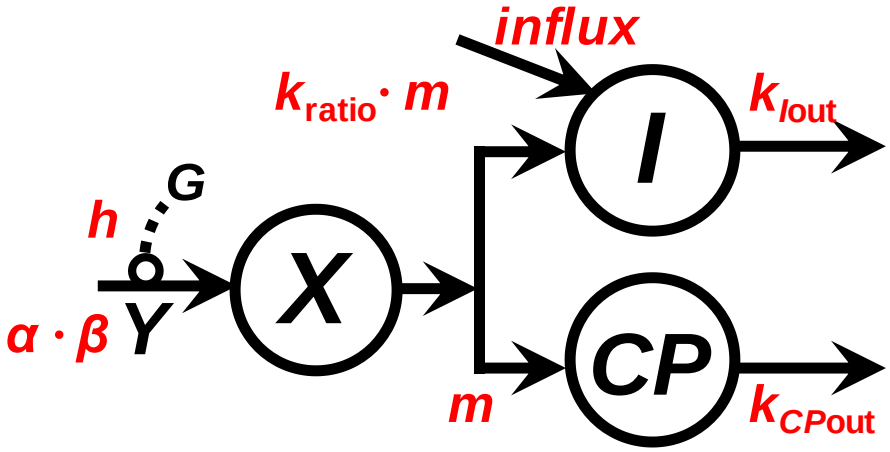

Figure 20. The model structures of serum insulin and C-peptide kinetics (see also Eqs. 32, 34, 36, and 37 and *Model VI* in Fig. 18). *I* and *CP* are serum insulin and C-peptide concentration, respectively. *X* is the amount of stored insulin and C-peptide, and *Y* is the provision rate controlled by plasma glucose concentration, *G*. Arrows indicate fluxes with corresponding parameters (red).

The differential equations of this model are following:

$$\frac{dY}{dt} = \begin{cases} a\{b(G-h)-Y\} & (G>h) \\ -aY & (G\le h) \end{cases}, \; Y(0)=0 \tag{32}$$

$$\frac{dX}{dt} = Y - v_{CPin} = \begin{cases} Y - m\cdot X & (G>h) \\ Y & (G\le h) \end{cases}, \quad X(0)=X_b \tag{36}$$

$$\begin{aligned} \frac{dI}{dt} &= k_{ratio}\cdot v_{CPin} - v_{Iout} + influx \\ &= \begin{cases} k_{ratio}\cdot m\cdot X - k_{Iout}\cdot(I-I_b) + f(t) & (G>h) \\ -k_{Iout}\cdot(I-I_b) + f(t) & (G\le h) \end{cases}, \quad I(0)=I_b \end{aligned} \tag{34}$$

$$\begin{aligned} \frac{dCP}{dt} &= v_{CPin} - v_{CPout} \\ &= \begin{cases} m\cdot X - k_{CPout}\cdot(CP-CP_b) & (G>h) \\ -k_{CPout}\cdot(CP-CP_b) & (G\le h) \end{cases}, \quad CP(0)=CP_b \end{aligned} \tag{37}$$

Table 4. Model selection based on the Akaike information criterion (AIC)

Model	No. subjects of min AIC	NGT	Borderline	T2DM	AIC mean ± SD
I	25	7	4	14	–21.1 ± 22.9*
II	5	3	1	1	–19.0 ± 24.2*
III	0	0	0	0	–16.2 ± 24.9*
IV	7	0	0	7	–17.2 ± 25.3*
V	8	4	3	1	–28.4 ± 26.2
VI	76	36	10	30	–31.4 ± 25.2
Total	121	50	18	53	

AIC was calculated for each model for each subject. The number of subjects who selected each model with minimum AIC is listed (see Methods). *AIC significantly differs from *Model VI* ($P < 0.01$, corrected by the number of *t*-tests, multiplied by 5).

$$\frac{dY}{dt} = \begin{cases} a\{b(G-h)-Y\} & (G>h) \\ -aY & (G\le h) \end{cases}, Y(0)=0 \tag{32}$$

$$\frac{dX}{dt} = Y - v_{CP\text{in}} = \begin{cases} Y - m\cdot X & (G>h) \\ Y & (G\le h) \end{cases}, \quad X(0)=X_{\text{b}} \tag{36}$$

$$\begin{aligned} \frac{dI}{dt} &= k_{\text{ratio}}\cdot v_{CP\text{in}} - v_{I\text{out}} + influx \\ &= \begin{cases} k_{\text{ratio}}\cdot m\cdot X - k_{I\text{out}}\cdot(I-I_{\text{b}}) + f(t) & (G>h) \\ -k_{I\text{out}}\cdot(I-I_{\text{b}}) + f(t) & (G\le h) \end{cases}, \quad I(0)=I_{\text{b}} \end{aligned} \tag{34}$$

$$\begin{aligned} \frac{dCP}{dt} &= v_{CP\text{in}} - v_{CP\text{out}} \\ &= \begin{cases} m\cdot X - k_{CP\text{out}}\cdot(CP-CP_{\text{b}}) & (G>h) \\ -k_{CP\text{out}}\cdot(CP-CP_{\text{b}}) & (G\le h) \end{cases}, \quad CP(0)=CP_{\text{b}} \end{aligned} \tag{37}$$

where I_{b} and CP_{b} correspond to fasting (basal) serum insulin and C-peptide concentration, respectively, directly given by the measurement, and X_{b} is an initial value of X to be estimated.

Eq. 32 describes how insulin provision rate Y increases according to $\alpha\beta(G - h)$ when $G > h$, otherwise zero, and decreases with αY. This means that provision of X, stored amounts of insulin and C-peptide, depends on parameter α and β, and stimulated only when the plasma glucose concentration exceeds the threshold value, h, which may correspond to the fasting plasma glucose concentration.

Eq. 36 describes how X increases according to the provision rate Y and decreases according to the insulin and C-peptide secretion $v_{CP\text{in}}$. $v_{CP\text{in}}$ is X secreted at the rate m when $G > h$, otherwise zero. Since X_{b}, which is the initial value of X, relates to the insulin and C-peptide secretion when $G > h$ for the first time during hyperglycemic clamp, X_{b} is responsible for the first-phase secretion[48].

Eq. 34 describes how serum insulin concentration I increases according to the post-hepatic insulin delivery, $k_{\text{ratio}} \cdot v_{CP\text{in}}$, and infused insulin, *influx*, and decreases according to peripheral insulin clearance $v_{I\text{out}}$. $k_{\text{ratio}} \cdot v_{CP\text{in}}$ is expanded as $k_{\text{ratio}} \cdot m \cdot X$, which corresponds to insulin delivered into peripheral circulation after passage through the liver, when $G > h$, otherwise zero. The parameter k_{ratio} is the molar ratio of post-hepatic insulin to secreted C-peptide, which represents the fraction of insulin delivered to the peripheral circulation without being extracted by the liver. Given that C-peptide is not extracted by the liver, k_{ratio} can represent the remaining fraction of insulin after the extraction by the liver over the total amount of secreted insulin, and ranges from 0 to 1. Therefore, $(1 - k_{\text{ratio}})$ represents the fraction of insulin extracted by the liver and not delivered to the peripheral circulation and corresponds to hepatic insulin clearance. *influx* is the insulin infusion rate during hyperinsulinemic-euglycemic clamp. The infusion rate at time t is represented by the function $f(t)$ (Methods). $v_{I\text{out}}$ represents serum insulin degradation with the rate parameter $k_{I\text{out}}$. Therefore, $k_{I\text{out}}$ represents insulin degradation in the periphery and corresponds to peripheral insulin clearance.

Eq. 37 describes how serum C-peptide concentration CP increases according to the C-peptide secretion $v_{CP\text{in}}$ and decreases according to peripheral C-peptide clearance $v_{CP\text{out}}$. $v_{CP\text{in}}$ is C-peptide secreted and delivered to peripheral serum without hepatic clearance. $v_{CP\text{out}}$ represents serum C-peptide degradation with the rate parameter $k_{CP\text{out}}$.

3.3.4 Comparing between *Model VI* and models selected by each subject

The 45 of 121 subjects did not selected this model (Fig. 20; *Model VI* in Fig. 18). I compared some aspects between *Model VI* and other models.

First, there seemed to be no bias in the distribution of the number of NGT, borderline type, and T2DM subjects among the models which were selected as the best model by subjects (Table 4). *Model VI* was selected even if AIC of each model was calculated using measured concentrations of all 121 subjects instead of using measured concentration of each subject (Table 5). The distributions of the residual sum of squares (RSS) between measured and simulated concentrations of serum insulin and C-peptide in this model were not significantly different between the 45 subjects who did not selected the model and the 76 subjects who selected this model with minimum AIC (Fig. 21). However, in the RSS distribution of all 121 subjects in this model, RSS values of three subjects were relatively high, and detected as outliers. These three subjects were excluded from the analysis in this study (Fig. 21).

Second, I examined the relationship between the temporal patterns of serum insulin and C-peptide concentrations and the model which was selected by the subjects who had those patterns. To classify the temporal patterns of serum insulin and C-peptide concentration among the subjects, I performed hierarchical clustering with actual measurements of serum insulin and C-peptide concentration of clamp analysis (Fig. 22 and 23).

Cluster 1: Serum insulin and C-peptide concentrations increase during both first-phase (0–15 min) and second-phase secretion (15–90 min) under hyperglycemic clamp, and serum

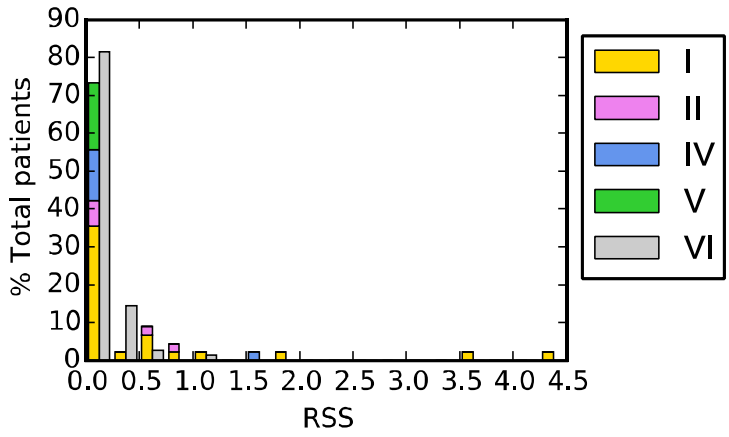

Figure 21. The distribution of residual sum of squares (RSS) between time courses of insulin and C-peptide concentrations reproduced by *Model VI* and serum measurement. Relative frequency histograms of 76 subjects who were optimal for *Model VI* (gray) and of 45 subjects who were not optimal for *Model VI* (yellow, pink, blue, and green indicate subjects who were optimal for *Models I*, *II*, *IV*, and *V*, respectively) are shown. The bin size of each histogram is 0.25. These two RSS distributions were not significantly different (Kolmogorov-Smirnov test, $P = 0.118$). The subjects with upper three RSS values (#104: T2DM, RSS = 4.42, #6: NGT, RSS = 3.58, #26: NGT, RSS = 1.96) were excluded as outliers of the RSS distribution of all 121 subjects (adjusted outlyingness, see Methods).

Table 5. AIC of each model calculated using measure time courses of all 121 subjects

Model	RSS	AIC	No. parameters
I	49.0	-1050	726
II	50.9	-479	968
III	53.2	-129	1089
IV	61.4	-272	847
V	29.2	-1320	1210
VI	31.8	-1600	968

RSS between the time courses of measurement and simulation of all 121 subjects is given by summing RSS (Eq. 21) for all subjects.

$$RSS = \sum_{subjects}\left[\sum_{\text{points}}\left\{\frac{I(t)-I_{\text{sim}}(t)}{I_{\text{mean}}}\right\}^2 + \sum_{\text{points}}\left\{\frac{CP(t)-CP_{\text{sim}}(t)}{CP_{\text{mean}}}\right\}^2\right] \tag{38}$$

AIC was calculated according to Eq. 24, where n is the total number of sampling time points of serum insulin and C-peptide for all subjects, and K is the number of estimated parameters of each model for all subjects as listed

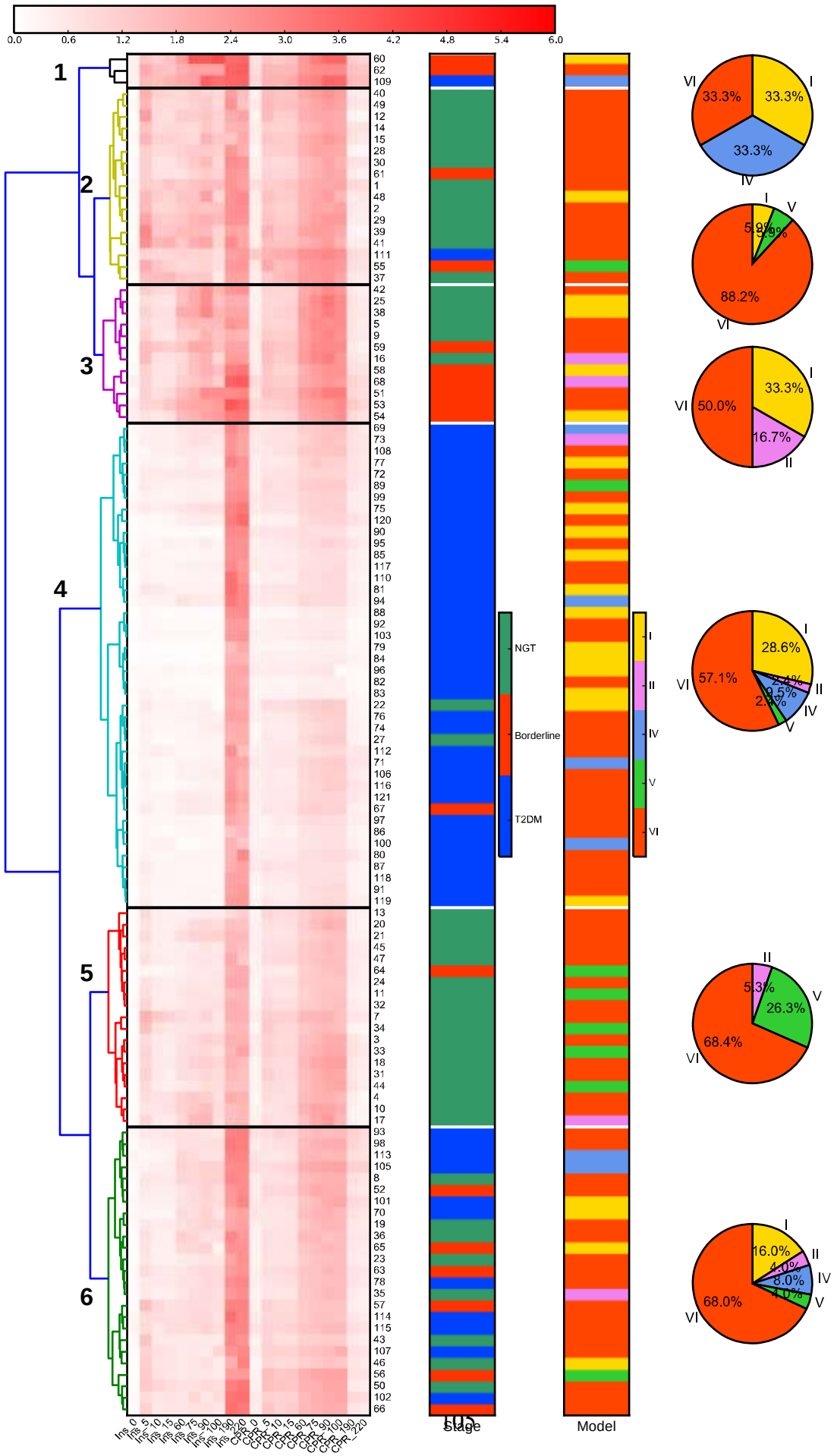
0.0 0.6 1.2 1.8 2.4 3.0 3.6 4.2 4.8 5.4 6.0
1
2
3
4
5
6
Ins_0 Ins_5 Ins_10 Ins_15 Ins_60 Ins_75 Ins_90 Ins_100 Ins_180 CPR_0 CPR_5 CPR_10 CPR_15 CPR_60 CPR_75 CPR_90 CPR_100 CPR_150 CPR_220
Stage
Model
NGT
Borderline
T2DM
I
II
IV
V
VI
33.3%
33.3%
33.3%
5.9%
88.2%
50.0%
16.7%
28.6%
57.1%
2.4%
9.5%
2.4%
5.3%
26.3%
68.4%
16.0%
4.0%
8.0%
4.0%
68.0%

Figure 22. The relationship between the clusters of time courses of serum insulin and C-peptide concentration and selected models. Normalized serum insulin and C-peptide concentration (see Methods) measured over 10 time points (0–220 min) for each subject were shown in the heat map. The analysis was performed using the Ward hierarchical clustering technique with Euclidean distance, and the hierarchy was cut at 0.25 times the maximum height. Two color bars on the right side of the heat map indicate the categorized stage of each subject (NGT, borderline type, or T2DM) and the optimal model for the subject. Pie charts show the proportion of the number of subjects optimal for each model among the subjects classified in each cluster.

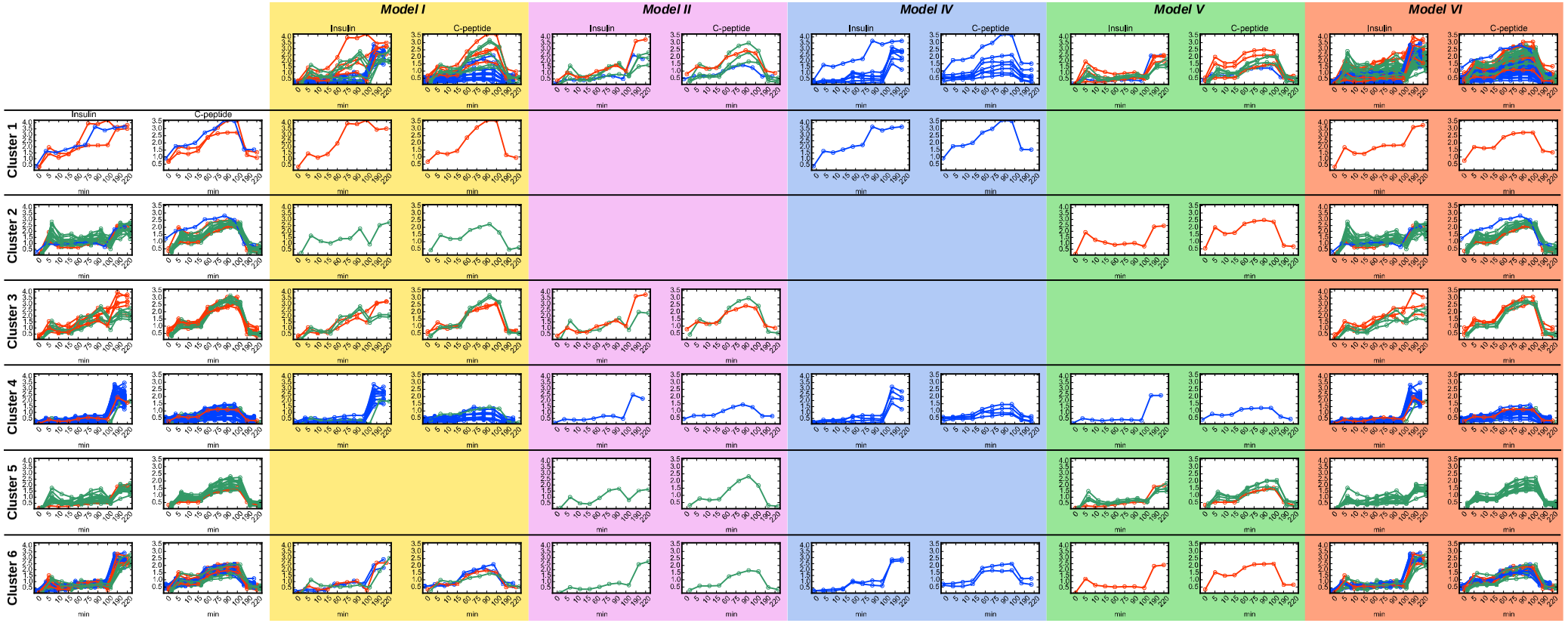
Model I
Model II
Model IV
Model V
Model VI
Insulin
C-peptide
Cluster 1
Cluster 2
Cluster 3
Cluster 4
Cluster 5
Cluster 6
min

Figure 23. Normalized time courses of serum insulin and C-peptide concentration of NGT (green), borderline type (red), and T2DM (blue) subjects classified in each cluster (column) and optimal for each model (row). Each panel in the leftmost column shows the time courses of subjects in each cluster, and each panel in the top row shows the time courses of subjects optimal for each model. The other panels show time courses of subjects in the cluster of the row and optimal for the model of the column.

C-peptide concentration returns to the fasting level during hyperinsulinemic-euglycemic clamp. The subjects in this cluster were optimal for *Model I*, *IV*, and *VI*.

Cluster 2: Serum insulin and C-peptide concentrations increase during the first-phase secretion, but do not increase much during the second-phase secretion. Most subjects in this cluster were in the NGT group and optimal for *Model VI*.

Cluster 3: Serum insulin and C-peptide concentrations do not increase much during the first-phase secretion, but increase during the second-phase secretion. Half the subjects in this cluster were in the NGT group and the others were in the borderline type group, and half of the subjects were optimal for *Model VI*.

Cluster 4: Serum insulin and C-peptide concentrations do not increase during both the first- and second-phase secretion. Most subjects in this cluster were in the T2DM group and optimal for *Model VI*.

Cluster 5: Serum insulin and C-peptide concentrations increase during both first- and second-phase secretions, and serum insulin concentration during hyperinsulinemic-euglycemic clamp was relatively low compared to that of the subjects in the other clusters. Most subjects in this cluster were in the NGT group and optimal for *Model VI*.

Cluster 6: Serum insulin and C-peptide concentrations moderately increase during both first- and second-phase secretions. NGT, borderline type, and T2DM subjects were included in this cluster, and most subjects were optimal for *Model VI*.

As described above, the cluster of time course of serum insulin and C-peptide concentrations corresponds to the stage of progression of glucose intolerance of the subjects

in the cluster to some extent. NGT, borderline type, and T2DM subjects account for the majority of *Clusters 2* and *5*, *Cluster 3*, and *Cluster 4*, respectively. NGT, borderline type, and T2DM subjects are included in *Cluster 6*, suggesting that it is possible to classify subjects independent of the stage of progression of glucose intolerance. However, optical models for the subjects were not significantly different among clusters in which the subjects were classified (Table 6), suggesting that there seems to be no bias of temporal patterns of serum insulin and C-peptide concentrations among the subjects who selected their own best model.

Therefore, I selected the model (Fig. 20; *Model VI* in Fig. 18) for further study because this model was good for reproducing time courses of serum insulin and C-peptide concentrations for the remaining 118 subjects with a simpler structure. The simulation with *Model VI* reproduced measured concentrations of insulin and C-peptide and reflected significant differences among the NGT, borderline type, and T2DM subjects (Fig. 17).

Seven subjects (one NGT, one borderline type, and five T2DM subjects) were excluded because their estimated model parameters were detected as outliers based on the adjusted outlyingness (Methods), and I analyzed the model for the remaining 111 subjects (47 NGT, 17 borderline type, and 47 T2DM) (Table 7).

Table 6. Significant differences in models selected by subjects among clusters

Cluster - Model	Classified in cluster Select model	Classified in cluster Not select model	Not classified in cluster Select model	Not classified in cluster Not select model	Corrected *P*
1 - I	1	2	21	94	1.39×10
1 - II	0	3	5	110	3.00×10
1 - IV	1	2	6	109	5.07
1 - V	0	3	8	107	3.00×10
1 - VI	1	2	75	40	8.64
2 - I	1	16	21	80	5.73
2 - II	0	17	5	96	3.00×10
2 - IV	0	17	7	94	1.77×10
2 - V	1	16	7	94	3.00×10^{-1}
2 - VI	15	2	61	40	8.84×10^{-1}
3 - I	4	8	18	88	6.99
3 - II	2	10	3	103	2.40
3 - IV	0	12	7	99	3.00×10
3 - V	0	12	8	98	3.00×10
3 - VI	6	6	70	36	1.03×10

Cluster - Model	Classified in cluster Select model	Classified in cluster Not select model	Not classified in cluster Select model	Not classified in cluster Not select model	Corrected *P*
4 - I	12	30	10	66	1.49
4 - II	1	41	4	72	1.96×10
4 - IV	4	38	3	73	7.34
4 - V	1	41	7	69	7.69
4 - VI	24	18	52	24	7.05
5 - I	0	19	22	77	6.61×10^{-1}
5 - II	1	18	4	95	3.00×10
5 - IV	0	19	7	92	1.79×10
5 - V	5	14	3	96	8.04×10^{-2}
5 - VI	13	6	63	36	2.39×10
6 - I	4	21	18	75	3.00×10
6 - II	1	24	4	89	3.00×10
6 - IV	2	23	5	88	1.92×10
6 - V	1	24	7	86	3.00×10
6 - VI	17	8	59	34	2.45×10

The number of subjects who were classified or not classified in the cluster, and selected or did not select the model are listed. *P* values for the bias of the number of subjects using Fisher exact test are shown, with the correction by the number of tests, multiplied by 30.

Table 7. Characteristics of the three groups of study subjects.

	NGT	Borderline	T2DM	Total
Number	47	17	47	111
Sex (male/female)	21/26	10/7	31/16	62/49
Age (years)	30.3 ± 8.68	42.0 ± 12.0	56.1 ± 12.7	43.0 ± 16.2
BMI (kg/m^2)	21.2 ± 3.47	26.9 ± 6.80	25.9 ± 5.03	24.1 ± 5.34
FPG (mg/dL)	85.4 ± 6.79	91.8 ± 14.7	111 ± 23.5	97.2 ± 20.7
2-h PG (mg/dL)	111 ± 17.2	167 ± 16.1	264 ± 76.9	184 ± 87.3
F-IRI (μU/mL)	5.44 ± 2.10	9.18 ± 5.63	6.65 ± 4.25	6.53 ± 3.95
F-CPR (ng/mL)	1.45 ± 0.394	2.13 ± 0.753	1.83 ± 0.872	1.71 ± 0.725

Data are means ± SD. BMI, body mass index; FPG, fasting plasma glucose concentration; 2-h PG, 2-h plasma glucose level during the oral glucose tolerance test; F-IRI, fasting serum immunoreactive insulin concentration; F-CPR, fasting serum immunoreactive C-peptide concentration.

3.3.5 Changes in opposite direction of hepatic and peripheral insulin clearance in development of glucose intolerance

I statistically compared the model parameters among the NGT, borderline type, and T2DM subjects (Fig. 24 and 25; Methods). Four of the nine parameters, $k_{I\text{out}}$, k_{ratio}, h, and X_{b}, were significantly different.

The parameter $k_{I\text{out}}$ is the degradation rate of serum insulin and corresponds to peripheral insulin clearance. The value of $k_{I\text{out}}$ in the NGT subjects was significantly higher than that in the borderline type and T2DM subjects (Fig. 25), indicating that peripheral clearance decreases in development of glucose intolerance, which is consistent with previous studies.

The parameter k_{ratio} is the ratio of post-hepatic insulin to C-peptide, and $(1 - k_{\text{ratio}})$ corresponds to the ratio of insulin extracted by the liver, that is, hepatic insulin clearance. The value of $(1 - k_{\text{ratio}})$ in the NGT subjects was significantly lower than that in the borderline type and T2DM subjects (Fig. 25), indicating the increase of hepatic insulin clearance in development of glucose intolerance. This is consistent with an earlier clinical observation.

The parameter h is the threshold of plasma glucose concentration for the insulin secretion and corresponds to the fasting plasma glucose concentration. This parameter in the T2DM subjects was significantly higher than that in the NGT subjects (Fig. 24), consistent with the fact that fasting plasma glucose concentration is higher in T2DM [97,98].

The parameter X_{b} is the initial value of X, which may correspond to stored amounts of insulin and C-peptide in β-cells or β-cell masses before the start of the hyperglycemic clamp. This parameter in the T2DM subjects was significantly lower than that in the NGT subjects

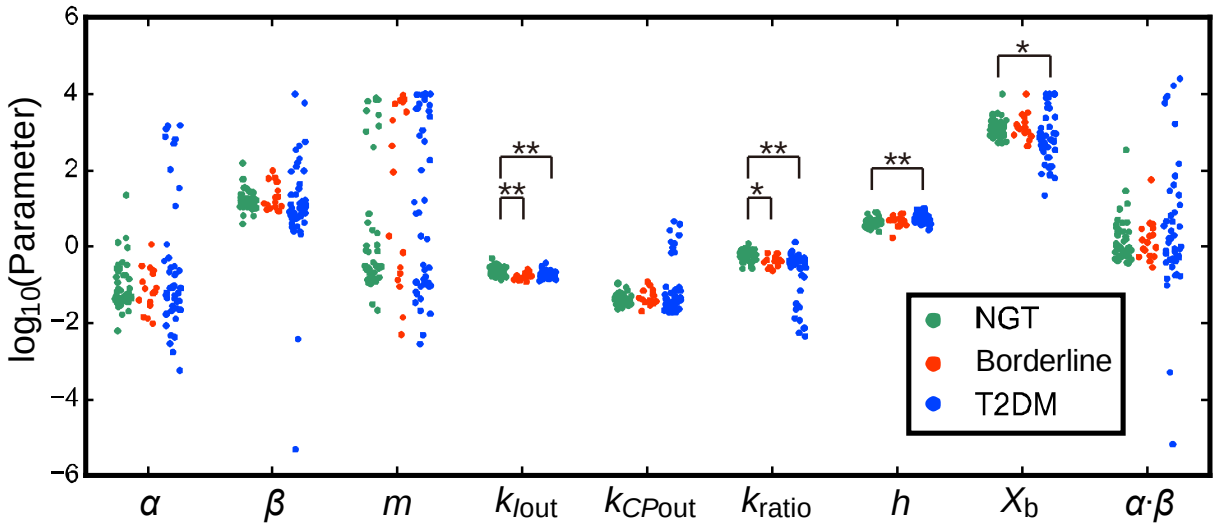

Figure 24. The estimated parameters for the NGT (green), borderline type (red), and T2DM (blue) subjects. Each dot corresponds to the indicated parameter for an individual subject. *P < 0.05, **P < 0.01, NS: not significant (two-sided Wilcoxon rank sum test with FDR-correction).

Model parameters for all subjects are provided in Ohashi et al. (in preparation) (Supplementary Table S9).

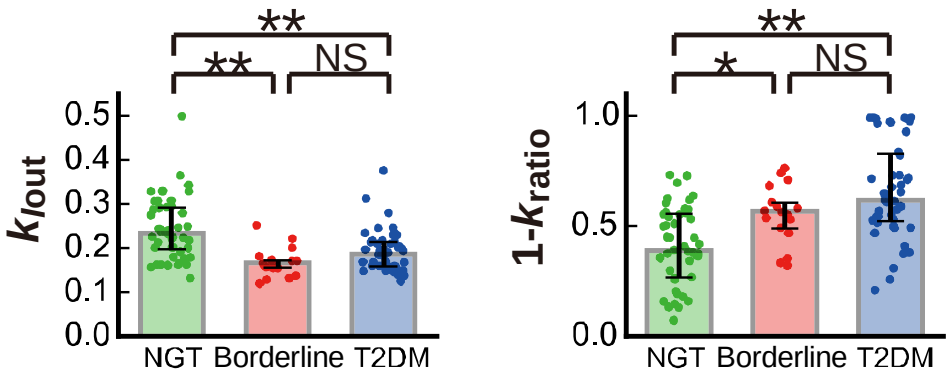

Figure 25. The parameters of k_{Iout} and (1 - k_{ratio}), corresponding to peripheral and hepatic insulin clearance, respectively. *P < 0.05, **P < 0.01, NS: not significant (two-sided Wilcoxon rank sum test with FDR-correction). The bar and error bar show the median and lower and upper quantiles, respectively. Each dot corresponds to the indicated parameter for an individual subject.

(Fig. 24), consistent with observations that β-cell masses and stored insulin decrease in T2DM patients [102-104].

In Chapter 2, using the same clamp data, I showed that insulin secretion decreases from NGT to borderline type to T2DM [17,52]. In this study, however, the parameters α and β, related to insulin secretion, did not show any significant differences among the NGT, borderline type, and T2DM subjects, possibly because previously defined insulin secretion [52] is described by insulin secretion and delivery in this model, which depends on other parameters such as h, m, X_b, and k_{ratio}, and the parameters involved in insulin secretion and delivery are too diverse.

The parameters k_{ratio}, k_{Iout}, k_{CPout}, h, and X_b show smaller variations than others (Fig. 24). This is probably because these parameters are directly related to the model compartments corresponding to measured concentrations of serum insulin and C-peptide and plasma glucose, and therefore can be accurately estimated, whereas other parameters are not, resulting in large variation possibly due to inaccurate estimation.

3.3.6 Relationship between parameters of hepatic and peripheral insulin clearance and clinical indices of serum insulin regulation

I examined the correlation of the estimated model parameters with clinical indices of circulating insulin regulation among 111 subjects (Fig. 26). The model parameter showing the highest correlation with insulin sensitivity index (ISI) and with the metabolic clearance rate (MCR), which is the index of insulin clearance (see Methods for details), was peripheral insulin clearance, k_{Iout} (r = 0.761 and 0.790, respectively, both $P < 0.001$). These correlations

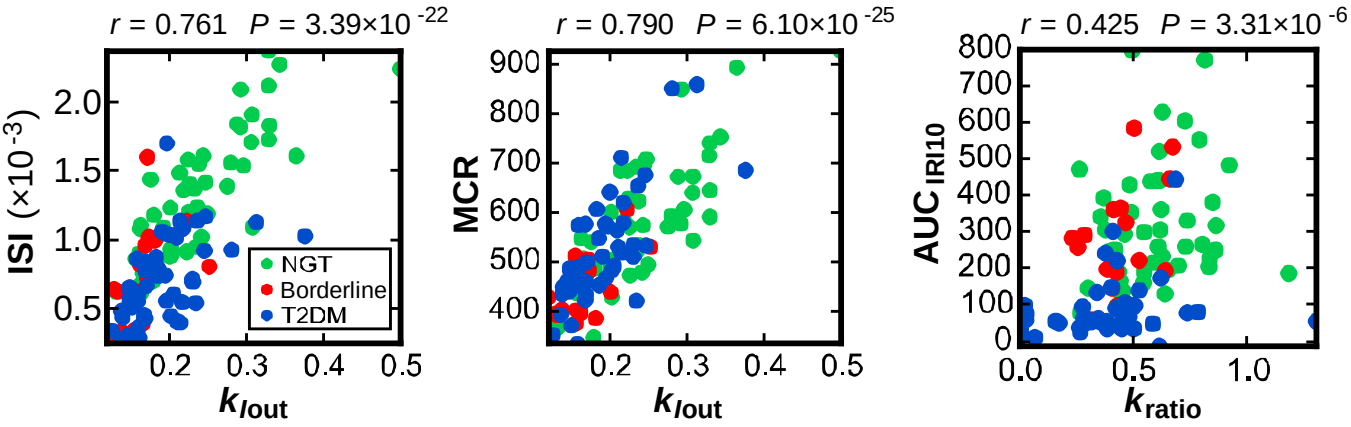

Figure 26. Correlations between clinical indices and model parameters. Scatter plots for the indicated measured clinical indices versus the highest correlated model parameters are shown. ISI, the insulin sensitivity index; MCR, the metabolic clearance rate; AUC_{IRI10}, amount of insulin secretion during the first 10 min of hyperglycemic clamp. Each dot indicates the value of an individual subject. The correlation coefficient, *r*, and the *P* value for testing the hypothesis of no correlation are shown. The partial correlation coefficients among k_{Iout}, ISI, and MCR are shown in Fig. 27.

Correlation coefficients of all clinical indices with model parameters are provided in Ohashi et al. (in preparation) (Supplementary Table S6).

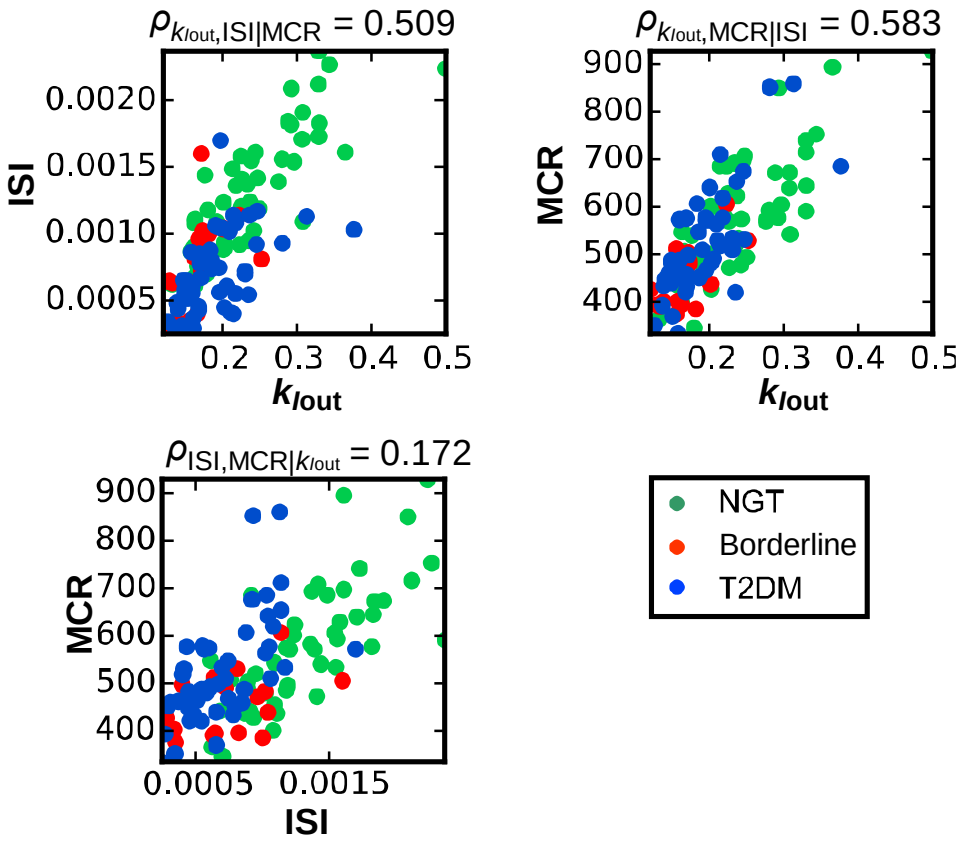

Figure 27. Scatter plots of k_{Iout}, ISI, and MCR. The partial correlation coefficient, $\rho_{X,Y|Z}$, defined as the correlation between X and Y conditioning of Z, is shown. Model parameter k_{Iout} shows the correlations with clinical indices after removing the effect of the other clinical index.

are consistent with finding in Chapter 2 that peripheral insulin clearance is highly correlated with ISI and MCR [52]. $k_{I\text{out}}$ is the degradation rate of serum insulin, which depends on the number of insulin receptors on target tissues [77], indicating that serum insulin degradation and insulin sensitivity are mutually correlated. Therefore, it is reasonable that $k_{I\text{out}}$ is correlated not only with MCR but also with ISI.

The model parameter showing the highest correlation with insulin secretion during the first phase, AUC_{IRI10} (see Methods), which is the index of insulin secretion, was k_{ratio} (r = 0.425, $P < 0.01$). Note that $(1 - k_{\text{ratio}})$ corresponds to hepatic insulin clearance. Because the parameter k_{ratio} is the ratio of insulin remaining after the hepatic extraction, and is related to increase in serum insulin concentration, its correlation with insulin secretion is reasonable.

In addition, the model parameter showing the highest correlation with both FPG and 2-h PG, the main indices of glucose tolerance, was h (r = 0.448 and 0.504, respectively, both $P <$ 0.001), which is the threshold glucose concentration for insulin secretion. This finding is consistent with h corresponding to fasting plasma glucose concentration. The model parameter showing the highest correlation with the clamp disposition index, clamp DI, which is calculated as the product of insulin secretion AUC_{IRI10} and ISI and is the index of glucose tolerance [17], was $k_{\text{ratio}} \cdot k_{I\text{out}}$ (r = 0.540, $P < 0.001$). Considering that k_{ratio} is related to post-hepatic insulin delivery, and $k_{I\text{out}}$ is related to insulin sensitivity, which depends on the number of insulin receptors on target organs, it is reasonable that the product $k_{\text{ratio}} \cdot k_{I\text{out}}$ shows the highest correlation with clamp DI, which is also the product of clinically estimated insulin secretion and sensitivity.

3.3.7 The roles of hepatic and peripheral insulin clearance on the regulation of amplitude and temporal patterns of serum insulin concentration

Because $k_{I\text{out}}$ and k_{ratio} were the parameters showing the highest correlation with clinical indices of insulin sensitivity and secretion, respectively, both of which are related to the temporal changes of serum insulin concentration related to the progression of glucose intolerance and T2DM, I analysed the effects of k_{ratio} and $k_{I\text{out}}$ on serum insulin concentration during the first- and second-phase insulin secretion (Fig. 28). I changed the originally estimated values of k_{ratio} or $k_{I\text{out}}$ or both by 2^{-1} to 2^{1} times and simulated the time course of *I*, serum insulin concentration, during hyperglycemic clamp for each subject. Similar temporal changes of *I* versus changes in the parameters were observed in all 111 subjects, so only the simulation result of subject #3 (NGT) is shown (Fig. 28).

The time course of *I* with the original parameters in the model of subject #3 showed the transient increase (Fig. 28A, black line). As k_{ratio} increased, *I* increased without changing the transient pattern (Fig. 28A, left panel, red line). Indeed, an increase of k_{ratio} affects the value of *I* similarly at any time point, because k_{ratio} controls the gain of time derivative of *I*. As $k_{I\text{out}}$ increased, *I* decreased and the temporal pattern became more transient with an earlier peak time (Fig. 28A, middle panel, red line). Conversely, as $k_{I\text{out}}$ decreased, *I* increased and the temporal pattern became more sustained with a delayed peak time (Fig. 28A, middle panel, blue line). This result suggests that $k_{I\text{out}}$ controls the shift in the temporal patterns of *I* from transient to sustained. These changes in the temporal pattern of *I* are characterized by a decrease in the difference between serum insulin concentration during the first-phase

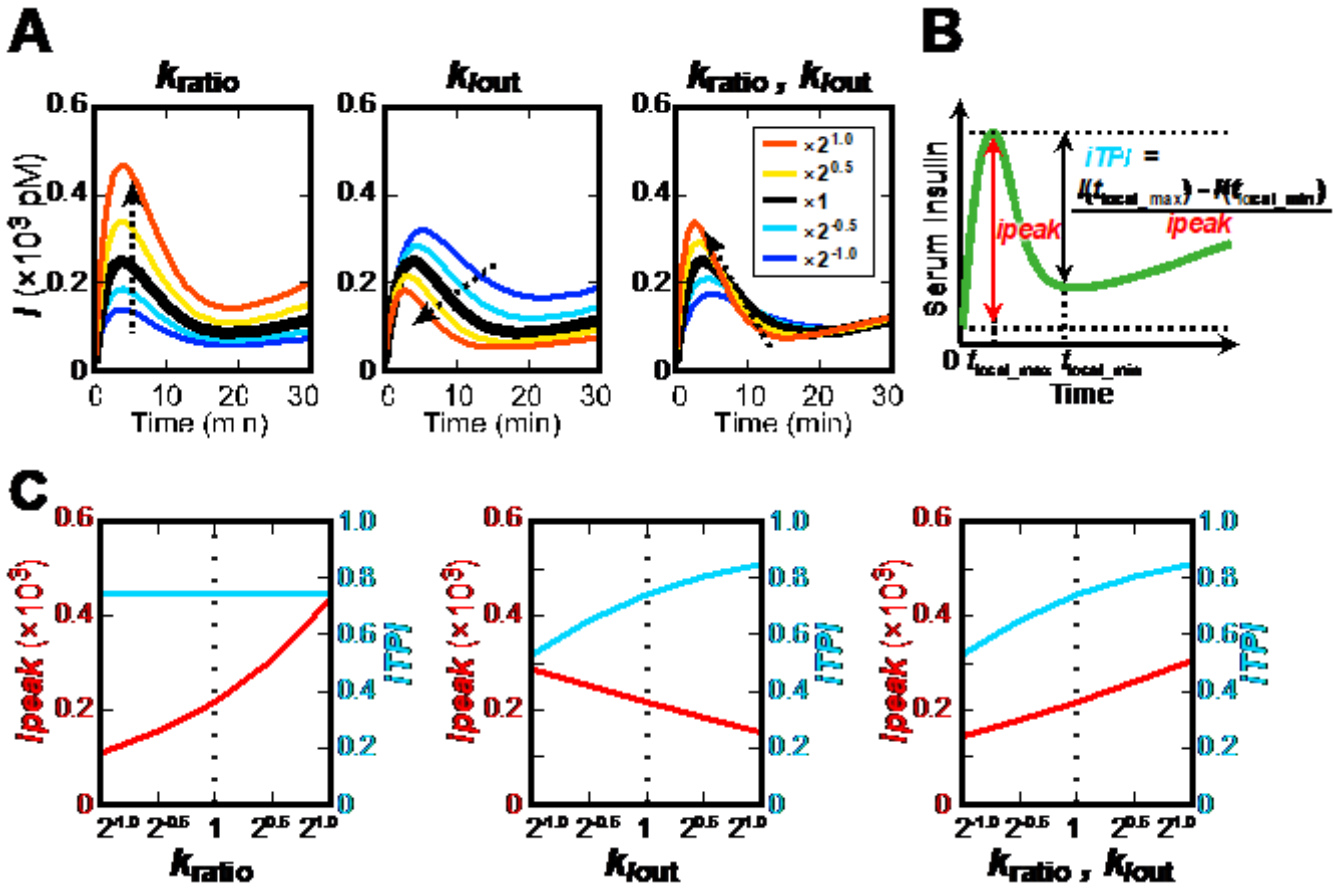

Figure 28. The effects of k_{ratio} and k_{Iout} on the amplitude and temporal patterns of serum insulin concentration.

(**A**) Simulated time course of serum insulin concentration *I* during hyperglycemic clamp of typical subject (#3: NGT) by changing k_{ratio} or k_{Iout} or both by scaling the fitted parameter value with $2^{-1.0}$, $2^{-0.5}$, 1, $2^{0.5}$, and $2^{1.0}$ (see Methods). Dotted arrows indicate the direction of the change in the temporal pattern as the parameter increases.

(**B**) The definition of *ipeak* (incremental peak) and iTPI (incremental transient peak index), reflecting the peak amplitude and the temporal pattern of serum insulin concentration *I*.

(**C**) Trajectories of *ipeak* and *iTPI* of *I* of subject #3 by changing k_{ratio} or k_{Iout} or both.

The results of this analysis on the all subjects are provided in Ohashi et al. (in preparation) (Supplementary Fig. S7).

secretion and that during the second-phase secretion. Note that the decrease in $k_{I\text{out}}$ also increases the amplitude of *I*.

Because both k_{ratio} and $k_{I\text{out}}$ decreased from NGT to borderline type and T2DM (Fig. 24), I examined the effect of the simultaneous changes of k_{ratio} and $k_{I\text{out}}$ on the amplitude and transient/sustained patterns of *I*. When both k_{ratio} and $k_{I\text{out}}$ increased with the same ratio, *I* increased during first-phase secretion (0–10 min), whereas *I* decreased during second-phase secretion (10–30 min) (Fig. 28A, right panel, red line). Thus, simultaneous increase of k_{ratio} and $k_{I\text{out}}$ results in the increase of peak amplitude of *I* and in changes in the temporal pattern of *I* from sustained to transient.

I quantified the effects of k_{ratio} and $k_{I\text{out}}$ on the peak amplitude and temporal patterns of *I*. I defined the index *ipeak* (incremental peak) for the peak amplitude of *I*, and the index *iTPI* (incremental transient peak index; modified from Kubota et al. [88]) for the temporal pattern of *I* (Fig. 28B), as follows:

$$ipeak = I(t_{\text{local\_max}}) - I(0), \quad I(t_{\text{local\_max}}) > I(t_{\text{local\_max\_next}}) \tag{39}$$

$$iTPI = \frac{I(t_{\text{local\_max}}) - I(t_{\text{local\_min}})}{ipeak}, \quad I(t_{\text{local\_min}}) < I(t_{\text{local\_min\_next}}), t_{\text{local\_min}} > t_{\text{local\_max}} \tag{40}$$

where $I(t)$ represents *I* at time *t*, $t_{\text{local\_max}}$ is the time at which *I* stops increasing for the first time from 0 min, $t_{\text{local\_max\_next}}$ is the next sampling time of $t_{\text{local\_max}}$, $t_{\text{local\_min}}$ is the time at which *I* stops decreasing for the first time after $t_{\text{local\_max}}$, and $t_{\text{local\_min\_next}}$ is the next sampling time of $t_{\text{local\_min}}$.

The index *ipeak* is the difference in *I* between the local maximum $I(t_{\text{local\_max}})$ and the initial fasting concentration $I(0)$ and represents the peak amplitude of *I* during the first-phase

secretion. The index *iTPI* is the ratio of the difference of *I* between the local maximum $I(t_{local\_max})$ and the local minimum $I(t_{local\_min})$ of *I* against *ipeak*, which reflects the ratio of *I* during the first- and second-phase secretions. As *iTPI* approaches 1, the difference in *I* between the first- and second-phase secretions becomes larger, meaning that the temporal change of *I* becomes more transient. Conversely, as *iTPI* approaches 0, the difference in *I* between the first- and second-phase secretions becomes smaller, meaning that the temporal change of *I* becomes more sustained.

I calculated *ipeak* and *iTPI* from the simulated time courses of *I* by changing the original estimates of k_{ratio} or k_{Iout} or both by 2^{-1} to 2^{1} times. As k_{ratio} increased, *ipeak* increased but *iTPI* did not change (Fig. 28C, left panel), indicating that increasing k_{ratio} increases the peak amplitude of *I* during the first-phase secretion without changing its temporal pattern. As k_{Iout} increased, *iTPI* increased and *ipeak* decreased (Fig. 28C, middle panel), indicating that increasing k_{Iout} changes the temporal patterns of *I* from sustained to transient and decreases the peak amplitude of *I* during the first-phase secretion.

When both k_{ratio} and k_{Iout} increased at the same ratio, both *ipeak* and *iTPI* increased (Fig. 28C, right panel), indicating that increasing both k_{ratio} and k_{Iout} increases the peak amplitude of *I* and changes the temporal pattern from sustained to transient. The increase in *ipeak* means that the effect of k_{ratio}, which increases *ipeak*, is stronger than that of k_{Iout}, which decreases *ipeak*. Given that both k_{ratio} and k_{Iout} decrease from NGT to borderline type and T2DM, both *ipeak* and *iTPI* decrease (Fig. 29). This finding is consistent with earlier clinical observations that the peak amplitude of circulating insulin concentration during the first-phase secretion

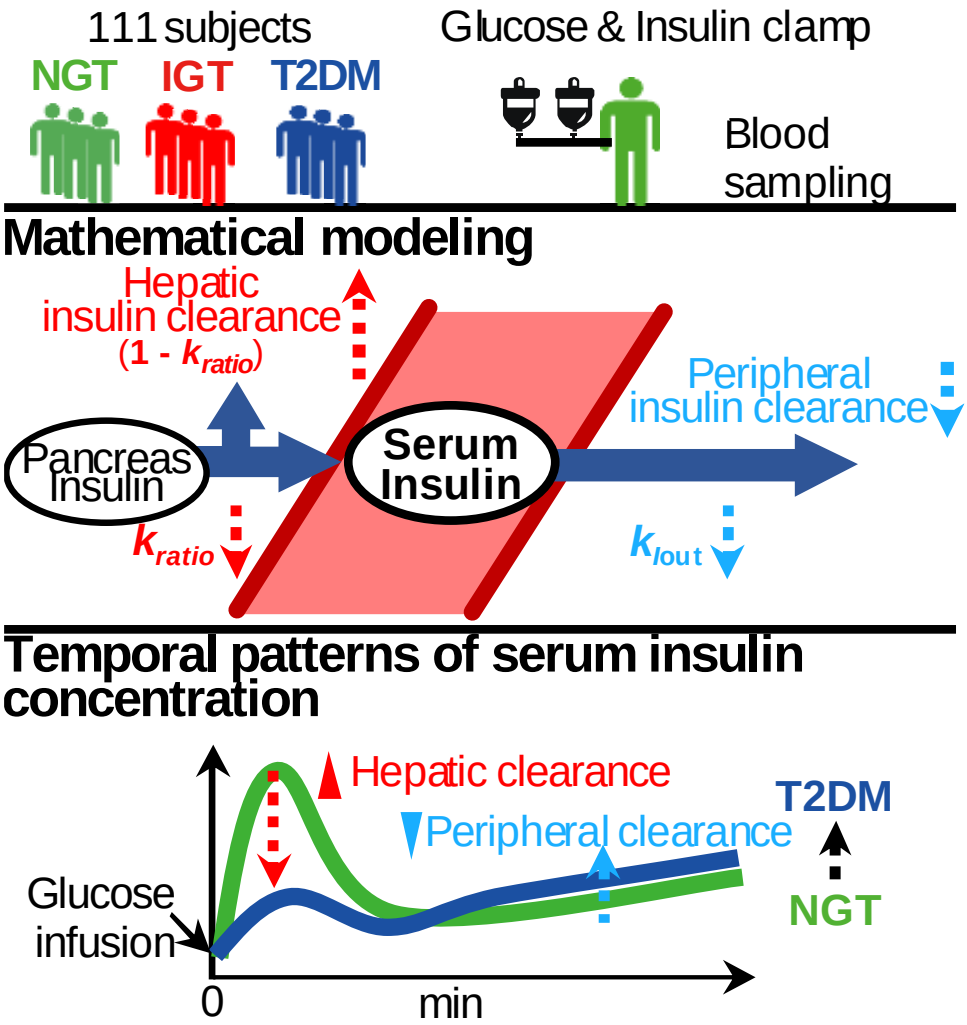

Figure 29. The summary of the study in Chapter 3. Mathematical model based on the measured concentrations of plasma glucose, serum insulin, and C-peptide revealed the increase in hepatic (1 - k_{ratio}) and decrease in peripheral (k_{Iout}) insulin clearance in development of glucose intolerance. These changes of hepatic and peripheral insulin clearance result in the decrease in peak amplitude and the change in the temporal pattern of serum insulin concentration from transient to sustained, respectively.

decreases and the temporal pattern becomes more sustained during the progression of glucose intolerance [19-21].

3.4 Discussion

I developed several alternative mathematical models using concentrations of plasma glucose, serum insulin, and C-peptide during the consecutive hyperglycemic and hyperinsulinemic-euglycemic clamp, and selected the model showing the best fit for most subjects. Although *Model VI* was selected for 76 of 121 subjects, 45 subjects were not optimal for *Model VI*. This suggests that some of the parameters of *Model VI* were unnecessary in subjects whose selected model is *Model I, II, IV,* or *V* by comparing the structure with *Model VI*. However, no parameter of *Model VI* showed significant difference between subjects who selected *Model I*, *II*, *IV*, or *V* and subjects who selected *Model VI* (Fig. 30), suggesting that there is no biased feature on the structure of the control of circulating insulin concentration in subjects who were not optimal for *Model VI*, and *Model VI* can be applied to all subjects.

During the progression of glucose intolerance, it has been shown that the peak amplitude of circulating insulin concentration during the first-phase secretion decreases and the temporal pattern becomes more sustained [19-21]. In this study, I found that both $k_{I\text{out}}$, corresponding to peripheral insulin clearance, and k_{ratio} decrease from NGT to borderline type and T2DM. Given that $(1 - k_{\text{ratio}})$, corresponding to hepatic insulin clearance, increases as the k_{ratio} decreases, these findings strongly suggest that, from NGT to borderline type and T2DM, the peak amplitude of serum insulin concentration decreases due to the increase in hepatic insulin clearance and the temporal pattern changes from transient to sustained occur because of a decrease in peripheral insulin clearance (Fig. 30). Importantly, the decrease in peripheral insulin clearance alone can explain only the temporal change of serum insulin concentration,

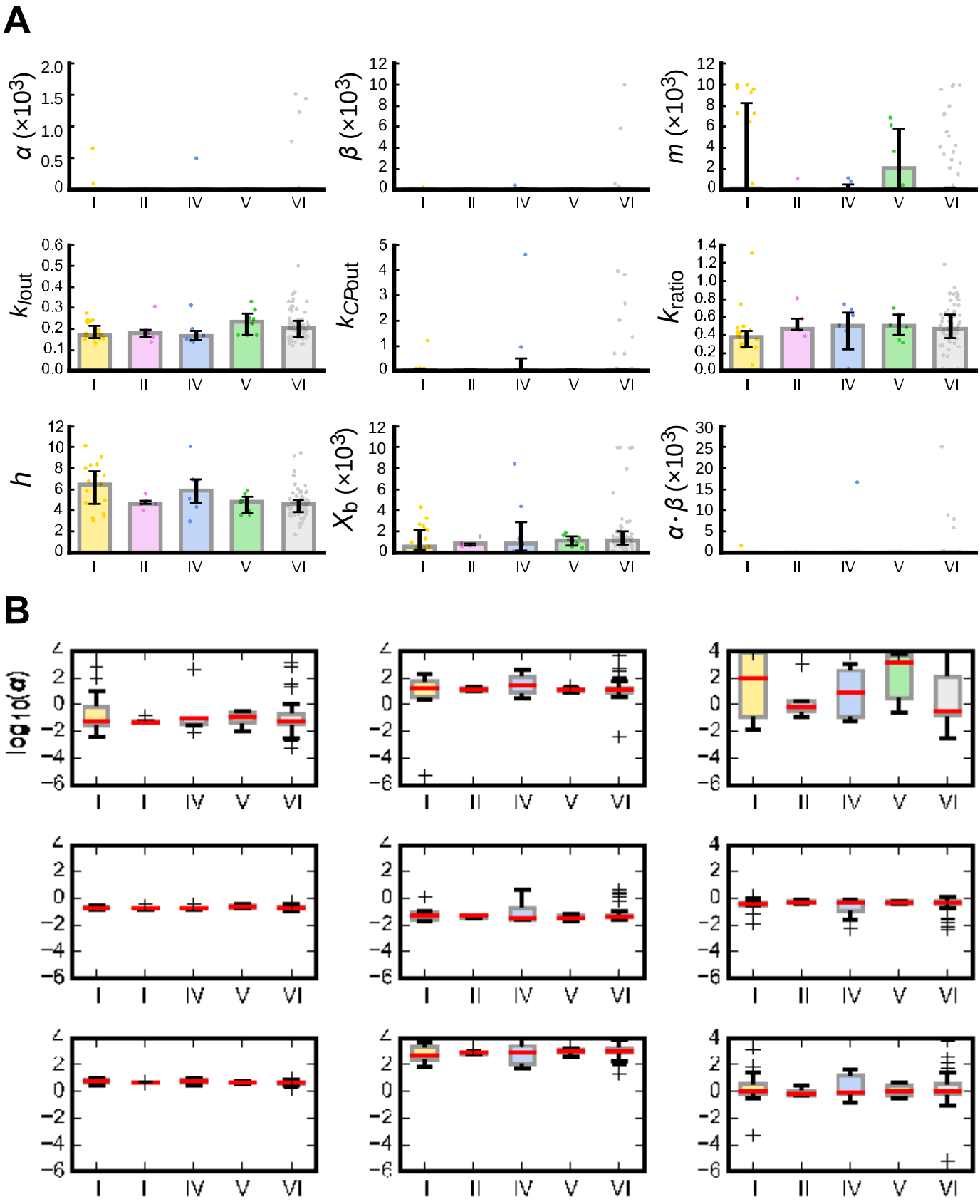

Figure 30. The estimated parameters of *Model VI* for subjects who selected each of Model *I*, *II*, *IV*, *V*, and *VI*.

(**A**) Medians and upper and lower quartiles of 76 subjects who were optimal for *Model VI* (gray) and of 45 subjects who were not optimal for *Model VI* (yellow, pink, blue, and green indicate subjects who were optimal for *Models I*, *II*, *IV*, and *V*, respectively) are shown. Each dot corresponds to the indicated parameter for an individual subject.

(**B**) Box plots of 76 subjects who were optimal for *Model VI* (gray) and of 45 subjects who were not optimal for *Model VI* are shown. Note that all graphs use a log-10 scale for the Y axis.

No parameter differed significantly between subjects who were optimal for each of *Models I*, *II*, *IV*, and *V* and subjects who were optimal for *Model VI*, using two-sided Wilcoxon rank sum test (36 tests were performed, FDR-corrected P value > 0.05).

not the decrease of peak amplitude. Thus, the increase of hepatic insulin clearance and decrease of peripheral insulin clearance simultaneously cause the decrease in the peak amplitude of serum insulin concentration during the first-phase secretion and change in temporal pattern from transient to sustained. This result demonstrates that, in addition to the decrease in insulin secretion [20,21], the increase in hepatic clearance also contributes to the decrease in peak amplitude of serum insulin concentration in the first-phase secretion from NGT to borderline type and T2DM.

In the model, as k_{ratio}, the ratio of post-hepatic insulin compared to C-peptide, increased, *ipeak*, the peak amplitude of peripheral insulin concentration, increased (Fig. 28C). According to clinical measurements, k_{ratio} was also correlated with *ipeak* calculated directly from the serum insulin concentration measured during the first-phase secretion in hyperglycemic clamp (Fig. 31A, $r = 0.423$, $P < 0.001$), indicating that hepatic insulin clearance is pathologically correlated with the peak amplitude in the first-phase secretion from NGT to borderline type and T2DM. On the other hand, in the model, as k_{Iout}, the peripheral insulin clearance, increased, *iTPI*, representing the temporal pattern of peripheral insulin concentration, increased (Fig. 28C). However, in clinical measurements, k_{Iout} was not highly correlated with *iTPI* calculated directly from the serum insulin concentration measured during hyperglycemic clamp (Fig. 31A, $r = 0.297$, $P < 0.01$). The reason for this lack of correlation between k_{Iout} and *iTPI* in clinical measurement remains unclear; however, it may be because little insulin was secreted during hyperglycemic clamp in some borderline type and T2DM subjects, and *iTPI* cannot be estimated accurately because of low concentration of serum insulin.

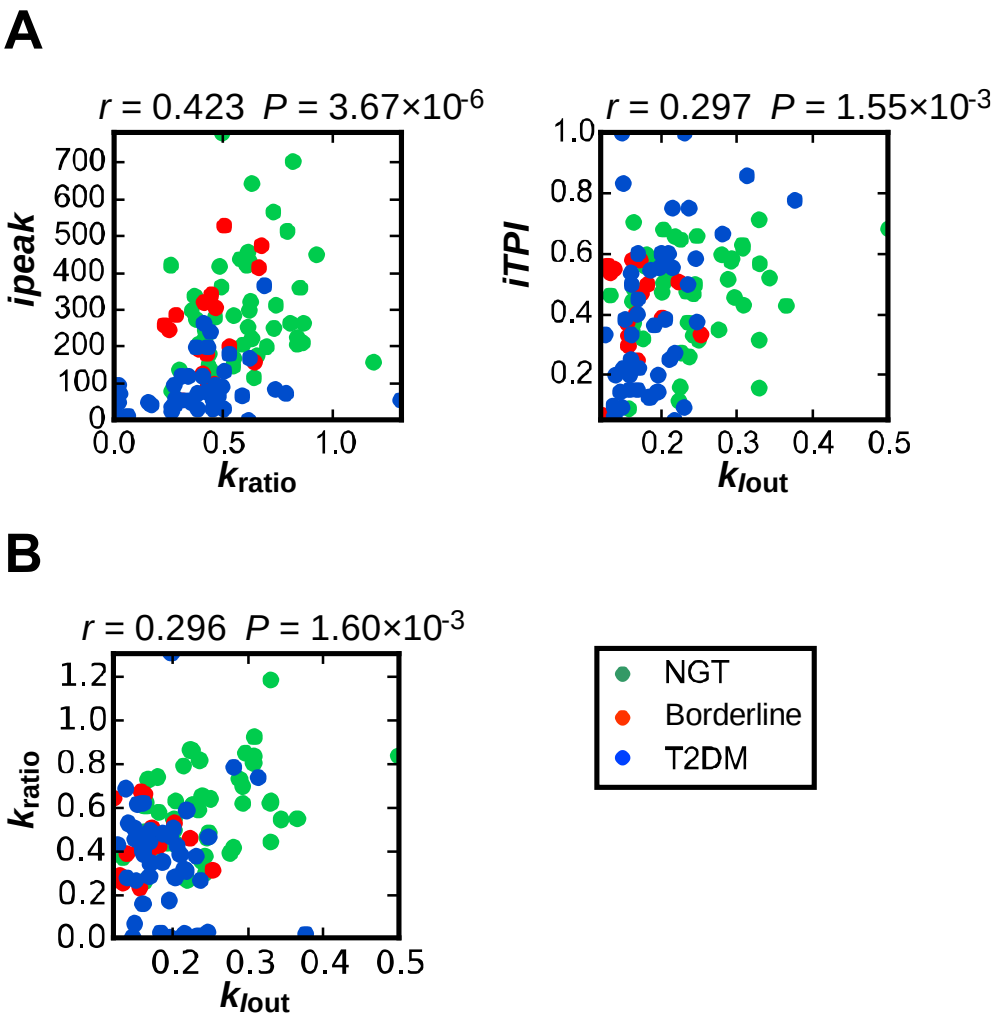

Figure 31. Distribution of model parameters and indices of peak amplitude and temporal pattern of serum insulin concentration. (**A**) Scatter plots of *ipeak* and k_{ratio} and of *iTPI* and k_{Iout}. *ipeak* and *iTPI* are calculated directly from the measured serum insulin concentration. (**B**) Scatter plot of k_{Iout} and k_{ratio}.

Many studies have shown that insulin clearance decreases in T2DM patients [78-83]. However, the change in hepatic insulin clearance in this condition has been controversial, with some studies finding an increase in T2DM subjects [85] and others a decrease [78,84]. In Chapter 2, I developed a mathematical model using data gathered during hyperglycemic and hyperinsulinemic-euglycemic clamps, and peripheral insulin clearance significantly decreased from NGT to borderline type to T2DM [52]. However, hepatic and peripheral insulin clearances were not estimated separately because I did not use C-peptide data. Recently, Polidori et al. [51] estimated both hepatic and peripheral insulin clearance by modeling analysis using plasma insulin and C-peptide concentrations obtained from the insulin-modified frequently sampled IVGTT. They found that the peripheral insulin clearance significantly decreased in borderline type subjects compared with NGT subjects, whereas hepatic insulin clearance did not significantly differ between the borderline type and NGT subjects [51]; the former finding is consistent with the result in Chapter 2 that peripheral insulin clearance decreases from NGT to borderline type to T2DM. In Chapter 3, I demonstrated that hepatic insulin clearance significantly increases, whereas peripheral insulin clearance significantly decreases from NGT to borderline type and T2DM. One difference between the study by Polidori et al. and this study is C-peptide kinetics. They used the reported two-compartment model of C-peptide kinetics for calculating insulin secretion rate by deconvolution, while I selected the structure of C-peptide kinetics that fitted for the clamp data, which may improve the accuracy of the parameter estimation of hepatic insulin clearance, estimated by use of serum insulin and C-peptide concentration.

The increase in hepatic insulin clearance may be caused by impaired suppression of endocytosis of insulin receptors on the liver [85], and the decrease in peripheral insulin clearance may be caused by a decrease of the number of insulin receptors on target tissues [77]. Polidori et al. [51] also found that hepatic and peripheral insulin clearances were not highly correlated. Consistent with their results, in this study the insulin clearance parameters k_{ratio} and k_{Iout} were not highly correlated (Fig. 31B, $r = 0.296$, $P < 0.01$), suggesting that both insulin clearances are independently regulated.

I am aware that some of the results of this analysis only hold if the parameters are identifiable based on serum insulin and C-peptide data. I performed 20 trials of parameter estimation for each subject (Methods), but most subjects (107 subjects) had only one trial which minimized RSS. The values of estimated parameters and RSS varied among the 20 trials of each subject. For the remaining four subjects, estimated parameters varied among trials that returned the same RSS, especially the parameters α and β differed to a large extent, while the parameters k_{Iout} and k_{ratio} did not largely differ (Fig. 32). If the number of estimated trials, parents, and generations of evolutionary programming increases, a trial that gives a different parameter solution with smaller RSS than that reported in this study might be obtained. Structural or a priori identifiability of parameters based on the system equations [92], which tests if model parameters can be determined from the available data, was not performed in this study. Large variability in the fitted parameters, like for instance in α and β, could be due to the identifiability of the parameters and not due to biological variance, and interpretation of the results has to take this into account.

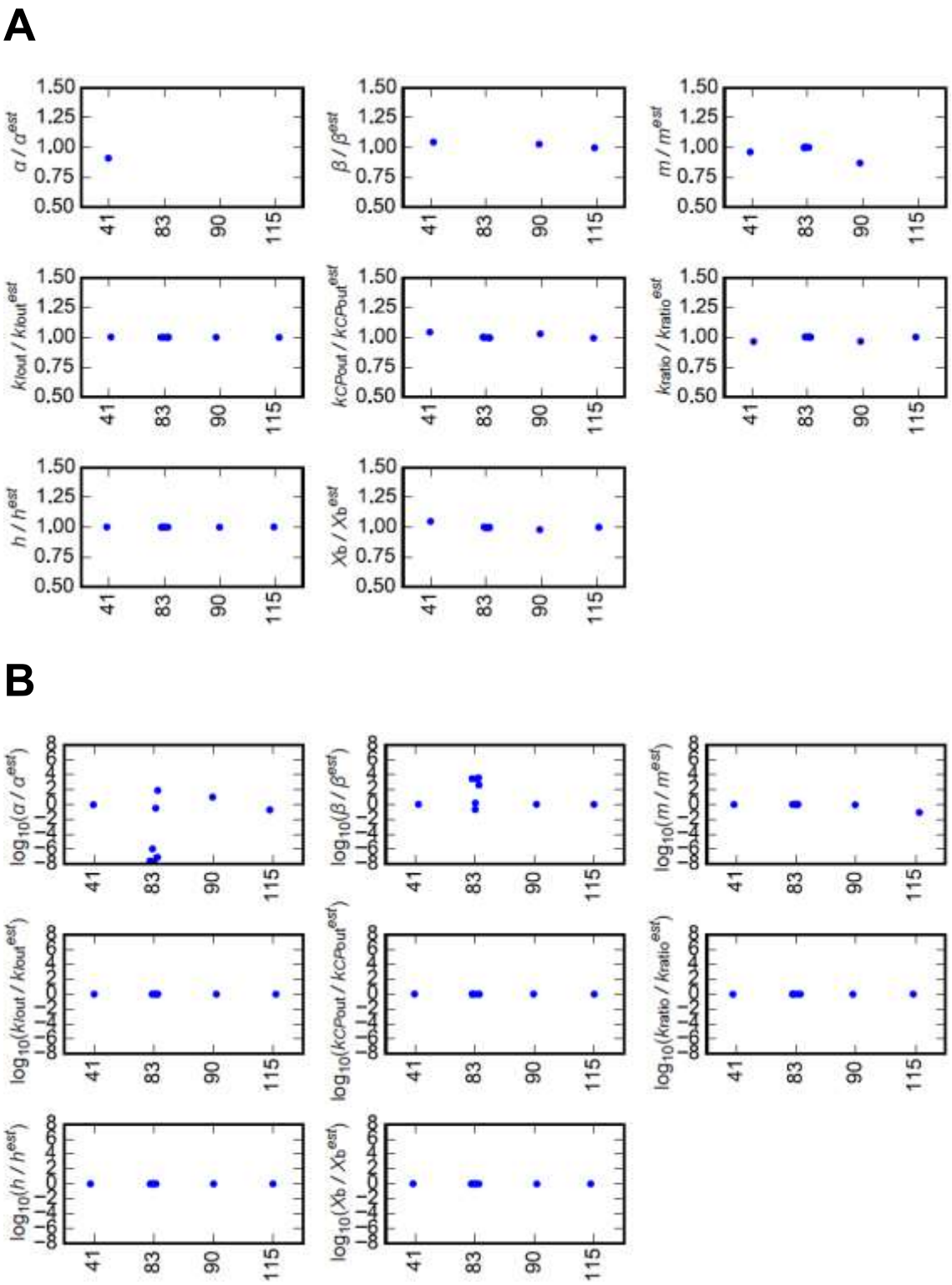

Figure 32. The ratio of parameters estimated in trials other than the trial used in this study to parameters estimated in the trial used in this study (*parameter*^{est}) of *Model VI* for subjects who had two or more trials which minimized RSS (#41: NGT, #83: T2DM, #90: T2DM,

#115: T2DM). Each dot corresponds to the indicated parameter ratio of an individual trial of an individual subject in linear (**A**) and log-10 (**B**) scale.

Insulin selectively regulates various functions, such as signalling activities, metabolic control, and gene expression, depending on its temporal patterns. For example, Kubota et al. [88] previously reported that pulse stimulation of insulin in rat hepatoma Fao cells, resembling the first-phase secretion, selectively regulated glycogen synthase kinase-3β (GSK3β), which regulates glycogenesis, and S6 kinase, which regulates protein synthesis, whereas ramp stimulation of insulin, resembling the second-phase secretion, selectively regulated GSK3β and glucose-6-phosphatase (*G6Pase*), which regulates gluconeogenesis. Noguchi et al. and Sano et al. [89,105] also found that insulin-dependent metabolic control and gene expression are selectively regulated by temporal patterns and doses of insulin in FAO cells. Sustained stimulation of insulin suppressed the expression of insulin receptors, leading to reduced insulin sensitivity in FAO cells [106-108] . Likewise, phosphorylation of the insulin receptor substrate (IRS)-1/2 in rat liver increased when pulsatile (rather than continuous) stimulation of insulin was imposed in the portal circulation [109]. This may have occurred through the negative feedback within the insulin signalling pathway, the phosphatidylinositide (PI) 3-kinase/Alt pathway, targeting IRS-1/2 [107,110]. In addition, IRS-2, rather than IRS-1, mainly regulates hepatic gluconeogenesis through its rapid downregulation by insulin [111], suggesting the selective roles of IRS-1/2 in response to temporal patterns of plasma insulin. These findings indicate that the amplitude and temporal pattern of circulating insulin concentration selectively regulate insulin actions on the target tissues. Given that hepatic and peripheral insulin clearances are responsible for the amplitude and temporal pattern of circulating insulin

concentration, these clearances are likely to be involved in selective control of insulin action, glucose homeostasis, and the pathogenesis of T2DM.

In Chapter 2, I developed a mathematical model for concentrations of plasma glucose and serum insulin measured during the consecutive hyperglycemic and hyperinsulinemic-euglycemic clamp and found significant decreases in insulin secretion, sensitivity, and peripheral insulin clearance from NGT to borderline type to T2DM [52]. The differences between studies in Chapter 2 and 3 are the model structure and C-peptide data. The previous model consisted of plasma glucose and serum insulin and required only glucose and insulin infusion as inputs. The model in this study does not have plasma glucose concentration but includes serum insulin and C-peptide concentrations, while plasma glucose concentration and insulin infusion are used as inputs (Fig. 18 and 20). In the previous study, only peripheral insulin clearance, but not hepatic insulin clearance, was estimated because C-peptide data were not used. The decrease of insulin clearance from NGT to T2DM in the previous study is consistent with the decrease of peripheral insulin clearance from NGT to T2DM in this study. In the previous study, the parameter corresponding to insulin secretion in the NGT and borderline type subjects was significantly higher than that in the T2DM subjects; however, the parameter related to insulin secretion in this study did not show a significant difference between the NGT, borderline type, and T2DM subjects, possibly because insulin secretion defined in Chapter 2 is described by insulin secretion and delivery in Chapter 3, and the parameters related to insulin secretion and delivery (α, β, h, m, X_b, and k_{ratio}) are too

diversified in this study. The parameter corresponding to insulin sensitivity was not incorporated in this study.

Many mathematical models to reproduce circulating C-peptide concentration have been developed. A two-compartment model for C-peptide kinetics was originally proposed [62]. A combined model that included both circulating insulin and C-peptide kinetics described by a single compartment structure was introduced to estimate hepatic insulin clearance [44]. The C-peptide minimal model describing peripheral insulin and C-peptide appearance and kinetics was also developed to assess hepatic insulin clearance [34,45-48], and several other model structures for circulating C-peptide concentration were reported [49,50]. One difference between their studies and this study is the experimental protocol in which data were applied to parameter estimation. IVGTT or hyperglycemic clamp were performed for parameter estimation in models of circulating C-peptide concentration, whereas I used hyperglycemic and hyperinsulinemic-euglycemic clamps, which may improve the accuracy of the parameter estimation of peripheral insulin clearance, $k_{I\text{out}}$.

Recently, a model of plasma insulin concentration including hepatic and peripheral insulin clearance and the delivery of insulin from the systemic circulation to the liver during the insulin-modified IVGTT was proposed [51]. In that model, the parameter of hepatic insulin clearance was negatively correlated with acute insulin secretion in response to glucose, and the parameter of peripheral insulin clearance was correlated with insulin sensitivity [51], consistent with the results in this study (Fig. 26). Since the age of subjects in this study differed between groups with NGT, borderline type, and T2DM (Table 7), the correlations

between the parameters and clinical indices may be affected by age. However, the age did not highly correlate with the clinical indices or model parameters (Fig. 33). In addition, the parameters showing the highest correlation with clinical indices of insulin secretion, AUC_{IRI10}, insulin sensitivity, ISI, and insulin clearance, MCR, were not changed with conditioning of age (Table 8). The high correlation between the parameter of hepatic insulin clearance, k_{ratio}, and the clinical index of insulin secretion, AUC_{IRI10}, suggests the possibility that hepatic insulin clearance considerably affects the clinical index of insulin secretion measured by peripheral insulin concentration because the clinical index of insulin secretion, AUC_{IRI10}, was measured by the post-hepatic insulin delivery, and therefore reflects both insulin secretion and hepatic insulin clearance. This suggests that insulin secretion *per se* in the clinical index of insulin secretion may be overestimated because of the involvement of hepatic insulin clearance. Further study is necessary to address this issue.

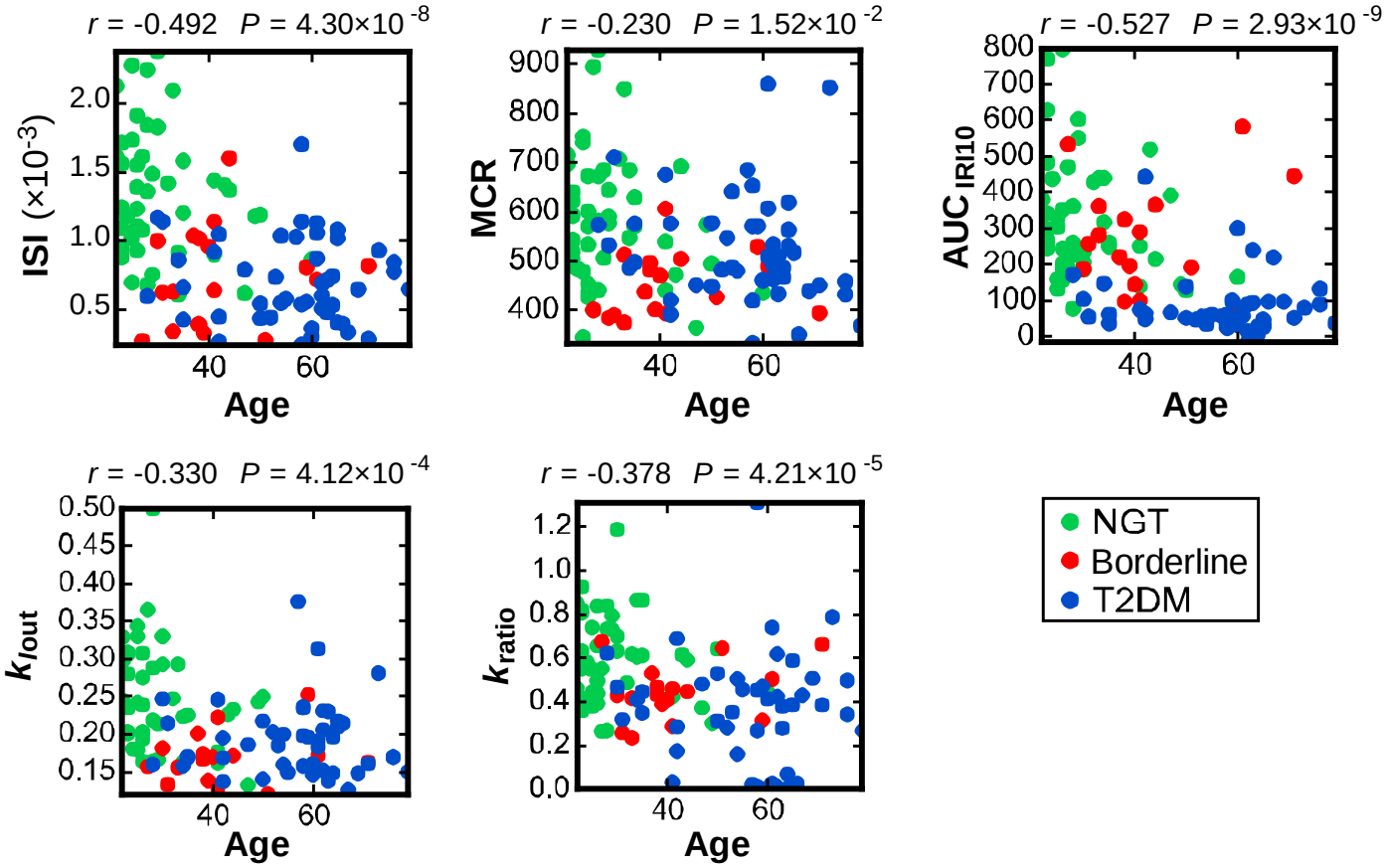

Figure 33. Correlations between the age and clinical indices and model parameters. Scatter plots for the indicated measured clinical indices and model parameters versus age are shown. ISI, the insulin sensitivity index; MCR, the metabolic clearance rate; AUC_{IRI10}, amount of insulin secretion during the first 10 min of hyperglycemic clamp. Each dot indicates the values of an individual subject. The correlation coefficient, *r*, and the *P* values for testing the hypothesis of no correlation are shown.

Table 8. Partial correlation between the model parameters and measured clinical indices

Rank	ISI		MCR		AUC_{IRI10}	
		ρ		ρ		ρ
1	$k_{I\text{out}}$	0.728	$k_{I\text{out}}$	0.778	k_{ratio}	0.287
2	$k_{\text{ratio}} \cdot k_{I\text{out}}$	0.633	$k_{\text{ratio}} \cdot k_{I\text{out}}$	0.516	$k_{I\text{out}}$	-0.202
3	k_{ratio}	0.343	k_{ratio}	0.187	α	-0.151
4	α	-0.146	X_{b}	0.0527	$k_{CP\text{out}}$	-0.126
5	β	-0.0734	β	-0.0518	X_{b}	0.101
6	$k_{CP\text{out}}$	-0.0555	m	0.0275	$k_{\text{ratio}} \cdot k_{I\text{out}}$	0.0941
7	X_{b}	-0.0554	α	0.0239	h	-0.0845
8	m	-0.0156	$k_{CP\text{out}}$	0.00347	m	-0.0699
9	h	0.00799	h	0.000521	β	-0.0637

The partial correlation coefficient (ρ), defined as the correlation between the model parameters and measured clinical indices conditioning of age, are listed in descending order of absolute value.

4. Conclusion

Due to the high social impact of Diabetes (particularly of T2DM in industrialized societies) and the potential simplicity in describing mathematically a two-variable system, the glucose-insulin homeostatic control has been one of the most intensely modeled biomedical problems. Although many models have been proposed to summarize the main functions of the system, using data observed in the OGTT and IVGTT which did not break the mutual relation between circulating glucose and insulin affected the estimation of the parameters corresponding to the functions, such as insulin secretion, sensitivity and clearance.

Throughout this study, I developed the mathematical models based on the consecutive hyperglycemic and hyperinsulinemic-euglycemic clamp analysis in order to improve the identification of the mechanisms involved in the glucose-insulin regulatory system. In Chapter 2, The model for the feedback loop between circulating glucose and insulin has revealed that the rate constant of insulin clearance represents both the capacity for glucose tolerance and a product of insulin sensitivity and insulin secretion among subjects with a range of glucose tolerance (Fig. 14). Further elucidation of underlying mechanism of this law may provide important insight into the physiology of glucose homeostasis and the pathology of glucose intolerance.

In Chapter 3, I developed the models for serum insulin and C-peptide kinetics based on the data of the consecutive clamps. The estimated model parameters revealed the increase of hepatic and decrease of peripheral insulin clearance from NGT to borderline type and T2DM, and these changes selectively regulate the amplitude and temporal patterns of serum insulin

concentration, respectively (Fig. 29). The changes in opposite direction of both types of clearance shed light on the pathological mechanism underlying the abnormal temporal patterns of circulating insulin concentration from NGT to borderline type and T2DM.

5. Acknowledgements

First of all, I would like to express my greatest appreciation to my supervisor, Professor Shinya Kuroda, for his direction with constructive discussion and constant encouragement throughout my graduate study. I greatly thank Dr. Hiroyuki Kubota for his advice on physiological techniques of experiments in mice and humans and the basis of mathematical modeling, and Dr. Shinsuke Uda and Dr. Masashi Fujii for teaching me the methods of mathematics, physics, and statistics and their helpful discussion and advice. I am also grateful to Dr. Yasunori Komori, Dr. Yu Toyoshima, Mr. Toshinao Iwaki, and Mr. Hiroki Fukuzawa for their insightful advice and suggestions, and all members of Kuroda laboratory for valuable discussion and fruitful days.

This study was achieved by collaborations with Dr. Hisako Komada, Dr. Kazuhiko Sakaguchi, and Professor Wataru Ogawa (Kobe University) for performing the clinical experiments in human subjects. I also greatly appreciate them for critical discussion in physiology and pathology. The computational analysis of this work was performed with support from the NIG supercomputer system at ROIS National Institute of Genetics.

This study was supported by the Creation of Fundamental Technologies for Understanding and Control of Biosystem Dynamics, CREST (JPMJCR12W3), of the Japan Science and Technology Agency (JST); the Human Frontier Science Project (HFSP) grant (RGP0061/2011); Japan Diabetes Foundation; Ono Medical Research Foundation; and the Japan Society for the Promotion of Science (JSPS) KAKENHI Grant Number (#21240025, 17H06300). I would like to thank Graduate Program for Leaders in Life Innovation (GPLLI) and JSPS Research Fellowship for Young Scientists for financial support during my graduate study.

Finally, I would like to offer my special thanks to my parents and grandparents for their financial support and daily encouragement.

6. References

1. Saltiel AR, Kahn CR. Insulin signalling and the regulation of glucose and lipid metabolism. *Nature* 2001; **414**(6865): 799-806.

2. Castillo MJ, Scheen AJ, Letiexhe MR, Lefèbvre PJ. How to measure insulin clearance. *Diabetes Metab Rev* 1994; **10**(2): 119-50.

3. World Health Organization. Diabetes: Fact Sheet N°312. 2013.

4. Whiting DR, Guariguata L, Weil C, Shaw J. IDF diabetes atlas: global estimates of the prevalence of diabetes for 2011 and 2030. *Diabetes Res Clin Pract* 2011; **94**(3): 311-21.

5. Alberti KG, Zimmet PZ. Definition, diagnosis and classification of diabetes mellitus and its complications. Part 1: diagnosis and classification of diabetes mellitus provisional report of a WHO consultation. *Diabet Med* 1998; **15**(7): 539-53.

6. Bergman RN, Ader M, Huecking K, Van Citters G. Accurate assessment of beta-cell function: the hyperbolic correction. *Diabetes* 2002; **51 Suppl 1**: S212-20.

7. Seino Y, Nanjo K, Tajima N, et al. Report of the committee on the classification and diagnostic criteria of diabetes mellitus. *J Diabetes Investig* 2010; **1**(5): 212-28.

8. Levine R, Haft DE. Carbohydrate homeostasis. *N Engl J Med* 1970; **283**(5): 237-46.

9. Myllynen P, Koivisto VA, Nikkilä EA. Glucose intolerance and insulin resistance accompany immobilization. *Acta Med Scand* 1987; **222**(1): 75-81.

10. YALOW RS, BERSON SA. Immunoassay of endogenous plasma insulin in man. *J Clin Invest* 1960; **39**: 1157-75.

11. Belfiore F, Iannello S, Volpicelli G. Insulin sensitivity indices calculated from basal

and OGTT-induced insulin, glucose, and FFA levels. *Mol Genet Metab* 1998; **63**(2): 134-41.

12. Matthews DR, Hosker JP, Rudenski AS, Naylor BA, Treacher DF, Turner RC. Homeostasis model assessment: insulin resistance and beta-cell function from fasting plasma glucose and insulin concentrations in man. *Diabetologia* 1985; **28**(7): 412-9.

13. Seltzer HS, Allen EW, Herron AL, Brennan MT. Insulin secretion in response to glycemic stimulus: relation of delayed initial release to carbohydrate intolerance in mild diabetes mellitus. *J Clin Invest* 1967; **46**(3): 323-35.

14. Matsuda M, DeFronzo RA. Insulin sensitivity indices obtained from oral glucose tolerance testing: comparison with the euglycemic insulin clamp. *Diabetes Care* 1999; **22**(9): 1462-70.

15. Perley MJ, Kipnis DM. Plasma insulin responses to oral and intravenous glucose: studies in normal and diabetic sujbjects. *J Clin Invest* 1967; **46**(12): 1954-62.

16. DeFronzo RA, Tobin JD, Andres R. Glucose clamp technique: a method for quantifying insulin secretion and resistance. *Am J Physiol* 1979; **237**(3): E214-23.

17. Okuno Y, Komada H, Sakaguchi K, et al. Postprandial serum C-peptide to plasma glucose concentration ratio correlates with oral glucose tolerance test- and glucose clamp-based disposition indexes. *Metabolism* 2013; **62**(10): 1470-6.

18. Pfeifer MA, Halter JB, Porte D. Insulin secretion in diabetes mellitus. *Am J Med* 1981; **70**(3): 579-88.

19. Cerasi E, Luft R. The plasma insulin response to glucose infusion in healthy subjects and in diabetes mellitus. *Acta Endocrinol (Copenh)* 1967; **55**(2): 278-304.

20. Del Prato S, Tiengo A. The importance of first-phase insulin secretion: implications for the therapy of type 2 diabetes mellitus. *Diabetes Metab Res Rev* 2001; **17**(3): 164-74.

21. Seino S, Shibasaki T, Minami K. Dynamics of insulin secretion and the clinical implications for obesity and diabetes. *J Clin Invest* 2011; **121**(6): 2118-25.

22. Weyer C, Bogardus C, Mott DM, Pratley RE. The natural history of insulin secretory dysfunction and insulin resistance in the pathogenesis of type 2 diabetes mellitus. *J Clin Invest* 1999; **104**(6): 787-94.

23. Bergman RN, Phillips LS, Cobelli C. Physiologic evaluation of factors controlling glucose tolerance in man: measurement of insulin sensitivity and beta-cell glucose sensitivity from the response to intravenous glucose. *J Clin Invest* 1981; **68**(6): 1456-67.

24. Bergman RN, Finegood DT, Kahn SE. The evolution of beta-cell dysfunction and insulin resistance in type 2 diabetes. *Eur J Clin Invest* 2002; **32 Suppl 3**: 35-45.

25. Denti P, Toffolo GM, Cobelli C. The disposition index: from individual to population approach. *Am J Physiol Endocrinol Metab* 2012; **303**(5): E576-86.

26. Retnakaran R, Shen S, Hanley AJ, Vuksan V, Hamilton JK, Zinman B. Hyperbolic relationship between insulin secretion and sensitivity on oral glucose tolerance test. *Obesity (Silver Spring)* 2008; **16**(8): 1901-7.

27. Utzschneider KM, Prigeon RL, Faulenbach MV, et al. Oral disposition index predicts the development of future diabetes above and beyond fasting and 2-h glucose levels. *Diabetes Care* 2009; **32**(2): 335-41.

28. Jauslin PM, Silber HE, Frey N, et al. An integrated glucose-insulin model to describe

oral glucose tolerance test data in type 2 diabetics. *J Clin Pharmacol* 2007; **47**(10): 1244-55.

29. Silber HE, Frey N, Karlsson MO. An integrated glucose-insulin model to describe oral glucose tolerance test data in healthy volunteers. *J Clin Pharmacol* 2010; **50**(3): 246-56.

30. Thomaseth K, Kautzky-Willer A, Ludvik B, Prager R, Pacini G. Integrated mathematical model to assess beta-cell activity during the oral glucose test. *Am J Physiol* 1996; **270**(3 Pt 1): E522-31.

31. Pedersen MG, Toffolo GM, Cobelli C. Cellular modeling: insight into oral minimal models of insulin secretion. *Am J Physiol Endocrinol Metab* 2010; **298**(3): E597-601.

32. Breda E, Cavaghan MK, Toffolo G, Polonsky KS, Cobelli C. Oral glucose tolerance test minimal model indexes of beta-cell function and insulin sensitivity. *Diabetes* 2001; **50**(1): 150-8.

33. Hovorka R, Chassin L, Luzio SD, Playle R, Owens DR. Pancreatic beta-cell responsiveness during meal tolerance test: model assessment in normal subjects and subjects with newly diagnosed noninsulin-dependent diabetes mellitus. *J Clin Endocrinol Metab* 1998; **83**(3): 744-50.

34. Toffolo G, Breda E, Cavaghan MK, Ehrmann DA, Polonsky KS, Cobelli C. Quantitative indexes of beta-cell function during graded up&down glucose infusion from C-peptide minimal models. *Am J Physiol Endocrinol Metab* 2001; **280**(1): E2-10.

35. Mari A, Pacini G, Murphy E, Ludvik B, Nolan JJ. A model-based method for assessing insulin sensitivity from the oral glucose tolerance test. *Diabetes Care* 2001; **24**(3): 539-48.

36. Dalla Man C, Caumo A, Cobelli C. The oral glucose minimal model: estimation of insulin sensitivity from a meal test. *IEEE Trans Biomed Eng* 2002; **49**(5): 419-29.

37. Dalla Man C, Caumo A, Basu R, Rizza R, Toffolo G, Cobelli C. Minimal model estimation of glucose absorption and insulin sensitivity from oral test: validation with a tracer method. *Am J Physiol Endocrinol Metab* 2004; **287**(4): E637-43.

38. Picchini U, De Gaetano A, Panunzi S, Ditlevsen S, Mingrone G. A mathematical model of the euglycemic hyperinsulinemic clamp. *Theor Biol Med Model* 2005; **2**: 44.

39. Sato H, Terasaki T, Mizuguchi H, Okumura K, Tsuji A. Receptor-recycling model of clearance and distribution of insulin in the perfused mouse liver. *Diabetologia* 1991; **34**(9): 613-21.

40. Duckworth WC, Hamel FG, Peavy DE. Hepatic metabolism of insulin. *Am J Med* 1988; **85**(5A): 71-6.

41. Rabkin R, Kitaji J. Renal metabolism of peptide hormones. *Miner Electrolyte Metab* 1983; **9**(4-6): 212-26.

42. Ahrén B, Thorsson O. Increased insulin sensitivity is associated with reduced insulin and glucagon secretion and increased insulin clearance in man. *J Clin Endocrinol Metab* 2003; **88**(3): 1264-70.

43. Cobelli C, Dalla Man C, Toffolo G, Basu R, Vella A, Rizza R. The oral minimal model method. *Diabetes* 2014; **63**(4): 1203-13.

44. Vølund A, Polonsky KS, Bergman RN. Calculated pattern of intraportal insulin appearance without independent assessment of C-peptide kinetics. *Diabetes* 1987; **36**(10):

1195-202.

45. Cobelli C, Pacini G. Insulin secretion and hepatic extraction in humans by minimal modeling of C-peptide and insulin kinetics. *Diabetes* 1988; **37**(2): 223-31.

46. Grodsky GM. A threshold distribution hypothesis for packet storage of insulin and its mathematical modeling. *J Clin Invest* 1972; **51**(8): 2047-59.

47. Ličko V, Silvers A. Open-loop glucose-insulin control with threshold secretory mechanism: Analysis of intravenous glucose tolerance tests in man. *Mathematical Biosciences* 1975; **27**(3): 319-32.

48. Toffolo G, Campioni M, Basu R, Rizza RA, Cobelli C. A minimal model of insulin secretion and kinetics to assess hepatic insulin extraction. *Am J Physiol Endocrinol Metab* 2006; **290**(1): E169-E76.

49. Chase JG, Mayntzhusen K, Docherty PD, et al. A three-compartment model of the C-peptide-insulin dynamic during the DIST test. *Math Biosci* 2010; **228**(2): 136-46.

50. Mari A, Tura A, Gastaldelli A, Ferrannini E. Assessing insulin secretion by modeling in multiple-meal tests: role of potentiation. *Diabetes* 2002; **51 Suppl 1**: S221-6.

51. Polidori DC, Bergman RN, Chung ST, Sumner AE. Hepatic and Extrahepatic Insulin Clearance Are Differentially Regulated: Results From a Novel Model-Based Analysis of Intravenous Glucose Tolerance Data. *Diabetes* 2016; **65**(6): 1556-64.

52. Ohashi K, Komada H, Uda S, et al. Glucose Homeostatic Law: Insulin Clearance Predicts the Progression of Glucose Intolerance in Humans. *PLoS One* 2015; **10**(12): e0143880.

53. Antuna-Puente B, Disse E, Rabasa-Lhoret R, Laville M, Capeau J, Bastard JP. How

can we measure insulin sensitivity/resistance? *Diabetes Metab* 2011; **37**(3): 179-88.

54. Antuna-Puente B, Disse E, Rabasa-Lhoret R, Laville M, Capeau J, Bastard JP. How can we measure insulin sensitivity/resistance? *Diabetes Metab* 2011; **37**(3): 179-88.

55. Bolie VW. Coefficients of normal blood glucose regulation. *J Appl Physiol* 1961; **16**: 783-8.

56. Ackerman E, Gatewood LC, Rosevear JW, Molnar GD. Model studies of blood-glucose regulation. *Bull Math Biophys* 1965; **27**: Suppl:21-37.

57. Gatewood LC, Ackerman E, Rosevear JW, Molnar GD, Burns TW. Tests of a mathematical model of the blood-glucose regulatory system. *Comput Biomed Res* 1968; **2**(1): 1-14.

58. Bergman RN, Ider YZ, Bowden CR, Cobelli C. Quantitative estimation of insulin sensitivity. *Am J Physiol* 1979; **236**(6): E667-77.

59. Denti P, Bertoldo A, Vicini P, Cobelli C. IVGTT glucose minimal model covariate selection by nonlinear mixed-effects approach. *Am J Physiol Endocrinol Metab* 2010; **298**(5): E950-60.

60. De Gaetano A, Arino O. Mathematical modelling of the intravenous glucose tolerance test. *J Math Biol* 2000; **40**(2): 136-68.

61. Silber HE, Jauslin PM, Frey N, Gieschke R, Simonsson US, Karlsson MO. An integrated model for glucose and insulin regulation in healthy volunteers and type 2 diabetic patients following intravenous glucose provocations. *J Clin Pharmacol* 2007; **47**(9): 1159-71.

62. Eaton RP, Allen RC, Schade DS, Erickson KM, Standefer J. Prehepatic insulin

production in man: kinetic analysis using peripheral connecting peptide behavior. *J Clin Endocrinol Metab* 1980; **51**(3): 520-8.

63. Watanabe RM, Steil GM, Bergman RN. Critical evaluation of the combined model approach for estimation of prehepatic insulin secretion. *Am J Physiol* 1998; **274**(1 Pt 1): E172-83.

64. Hovorka R, Soons PA, Young MA. ISEC: a program to calculate insulin secretion. *Comput Methods Programs Biomed* 1996; **50**(3): 253-64.

65. Toffolo G, De Grandi F, Cobelli C. Estimation of beta-cell sensitivity from intravenous glucose tolerance test C-peptide data. Knowledge of the kinetics avoids errors in modeling the secretion. *Diabetes* 1995; **44**(7): 845-54.

66. Mari A, Schmitz O, Gastaldelli A, Oestergaard T, Nyholm B, Ferrannini E. Meal and oral glucose tests for assessment of beta -cell function: modeling analysis in normal subjects. *Am J Physiol Endocrinol Metab* 2002; **283**(6): E1159-66.

67. Campioni M, Toffolo G, Basu R, Rizza RA, Cobelli C. Minimal model assessment of hepatic insulin extraction during an oral test from standard insulin kinetic parameters. *Am J Physiol Endocrinol Metab* 2009; **297**(4): E941-8.

68. Nicholls JG. From neuron to brain. 5th ed. Sunderland, Mass.: Sinauer Associates; 2012.

69. Choi E, Ahn W. A new mixture ratio of heparin for the cell salvage device. *Korean J Anesthesiol* 2011; **60**(3): 226.

70. Lagarias J, Reeds J, Wright M, Wright P. Convergence properties of the Nelder-Mead

simplex method in low dimensions. *Siam Journal on Optimization* 1998; **9**(1): 112-47.

71. Fujita KA, Toyoshima Y, Uda S, Ozaki Y, Kubota H, Kuroda S. Decoupling of receptor and downstream signals in the Akt pathway by its low-pass filter characteristics. *Sci Signal* 2010; **3**(132): ra56.

72. Hubert M, Van der Veeken S. Outlier detection for skewed data. *Journal of Chemometrics* 2008; **22**(3-4): 235-46.

73. Brys G, Hubert M, Struyf A. A robust measure of skewness. *Journal of Computational and Graphical Statistics* 2004; **13**(4): 996-1017.

74. Alon U. An introduction to systems biology: design principles of biological circuits: CRC Press; 2006.

75. Komada H, Sakaguchi K, Takeda K, et al. Age-dependent decline in β-cell function assessed by an oral glucose tolerance test-based disposition index. *Journal of Diabetes Investigation* 2011; **2**(4): 293-6.

76. Benjamini Y, Hochberg Y. Controlling the False Discovery Rate: A Practical and Powerful Approach to Multiple Testing. *Journal of the Royal Statistical Society B* 1995; **57**(1): 289-300.

77. Duckworth WC, Bennett RG, Hamel FG. Insulin degradation: progress and potential. *Endocr Rev* 1998; **19**(5): 608-24.

78. Marini MA, Frontoni S, Succurro E, et al. Differences in insulin clearance between metabolically healthy and unhealthy obese subjects. *Acta Diabetol* 2014; **51**(2): 257-61.

79. Lee CC, Haffner SM, Wagenknecht LE, et al. Insulin clearance and the incidence of

type 2 diabetes in Hispanics and African Americans: the IRAS Family Study. *Diabetes Care* 2013; **36**(4): 901-7.

80. Rudovich NN, Rochlitz HJ, Pfeiffer AF. Reduced hepatic insulin extraction in response to gastric inhibitory polypeptide compensates for reduced insulin secretion in normal-weight and normal glucose tolerant first-degree relatives of type 2 diabetic patients. *Diabetes* 2004; **53**(9): 2359-65.

81. Jones CN, Pei D, Staris P, Polonsky KS, Chen YD, Reaven GM. Alterations in the glucose-stimulated insulin secretory dose-response curve and in insulin clearance in nondiabetic insulin-resistant individuals. *J Clin Endocrinol Metab* 1997; **82**(6): 1834-8.

82. Benzi L, Cecchetti P, Ciccarone A, Pilo A, Di Cianni G, Navalesi R. Insulin degradation in vitro and in vivo: a comparative study in men. Evidence that immunoprecipitable, partially rebindable degradation products are released from cells and circulate in blood. *Diabetes* 1994; **43**(2): 297-304.

83. Polonsky KS, Given BD, Hirsch L, et al. Quantitative study of insulin secretion and clearance in normal and obese subjects. *J Clin Invest* 1988; **81**(2): 435-41.

84. Bonora E, Zavaroni I, Coscelli C, Butturini U. Decreased hepatic insulin extraction in subjects with mild glucose intolerance. *Metabolism* 1983; **32**(5): 438-46.

85. Tamaki M, Fujitani Y, Hara A, et al. The diabetes-susceptible gene SLC30A8/ZnT8 regulates hepatic insulin clearance. *J Clin Invest* 2013; **123**(10): 4513-24.

86. Kashyap S, Belfort R, Gastaldelli A, et al. A sustained increase in plasma free fatty acids impairs insulin secretion in nondiabetic subjects genetically predisposed to develop type

2 diabetes. *Diabetes* 2003; **52**(10): 2461-74.

87. Ader M, Stefanovski D, Kim SP, et al. Variable hepatic insulin clearance with attendant insulinemia is the primary determinant of insulin sensitivity in the normal dog. *Obesity (Silver Spring)* 2013.

88. Kubota H, Noguchi R, Toyoshima Y, et al. Temporal coding of insulin action through multiplexing of the AKT pathway. *Mol Cell* 2012; **46**(6): 820-32.

89. Noguchi R, Kubota H, Yugi K, et al. The selective control of glycolysis, gluconeogenesis and glycogenesis by temporal insulin patterns. *Mol Syst Biol* 2013; **9**: 664.

90. Matveyenko AV, Veldhuis JD, Butler PC. Mechanisms of impaired fasting glucose and glucose intolerance induced by an approximate 50% pancreatectomy. *Diabetes* 2006; **55**(8): 2347-56.

91. Toyoshima Y, Kakuda H, Fujita KA, Uda S, Kuroda S. Sensitivity control through attenuation of signal transfer efficiency by negative regulation of cellular signalling. *Nat Commun* 2012; **3**: 743.

92. Raue A, Karlsson J, Saccomani MP, Jirstrand M, Timmer J. Comparison of approaches for parameter identifiability analysis of biological systems. *Bioinformatics* 2014; **30**(10): 1440-8.

93. DeFronzo RA, Bonadonna RC, Ferrannini E. Pathogenesis of NIDDM. A balanced overview. *Diabetes Care* 1992; **15**(3): 318-68.

94. Lindsay JR, McKillop AM, Mooney MH, Flatt PR, Bell PM, O'harte FP. Meal-induced 24-hour profile of circulating glycated insulin in type 2 diabetic subjects measured by

a novel radioimmunoassay. *Metabolism* 2003; **52**(5): 631-5.

95. Polonsky KS, Given BD, Van Cauter E. Twenty-four-hour profiles and pulsatile patterns of insulin secretion in normal and obese subjects. *J Clin Invest* 1988; **81**(2): 442-8.

96. Stumvoll M, Mitrakou A, Pimenta W, et al. Use of the oral glucose tolerance test to assess insulin release and insulin sensitivity. *Diabetes Care* 2000; **23**(3): 295-301.

97. Hayashi T, Boyko EJ, Sato KK, et al. Patterns of insulin concentration during the OGTT predict the risk of type 2 diabetes in Japanese Americans. *Diabetes Care* 2013; **36**(5): 1229-35.

98. Abdul-Ghani MA, Tripathy D, DeFronzo RA. Contributions of beta-cell dysfunction and insulin resistance to the pathogenesis of impaired glucose tolerance and impaired fasting glucose. *Diabetes Care* 2006; **29**(5): 1130-9.

99. Saisho Y, Kou K, Tanaka K, et al. Postprandial serum C-peptide to plasma glucose ratio as a predictor of subsequent insulin treatment in patients with type 2 diabetes. *Endocr J* 2011; **58**(4): 315-22.

100. Vølund A, Brange J, Drejer K, et al. In vitro and in vivo potency of insulin analogues designed for clinical use. *Diabet Med* 1991; **8**(9): 839-47.

101. Akaike H. Information theory and an extension of the maximum likelihood principle. In: Petrov BN, Csáki F, eds. Proceedings of the 2nd International Symposium on Information Theory. Budapest: Akadémiai Kiadó; 1973: 267-81.

102. Butler AE, Janson J, Bonner-Weir S, Ritzel R, Rizza RA, Butler PC. Beta-cell deficit and increased beta-cell apoptosis in humans with type 2 diabetes. *Diabetes* 2003; **52**(1): 102-

10.

103. Inaishi J, Saisho Y, Sato S, et al. Effects of Obesity and Diabetes on α- and β-Cell Mass in Surgically Resected Human Pancreas. *J Clin Endocrinol Metab* 2016; **101**(7): 2874-82.

104. Mizukami H, Takahashi K, Inaba W, et al. Involvement of oxidative stress-induced DNA damage, endoplasmic reticulum stress, and autophagy deficits in the decline of β-cell mass in Japanese type 2 diabetic patients. *Diabetes Care* 2014; **37**(7): 1966-74.

105. Sano T, Kawata K, Ohno S, et al. Selective control of up-regulated and down-regulated genes by temporal patterns and doses of insulin. *Sci Signal* 2016; **9**(455): ra112.

106. Goodner CJ, Sweet IR, Harrison HC. Rapid reduction and return of surface insulin receptors after exposure to brief pulses of insulin in perifused rat hepatocytes. *Diabetes* 1988; **37**(10): 1316-23.

107. Hirashima Y, Tsuruzoe K, Kodama S, et al. Insulin down-regulates insulin receptor substrate-2 expression through the phosphatidylinositol 3-kinase/Akt pathway. *J Endocrinol* 2003; **179**(2): 253-66.

108. Hori SS, Kurland IJ, DiStefano JJ. Role of endosomal trafficking dynamics on the regulation of hepatic insulin receptor activity: models for Fao cells. *Ann Biomed Eng* 2006; **34**(5): 879-92.

109. Matveyenko AV, Liuwantara D, Gurlo T, et al. Pulsatile portal vein insulin delivery enhances hepatic insulin action and signaling. *Diabetes* 2012; **61**(9): 2269-79.

110. Sedaghat AR, Sherman A, Quon MJ. A mathematical model of metabolic insulin

signaling pathways. *Am J Physiol Endocrinol Metab* 2002; **283**(5): E1084-101.

111. Kubota N, Kubota T, Itoh S, et al. Dynamic functional relay between insulin receptor substrate 1 and 2 in hepatic insulin signaling during fasting and feeding. *Cell Metab* 2008; **8**(1): 49-64.

7. List of Publications

Kaoru Ohashi, Hisako Komada, Shinsuke Uda, Hiroyuki Kubota, Toshinao Iwaki, Hiroki Fukuzawa, Yasunori Komori, Masashi Fujii, Yu Toyoshima, Kazuhiko Sakaguchi, Wataru Ogawa, Shinya Kuroda. Glucose Homeostatic Law: Insulin Clearance Predicts the Progression of Glucose Intolerance in Humans. *PLoS One* 2015; **10**(12): e0143880

Kaoru Ohashi, Masashi Fujii, Shinsuke Uda, Hiroyuki Kubota, Hisako Komada, Kazuhiko Sakaguchi, Wataru Ogawa, Shinya Kuroda. Increase in hepatic and decrease in peripheral insulin clearance characterize abnormal temporal patterns of serum insulin in diabetic subjects. (in preparation, Preprint: bioRxiv: 121392)

大橋 郁, 藤井 雅史, 小川 渉, 黒田真也. 血糖恒常性システムの数理モデル解析. 実験医学増刊 (羊土社) 2017; **35**(5):